FG.

RAYTHEON **LASER ADVANCED DEVELOPMENT CENTER**

(12)

NRL-N00014-73-C-0199
INTER SATELLITE LASER RFDR

DEVELOPMENT AND FABRICATION OF A SPACE HARDENED Nd^{+3} YAG LASER TRANSMITTER SYSTEM

for

ORBITAL RANGE AND ALTITUDE CONTROL

by

Lorand J. Wargo

RAYTHEON COMPANY
Laser Advanced Development Center
Special Microwave Devices Operation
130 Second Avenue
Waltham, Massachusetts 02154

Contract No. N00014-73-C-0199

FINAL REPORT
Period Covered: January 1, 1973 through May 6, 1975
Date of Report: May 6, 1975
Contract Monitor: Dr. Steven Melman

Prepared for:

Naval Research Laboratory
4555 Overlook Avenue S. W.
Washington, D.C. 20390

NRL-N00014-73-C-0199
INTER SATELLITE LASER RFDR

(6) DEVELOPMENT AND FABRICATION OF A SPACE HARDENED Nd(+3) YAG LASER TRANSMITTER SYSTEM for ORBITAL RANGE AND ALTITUDE CONTROL

by

(10) Lorand J. Wargo

(12) 131 p.

RAYTHEON COMPANY
Laser Advanced Development Center
Special Microwave Devices Operation
130 Second Avenue
Waltham, Massachusetts 02154

(11) 6 May 75

Contract No. N00014-73-C-0199
(15)

(9) FINAL REPORT,
Period Covered: 1 Jan [redacted] 73 - [redacted] May [redacted] 75,
Date of Report: May 6, 1975
Contract Monitor: Dr. Steven Melman

Prepared for:

Naval Research Laboratory
4555 Overlook Avenue S.W.
Washington, D.C. 20390

402 847

DISTRIBUTION LIST

ADDRESSEE	DODAAD	No. of Copies (U)
Scientific Officer	N00173	1
Administrative Contracting Officer	S2205A	1
Director, U.S. Naval Research Lab Washington, D.C. 20390	N00173	
Attention: Code 2629		6
Attention: Code 2627		6
Defense Documentation Center Building 5 Cameron Station Alexandria, Virginia 22314		12

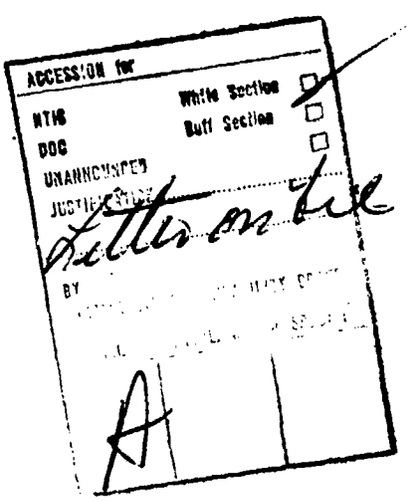

PREFACE

THE SCOPE OF THE PROGRAM

1) During the program, research and development was conducted for space hardening the Raytheon SS-219 miniature Nd^{+3} YAG system, to be able to operate in a ground launched satellite.

2) Study was conducted to identify and eliminate all sources of laser degradation resulting from the space environment with special consideration of the radiation conditions as they exist at an altitude of 666 nautical miles and the shock and vibrational environment (mechanical and acoustical) encountered during the launch period.

3) Investigation sought ways of reducing and minimizing the electrical power drain required by the Laser System.

4) Development of thermal control was attempted, to make the Laser System compatible with the Spacecraft radiational cooling.

BRIEF SYNOPSIS OF THE PROGRAM

The basic Raytheon Model SS-219 was described and the specifications of the Laser Transmitter, such as size, weight and performance were reported. Radiation tests were conducted on the Laser Crystal and the passive Q-Switch. The tests indicated, that the Laser Crystal will not suffer adverse consequences from the radiation, but the matrix imbedded dye Q-switch will.

A brief treatment of the various Q-switches and optical elements, with some recommendations and exclusions, established the basic guidelines for further studies and the design of the space-hardened Laser Transmitter. The study included such topics as general interferometer stability, internally generated perturbances, external perturbations and their effects on the laser stability.

Further study covered the Laser Crystal parameters such as the effect of the Neodymium concentration, spectrum matching, reflectivity and pumping efficiency and mode structure details. These parameters permitted the finalization of the Laser Crystal characteristics, the pumping lamp requirements and cavity geometry.

After the design of the final space hardened laser transmitter and the study of the mechanical subassemblies terminated, the drawings were released for fabrication. Detailed description of the mechanics of the SS-219 optical system was presented and the applicable details for the conversion of the SS-219 into SS-223 were highlighted. The problems of the existing mechanical suspensions for optical elements were described in detail and conclusions were drawn that the need for an unconventional but super stable optical mounting system was evident. A detailed analysis of the problems was presented and solution to the problems was suggested by the use of a Ball-Socket Joint Optical Suspension System.

The program continued with the detailed study of the final layout of the SS-223 opto-mechanical parts, including the housing, PFN, outlets and the complete laser resonator.

The final phase of the program dealt with the electronic space hardening of the SS-223 system. Radiation hazards were studied and reported, and the necessary precautions were taken. The achievement of low power drain and low cooling requirements was successful.

The program ended with the summary of the final tests and measurements at the acceptance, and the composition of this final report.

TABLE OF CONTENTS

TABLE OF CONTENTS (Continued)

LIST OF ILLUSTRATIONS

LIST OF ILLUSTRATIONS (Continued)

LIST OF ILLUSTRATIONS (Continued)

1.0 INTRODUCTION

Since the first successful demonstration of a working laser by Theodore Maiman in 1960, Raytheon LADC was leading the very early effort in the manufacture of laboratory laser systems.

A great number of gas and solid state lasers were constructed and placed in various scientific research centers by Raytheon Company.

The past decade presented a great opportunity for continuous improvement of the performance of such lasers.

Presently, LADC manufactures a broad line of Solid State Lasers. Our standard line of products features Ruby and YAG lasers and laser accessories such as Polarizers, Q-Switches, Harmonic Generators and mode control optics.

Our Ruby Lasers operate with efficiency of over 1% at repetition rates up to 10 pulses per second with average output power of 20W.

The YAG lasers deliver several joules per pulse at efficiency over 2% in millisecond pulses.

The present SS-219 miniature Nd^{+3} YAG Laser System was developed for test trial use in limited field environment, by an operator holding the equipment in his hands or to be fixed to a tripod.

1.1 SPECIFICATIONS : SS-219

Optical

Laser Crystal Material:		$LuNd^{+3}$ YAG
Size:		5 mm dia. x 50 mm long
Weight:		.25 oz.
Finish:	Ends	1/10th of λ flat - 3 sec. of arc parallel
	Side	Fine ground

Output Optics:	Front end of the crystal 55% reflective at 1.06 μ MgO-SiO super hard multi-layer, dielectric. Back end AR - .25% reflective. Magnesium Floride, single layer.
Retro-Optics Back Mirror:	
Size:	1/4" thick 1/2" diameter
Material:	Supersil, 10 meter, 1/10 λ radius mirror.
Coating:	100% reflective at 1.06 μ MgO-SiO super hard multi-layer, dielectric.
Weight:	.1 oz.
Polarizer Size:	8 mm x 8 mm; 10 mm long
Material:	Select optical calcite
Coating:	AR-AR; .25% reflective Magnesium Floride single layer.
Weight:	.08 oz.
Pockels Cell:	
Size:	8 mm x 8 mm x 25 mm long
Material:	Lithium Niobate
Finish:	1/10 flat - 3 sec. parallel
Coating:	AR-AR .25% reflective Magnesium Floride single layer
Weight:	.95 oz.
Flash Lamp; L-1454 Envelope:	Germisil 1 mm thick wall tubing
Electrodes:	Tungsten-Thoriated
Seal:	Graded U. glass
Plasma dia:	3 mm
Length:	44.44 mm
Gas fill:	Krypton
Gas pressure:	1500 Torr
End Caps:	4.76 mm dia.; 12.7 mm long
Lamp length:	96 mm

Cavity Reflector:

Surface finished:	per ESL-61125 Optical Silver

Electrical

Input Power:	min. 18 VDC 2.2 ADC .950 Sec. charging time max. 32 VDC 3.3 A .450 sec. charging time
Trigger Voltage:	16-20 kilovolts
Series injection:	50 microseconds
PFN Capacitor:	20 microfarads 1000 VDC
Energy:	10 joules
Pulse length:	110 microseconds
Q-switch voltage: switch speed:	2400 VDC at 2 nS
Logic Voltage:	15 VDC High noise immunity logic
Logic System:	All integrated circuit
Clock System:	HF unijunction oscillators (adjustable)
Alternate input:	115 VAC 50-60 Hz 25 Watts

Mechanical

Laser Head:

Size:	1.125" x 1.25", 6.75"
Material:	6062 aluminum hard drawn brass
Weight:	10 oz.

Total Transmitter:

Size:	2" x 3.25" x 7"
Weight:	3 lbs.

Performance

Output:	50 millijoules
Pulse Width (Q-switched)	10-15 nS
Beam Divergence	5 mr (nominal)
Repetition Rate:	1 pps
Trigger:	manual auto rep. external
Ambient:	-40° $+50^{\circ}C$
Enclosure:	dust proof
P.M.I.:	shielded; min.

This system served as starting point for the study, investigations, research and development. Design and final fabrication and testing of the new space hardened miniature Nd^{+3}YAG Laser System bearing the model number SS-223 will follow in the next reporting period. (See pictures #1 and #2)

1.2 Space Hardening Considerations

The space hardened SS-223 system must survive two major environmental conditions.

First, the initial launching and insertion into orbit; second, the full expected life span in the zero-gravity in the rarified atmosphere. Structurally, the design must take into consideration opto-mechanical functions and electronic circuit functions, as they are exposted to launching and space environments. (See attached chart for critical areas.)

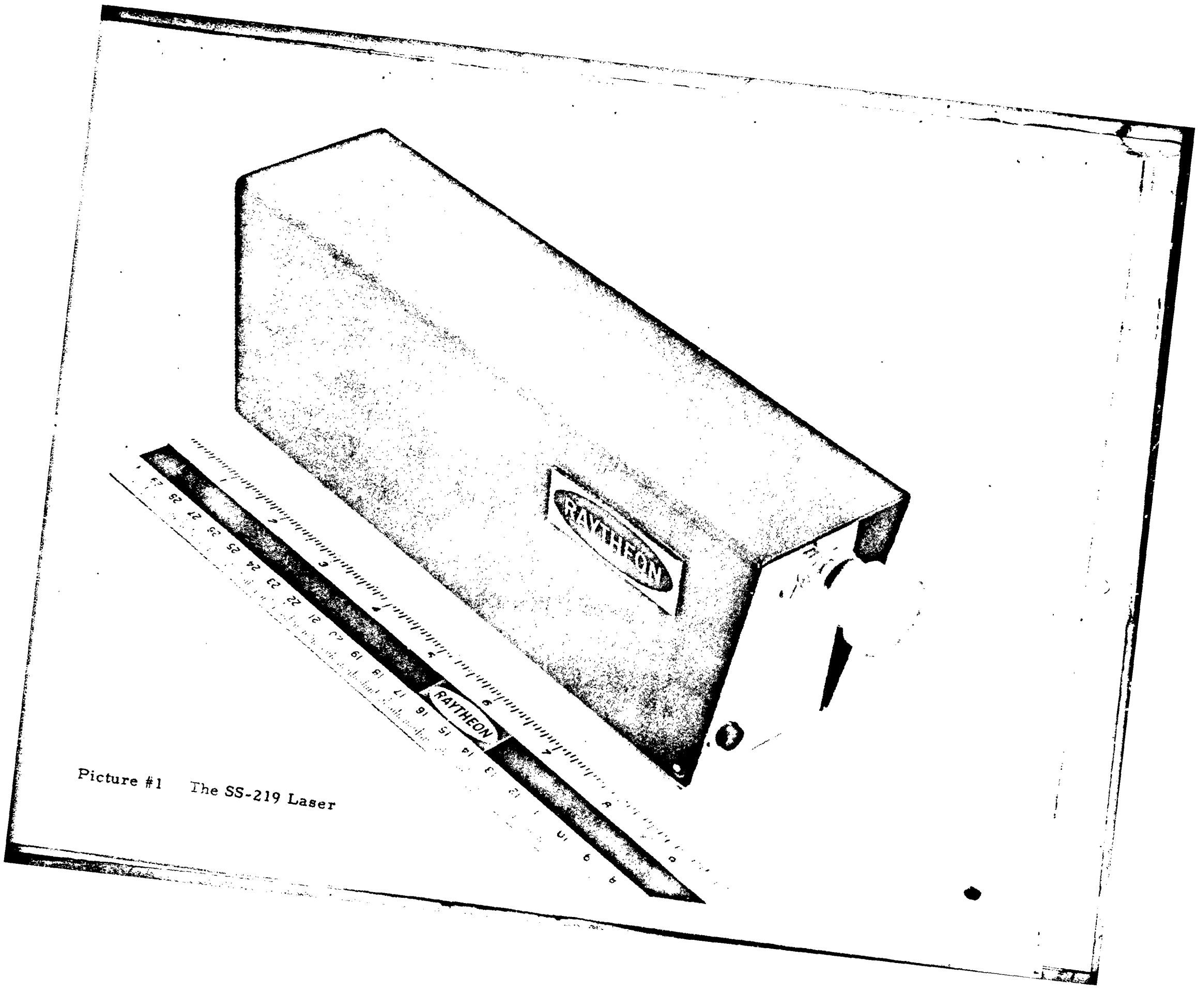

Picture #1 The SS-219 Laser

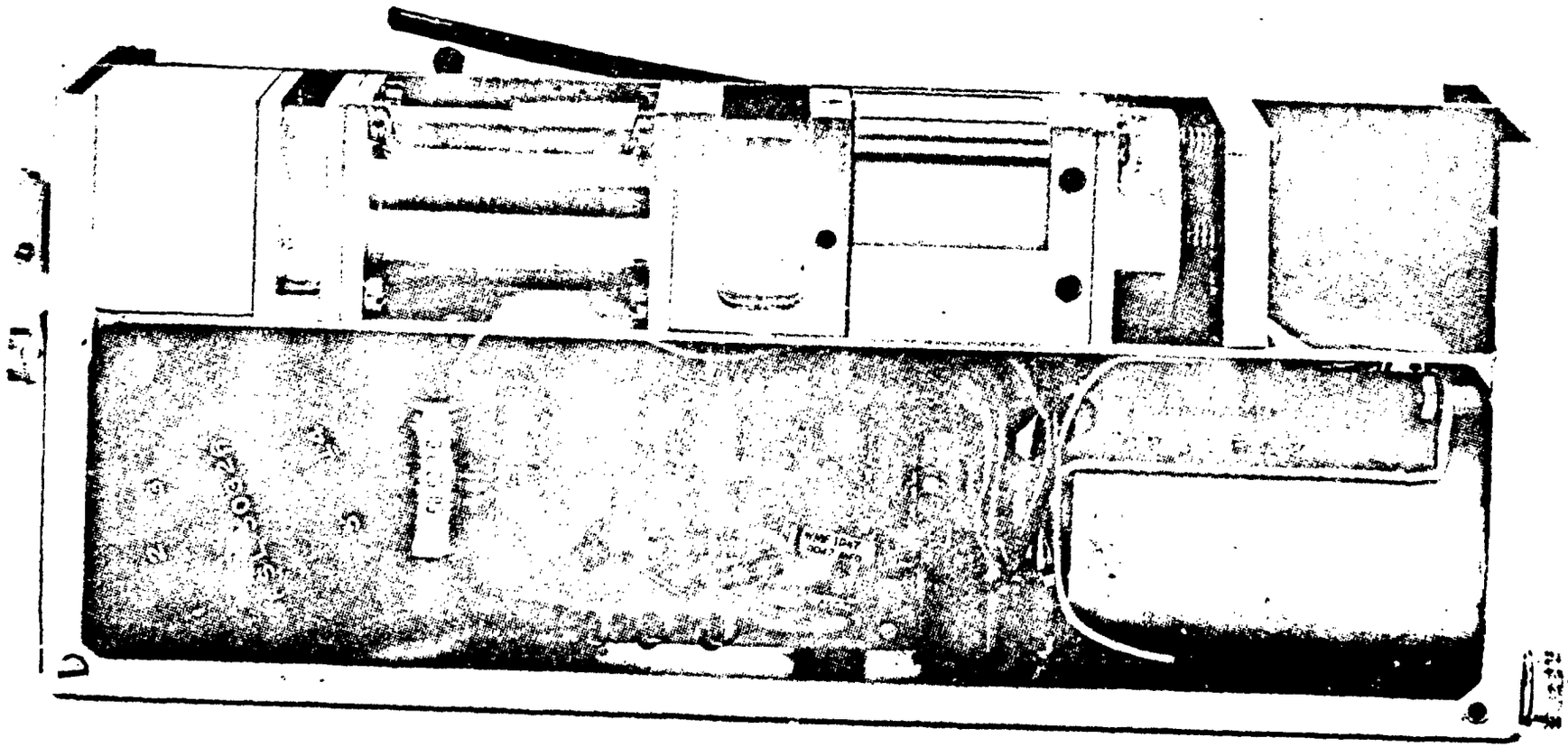

Picture #2 SS-219 Laser-Cover Removed

Task: Space Hardening of SS-223 Laser System

Environment:	Launch Environment		Orbiting Environment	
Design Area:	Opto-Mechanical	Electronic	Opto-Mechanical	Electronic
Exposure:	Shock, vibration, acoustics, acceleration, thermal, internal contamination.		Radiation, sublimation, cold weld, high vapor pressure deposition, out-gassing contamination, thermal differential distortion.	
Affected Area:	Mechanical stabilization of components, balanced distribution of the mass, cantilever suppression, fastener location, and selection, thermal depletion by conduction, thermal balance and radiation suppression. Choice of low vapor pressure materials		Stabilization of optical mounts. Choice of optical coatings. Choice of flashlamp. Interface of dissimilar metals and insulation. Shielding against radiation. Choice and protection of opto-electronic crystals, polarizers.	Stabilization of electronic parts. Balanced distribution of the circuits. Thermal depletion of the components. Electronic circuit stability. Radiation resistance. MTBF study. Outgassing contamination. Galvanic contamination.

1.3 Study and Conclusions

Certain component characteristics of the space hardened laser system are determined by the functional requirements of the laser. Such components are; the Nd^{+3} YAG laser crystal, the Glan-Laser Calcite polarizer, the Lithium Niobate Pockels cell and the dielectric coated mirrors in the resonator. At the present state of the art, no alternates are available in place of these components.

Possible alternate for the Nd^{+3} YAG would be the Nd-glass, but this material has poor thermal characteristics and lower hardness and mechanical stability than YAG. Another possible alternate would be YALO host material for the Nd-doping, but at present time the crystal growing technology does not produce reliable crystals and the ever-present twining tendency of the YALO host increases the risk factor beyond safe level.

The dielectric coatings have a safe past record in space application and if produced and inspected properly, the risk factor is very low.

Alternate to Electro-Optical "Q" switching is the Opto-Mechanical or an Opto-Chemical "Q" switch.

The opto-chemical (dye) "Q" switch in the solution form is not recommended for vacuum operation and the plastic matrix embedded dye cells do not possess proven long term stability. This leads us to believe that either one would be a poor choice for the space environment.

During the present study, samples of several Plastic "Q" switches and liquid "Q" switches were exposed to radiation of various levels and the results are tabulated with the results of Nd^{+3} YAG radiation experiments.

All the radiation tests were conducted in an LC-42 series cavity which is presently used in the SS-219 system (see picture # 3).

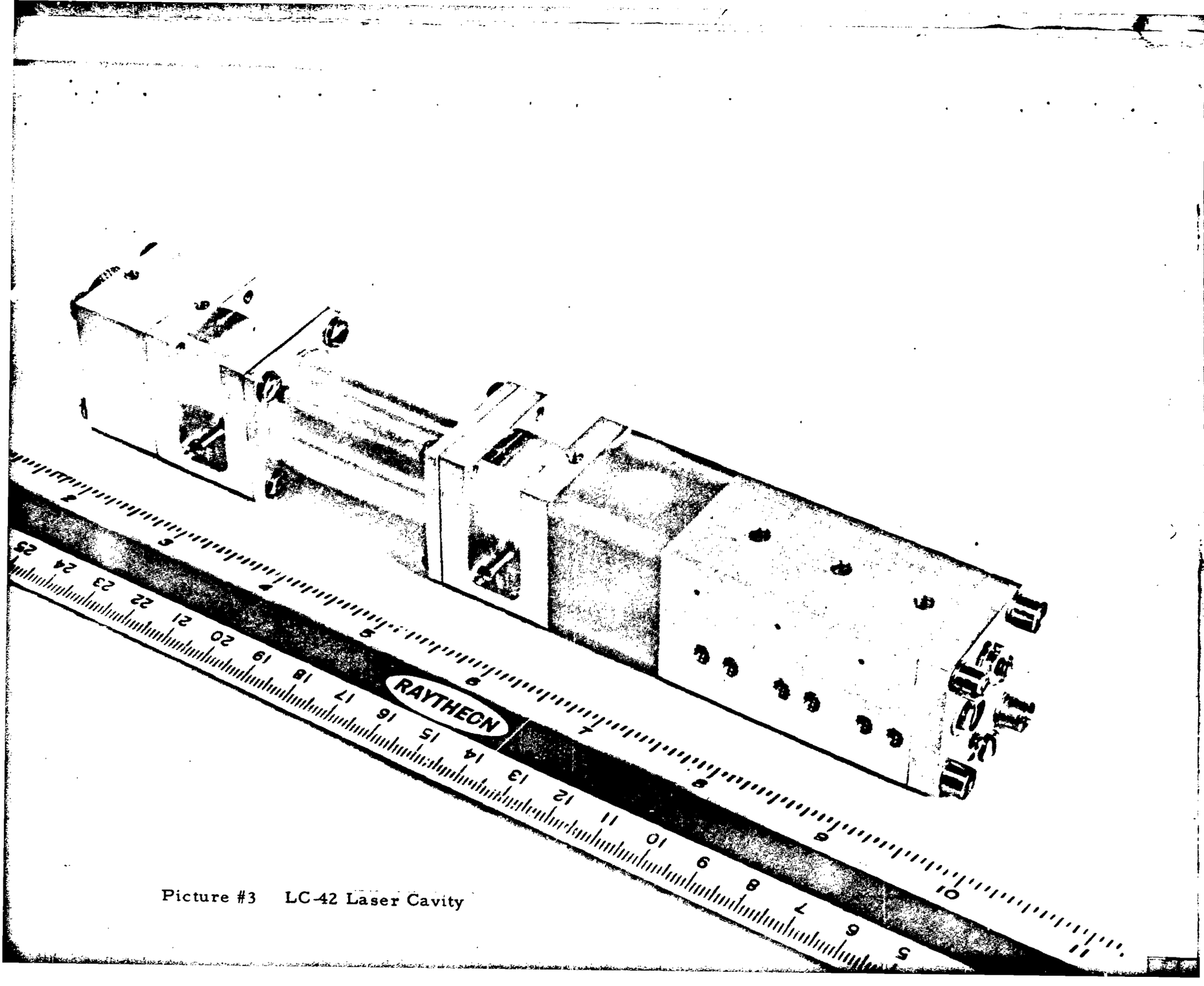

Picture #3 LC-42 Laser Cavity

The radiation test of the laser crystal was conducted on an Nd^{+3} YAG sample of dimension as follows:

Diameter:	5 millimeters $\pm$ .05
Length:	52 millimeters $\pm$ .1
Dopant Level:	approximately 1.1%
Side:	fine ground
Faces:	Flat to 1/10 λ parallel to 1 sec. antireflection coated at 1.06 microns on both faces.

Before irradiation, a TWYMAN-GREENE photograph was taken of the crystal. The picture indicated a poor quality crystal of about 2 fringes per inch and a strong color center at one place. We selected a poor quality crystal to reduce the financial risk involved in the case of total destruction during the irradiation testing.

The crystal was placed into the LC-42 pumping cavity and a selected pilot Xenon flashlamp (XFX-125-C-175) was installed into the same. The pumping cavity was placed into a 12-inch long resonator, containing a HR (99.5% reflectivity) and an MR (45% reflectivity) pair of mirrors coated for 1.06 microns. The flashlamp was pumped from a single stage C-L network, where the C was set at 50 microfarads and the L was represented by the saturated inductance of the series injection trigger transformer. The lamp impedance was extrapolated at 1.5 ohms.

The discharged network produced a 120 microsecond current pulse in the lamp. Measurements were taken of the input output characteristics of the laser, from zero to 25 joules input. Picture #4 indicates the input-output characteristics of the laser (solid line) before and (broken line) after irradiation.

After several attempts to optimize the alignment, the results indicated that optimum alignment was achieved and the recorded E. in E. out curve is the best obtainable.

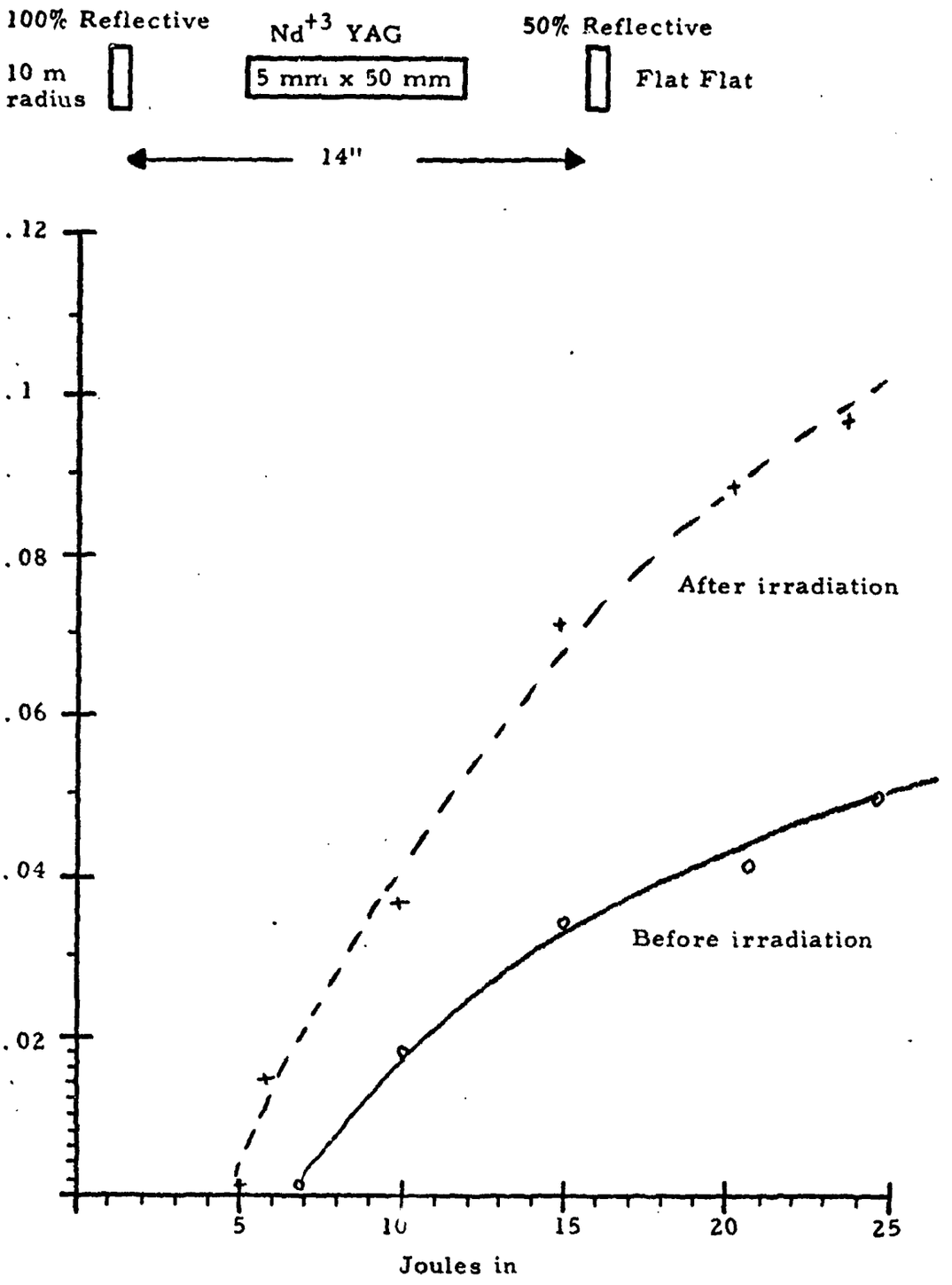

The Effect of Irradiation on the Output of Nd^{+3}YAG Crystal

Picture #4

After this test, the entire pumping cavity was shipped to NRL Laboratory in Washington, where Dr. S. Melman exposed the same to radiation at 5500 rad. level.

After the irradiation, the unit was shipped back to our laboratory at LADC, and the tests were repeated. The cavity was placed into the same resonator as the first time, and the output of the laser was maximized by repeated realignments.

As indicated on the picture (#4), in comparison with the nonradiated measurements, the output of the radiated crystal was considerably improved.

To verify the possibility of further improvement of the laser crystal, the cavity was sent back to NRL and was re-exposed to additional radiation. After the return of the cavity to LADC, we have repeated again the same measurements, but no further improvement of the laser crystal was noticed, and therefore no further radiation tests were made We have concluded, that no detrimental effect is induced into the laser crystal by simulated radiation of the levels expected at 666 nautical miles. (See Picture #5)

The radiation tests were conducted on the plastic "Q" switch cell and they indicated that the plastic cell bleached out at relatively low radiation levels. The liquid dye cell was subjected to radiation levels of 100-200-500-1000-2000 and 5500 rad. levels. All the tests were conducted on the same pilot solution that was normalized to 20 millijoules switching level at 5 millimeter aperture. All samples were tested and all produced the same output. We concluded that the plastic cell will not be suitable for the space laser and the liquid "Q" switch dye cell, will survive the radiation, but due to the fact that the cell contains a dye, whose long term characteristics are as yet unknown, we examined the third alternative; the opto-mechanical "Q" switch.

The main problem areas on this type of "Q" switch are in the bearing lubricant diffusion, the generation of debris in the collector-brush area and mainly, the short life expectancy of the driving motor (5000 hours). None of these characteristics is desirable for a satellite born laser.

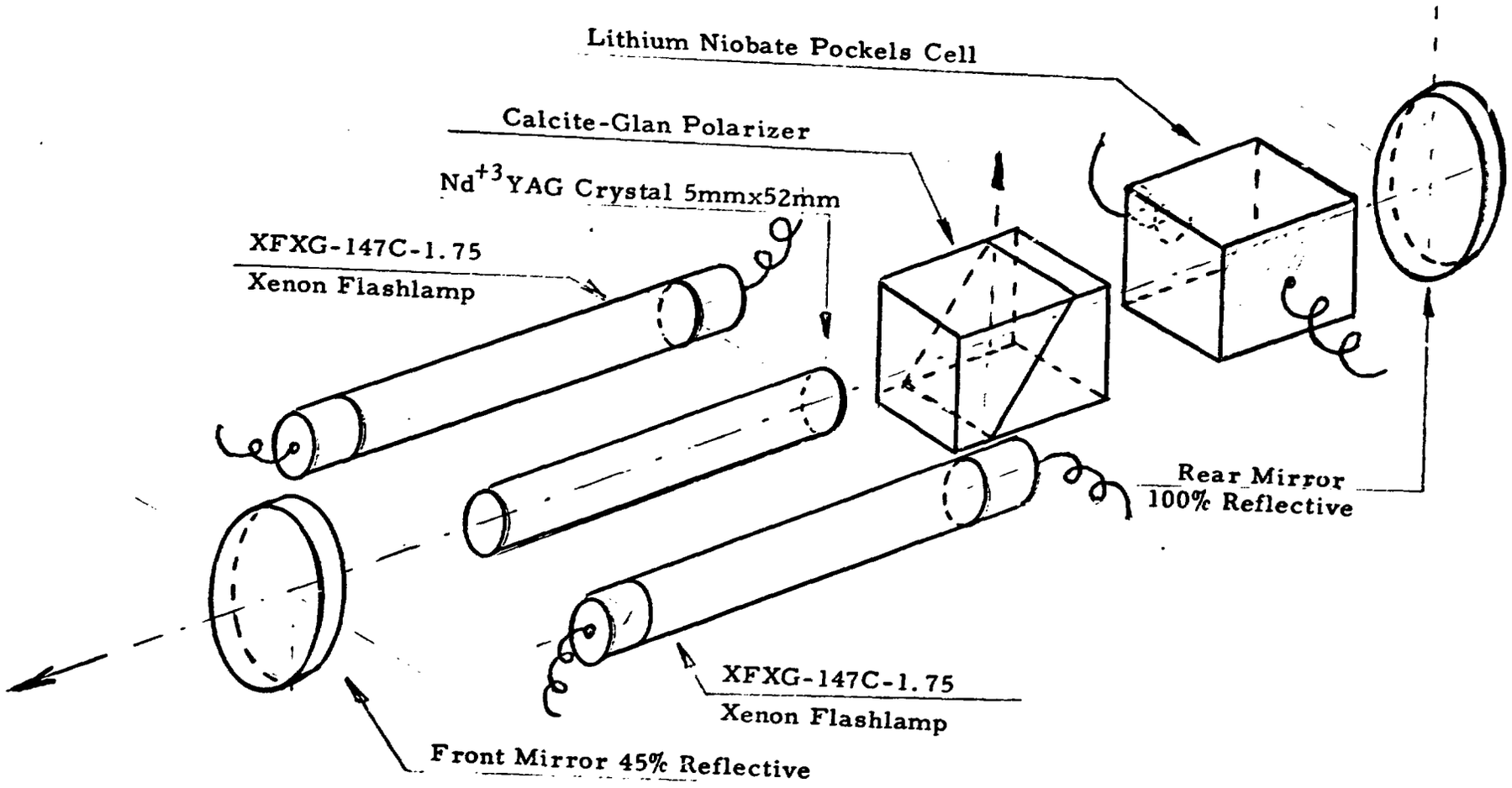

Picture 5

SS-223 Space Hardened Laser - Optical Diagram

2.0 THE SPACE HARDENING OF THE LASER INTERFEROMETER

2.1 Stability

In Laser interferometers, stability is of primary importance. Stability of an interferometer is determined by a wide variety of conditions, that lead to reliable and repeatable operation. A practical interferometer or resonator is exposed to a considerable amount of variations of ambient temperature, mechanical, acoustical and thermal shock, generated by the resonator and the surrounding environment. The influence of these environmental conditions can cause changes in the structure of the resonator and the optical elements attached to the structure. In an ideal optical system, all the changes induced by external perturbations should be minimal, or preferably none. The space hardening of the laser should start with the examination of the stability requirements.

2.2 General Interferometer Stability

A basic interferometer is determined by two optically reflecting surfaces, held in such a relative position, that a wave of electromagnetic radiation can freely travel between the reflecting surfaces in an oscillatory mode. These surfaces can be either plano parallel or can possess curvatures.

As long as the reflecting surfaces do not change relative positions (alignment), the wave front will oscillate until the absorption losses and radiation, consume all the energy represented by the wave disturbance. If the alignment is disturbed, the wave front will not be reflected back into the resonator and therefore oscillations cannot be sustained. If a Laser Crystal is placed between the two aligned reflecting surfaces, the interferometer becomes a Laser interferometer, also called a Laser resonator.

The stability requirements no longer apply only to the reflecting surfaces of the resonator (mirrors) but also to the Laser Crystal and any further optical elements (polarizer, Pockels Cell, etc.) placed between the reflecting surfaces, since the presence or change in position or orientation of the optical elements will alter the alignment of the resonator.

The general stability of the resonator can be perturbed momentarily or permanently. Temporary perturbance is caused by a shock, not exceeding the modulus of elasticity of the materials involved. If the modulus of elasticity is exceeded or the connections between the elements are interrupted, permanent failure and misalignment of the resonator will result.

In practical Laser resonators, a negligible amount of short term perturbance is always present in the form of vibrations and shocks. Pulsed laser resonators are more susceptible to the short term perturbances. Continuous Wave Laser Resonators are more prone to long term variations.

2.3 Internally Generated Perturbances

The internally generated shocks and vibrations in a Pulsed Laser Resonator originate in the pumping cavity. The pumping cavity can have a variety of well-defined enclosures such as a circular cylinder, elliptical cylinder, an ellipsoidal, an integrating sphere or a close-coupled flattened cylinder. The enclosure contains the Lasing Crystal and the flashlamp or lamps. The construction of the pumping cavity requires a good seal and solid mount between the cylindrical center and the end plates. The flashlamp carries up to a thousand amperes current in the contained plasma. The sudden current pulse of such high magnitude produces an acoustical shock wave that reverberates the entire resonator introducing vibrations into the structure, holding the aligned mirrors and all the optical elements contained in the resonator. The second main shock source is the instantaneous thermal expansion of the air (or nitrogen) inside the pumping cavity. The third main source of the vibrations is the induction of Focault Currents into the pumping cavity walls. The plasma inside the pumping cavity acts as a single turn conductor and the cavity walls act as a shorted turn. The current induced into the walls of the pumping cavity, acts upon the magnetic field generated by the plasma of the flashlamp, and causes the cavity walls to move across the magnetic field.

The pumping cavity excited phonons couple into the optical supports and reverberate the resonator. The phonon and photon coupled energy also causes the Lasing Crystal to reverberate. The crystal will flex and create an instantaneous mechanical deformation of the crystal matrix structure.

The effect of vibrations and shocks is the modulation of the path length (gain path) and the angular displacement of the beam, (see picture number 6).

2.4 Gain Path Modulation and Beam Angle Deflection

The internally induced mechanical perturbations are not necessarily the primary cause of failure, since the energy represented by the perturbations is never high enough to cause permanent structural changes. The thermally induced perturbations are more significant, and can degrade the laser performance on short and long term. But with a careful design, the permanent nature of damage can be easily avoided.

The primary effect of the gain path modulation and beam perturbation can be easily simulated in practically any cavity. This simulation is an excellent test to verify the mechanical and optical stability of a cavity.

The setup requires a cavity under test, power supply, a fast detector (integrating) and a fast scope.

The input energy to the flashlamp is to be set at threshold. The integrated output displayed on the scope will reveal spontaneous Q-switching. This multiple, spontaneous Q-switching is caused by the beam path modulation, due to the mechanical and thermal perturbation of the laser crystal and cavity.

The period of relaxation is typical of the volume of the crystal, the coolant and jacket, and the damping factor of the cavity (mechanical rigidity, stability).

Reproduction of photographs of normal lasing, Q-switched pulse and self-Q-switching.

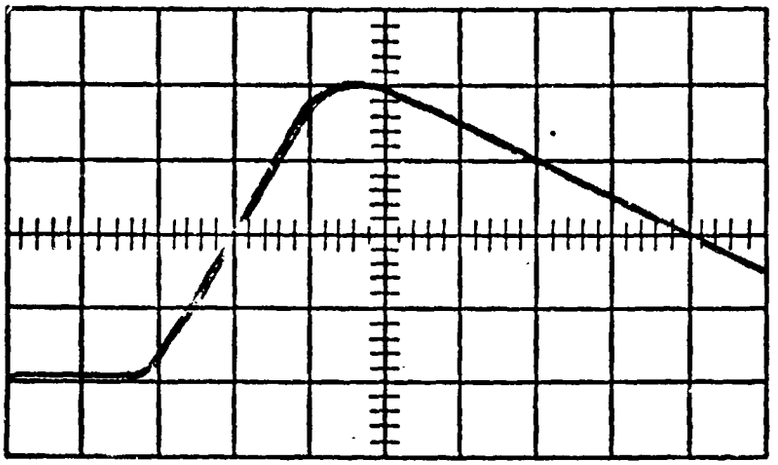

Picture A Vertical 10V/cm
Horizontal 50 microsec/cm

Resonator containing 100% rear mirror, 50% reflective front mirror and Nd^{+3} YAG crystal. Pumped by an FX-33-C-2 lamp.
Input = 10 joules; 150 micro-seconds pulse.
The crystal size is 50 mm x 54 millimeters. Lamp and crystal water cooled at 70°F.

Picture A displays the integrated energy output of the normal multimode pulse. The pulse width is 150 micro-seconds (measured from the base to the peak of the S curve).

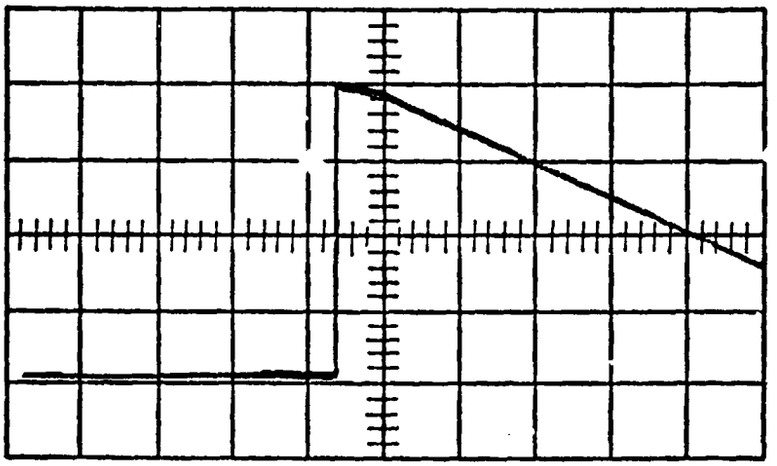

Picture B Vertical 5V/cm
Horizontal 50 microsec./cm

Picture B displays the same pulse Q-switched. The pulse width is 12 nanoseconds.

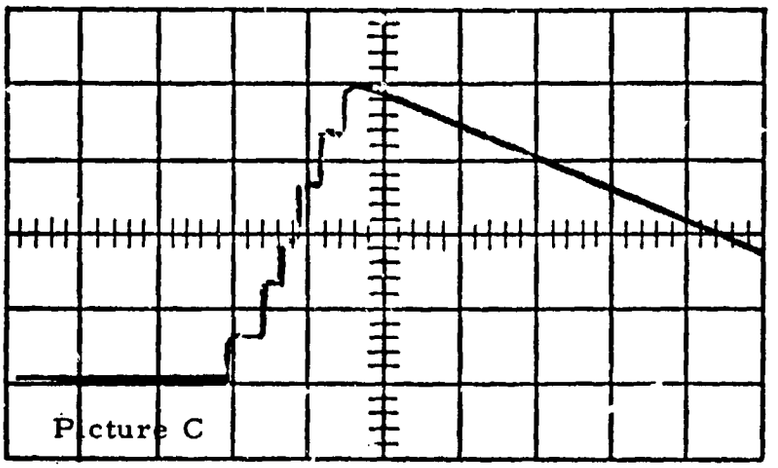

Picture #6 Vertical 0.05V/cm
Horizontal 50 microsec/cm

Picture C displays a self-Q-switched pulse. (the Q-switch and polarizer removed from the resonator) Q-switching occurs due to perturbation of the crystal induced modulation (periodic Q-spoiling).

The beam angle modulation is mainly due to unbalanced mechanical design of the supporting elements of the resonator, optics holders, bases and covers. One of the primary offenders is the cantilever type optical suspension when used, without proper truss-link stabilization.

2.5 External Perturbations

The external perturbations, causing instability in the resonators are primarily mechanical and thermal in nature.

The origin of the mechanical perturbation can be conducted, caused by solenoids, relays, motors, etc. mounted on the same base as the resonator. The oscillations and vibrations generated by the mechanical devices are conducted by the common mounting plate or the housing of the device to the resonator (laser interferometer).

Unfortunately, in most of the cases it is impossible to shock or vibration mount the Laser Interferometer, because the bore-sighting of the laser cannot suffer variations, that the highly compliant shock-mounts would offer.

The external thermal perturbations can be radiative or conductive. The radiative are primarily high temperature heat-sinks, or thermo-ionic components. The conductive thermal input is usually transmitted through the common base plate or adjacent cover via contacting surfaces.

Perturbances transmitted through the air can cause severe modulation of the laser beam within the resonator. Such vibrations are usually generated by jet motors, rocket engines, and contain a great deal of acoustical energy. Often the frequency content of the acoustical vibrations falls within the resonance of one or several optical elements. In such case, a great deal of instability can be expected. To prevent most of these inconveniences, a properly damped mechanical structure is recommended.

Long term instability can be induced into the resonator, if the base plate of the resonator is rigidly bolted to a structural member of the higher system assembly. Mechanically or thermally introduced stresses will deform the mounting surface, and the resonator base plate will follow the distortion. This will displace or deflect a cantilevered or stress sensitive optical mount, and it will induce instability into the laser interferometer.

In the space-hardened laser transmitter, we can expect that almost all the internal and external perturbations will be present during one or the other phase of the life cycle of the satellite.

Before we proceed with the final design of the stabilized and space hardened resonator, most of the non-variable components should be examined and selected. The first consideration of the selection must be given to the small size, light wieght and high efficiency.

The first element to be examined is the heart of the laser resonator, the Nd^{+3} YAG crystal. In our applications it is desirable to have a covert monochromatic source with a reasonable short wave length to match the sensitivity of a proper detector with high Quantrum efficiency and preferably at room temperature operation. The high gain of the neodymium (Trivalent) doped Yttrium Aluminum Garnet with a typical emission in the 1.06 micron band, seems to be a preferential choice. The size of such a crystal in an actual pumping cavity is determined by the required output energy. Such crystals vary from 2 millimeters to 20 millimeters diameter and 10 millimeter to 150 millimeters in length.

The ratio of the length to diameter is determined by the choice of the specific type of pumping geometry. The preferential ratio is 1:10 in diameter to length. A compromise in the extension of the length of the crystal usually limits the energy storage capacity of the crystal and therefore the penalty , especially in "Q" switched operation is a lower output limit.

From the state of the art of the laser technology we know that a certain volume of active crystal is required to store and convert a certain amount of energy. This volume will depend also on the level of dopant concentration in the YAG host material.

2.6 The Effect of Neodymium Concentration on the Performance of the Resonator

In a typical host crystal, such as Yttrium Aluminum Garnet for short YAG, the amount of impurity induced into the crystal lattice can vary from zero (undoped YAG) to a saturation level, where further increase of the doping, limits the useful speed of crystal growing. At this level the crystal becomes over strained and the growing process slows down to unacceptable yield levels.

In a Czochralski growing process (melt-pull) the highest practical level of doping is about 2.5% by weight. In the flux grown method, the dopant level may be as high as 5%. We have examined a large number of Nd^{+++} YAG crystals of different Nd concentration and various samples were tested in active lasers for the best ratio of doping versus output efficiency.

Since we are concerned mainly with the pulsed and Q-switched operation of the Nd^{+++} YAG crystal, in our idealized transmitter the most important factors to be examined are the ones, that contribute to the mode stability, lowest thermally induced birefringence and most efficient pumping of such crystal. The doping concentration of a crystal cannot be expressed by a simple percentage number because the Nd atoms are not distributed evenly through the crystal. The crystal growing process does not favor such distribution. Examination of many crystal samples revealed that concentration distribution can vary axially as much 0%. The dopant distribution non-uniformity will not be as drastic in the radial direction, but we should remember that a finished crystal is cut from a pie shaped section of a crystal boule and therefore the Nd concentration gradient will not show radial symmetry about the mechanical axis of the crystal. This may be a point to observe in YAG laser design, especially in the case of a single lamp pumped elliptical cavity. The orientation of the dopant concentration

gradient across the laser-rod becomes more important with increasingly higher differntial of concentration of the doping. The laser crystal side, facing the pump lamp will absorbe the highest level of the pumping energy, therefore the orientation of the YAG crystal may influence the uniformity of the output beam and the formation of the modes in the laser crystal. Our laboratory studies indicate that a perfectly doped crystal will show no difference in the mode pattern of the output beam, when rotated about its mechanical axis in the pumping cavity. A crystal with great radial doping differential will show mode pattern change and also mode switching instability at different excitation levels, if the orientation of the doping gradient is changed. The best output of such crystal was obtained when the lower doping concentration side of the crystal faced the pumping lamp in the cavity.

This effect will vary largely with the geometry of the cavity and the degree of imaging of the plasma into the crystal. In highly focusing cavity, the orientation becomes more important. In highly diffusive cavity the importance of crystal orientation becomes negligible. Several methods of minimizing the influence of the crystal orientation were studied and the favorable results will be described under another section.

Assuming an acceptable uniformity in the doping distribution, the doping level in a crystal will be one of the primary determinants of the pumping efficiency, because of the fluorescent lifetime of the Nd^{+++} in the YAG. Lower concentration levels tend to increase the fluorescence and higher concentration levels tend to decrease the fluorescent life-time. Typically 0.1% to 0.7% dopant concentration by weight, will yield 230 microseconds while 1.5% to 2% will yield fluorescent lifetime of 100 to 150 microseconds.

For Q-switched operation, a shorter fluorescence with higher efficiency would produce higher Q-switched output and shorter pulse, unfortunately at high concentration of dopant, the optical quality of the crystal becomes inferior due to the high number of inclusions, stresses and zones in the crystal lattice. Such poor optical characteristics actually degrade the laser output more, than the increased dopant concentration contributes to the gain of the resonator.

The longitudinal gradient of dopant concentratio is less significant in the performance of the Nd^{+++} YAG laser since this gain vector is parallel with the axis of the resonator.

In practical applications, the recommended level of dopant is between .7% and 1.5%. At these levels the crystal does not suffer from an excess of optical imperfections, stresses and growth rate problems and yields sufficiently high levels of Q-switched energy.

2.7 Radiated Spectrum Matching

The radiated pump spectrum is a function of the lamp geometry, the gas fill and pressure. To obtain the best excitation of the crystal, we studied the best combinations of the spectrum matching.

Combinations of 2mm; 3mm; 4 and 5 mm plasma diameter test lamps at energy levels between 2 and 25 joules input to the lamp were used, pumping a selection of different Nd^{+3} YAG crystals. The tests revealed the influence of the plasma characteristics on the output of the laser. Both Xenon and Krypton filled lamps were used during these tests. The lamps were filled to pressures of one to four atmospheres. The envelopes of the lamps were selectively chosen from quartz supersill, germisil and pyrex.

The pumping bands of Nd^{+3} YAG laser crystals are well known in the stateof the art and therefore we will concentrate only on the interaction of the plasma radiation upon these bands. (See Pictures 7 & 8).

It has been documented, that at plasma levels of 6 to 8 joules of input to the lamp with 3 mm bore, the plasma does not fill the available lamp volume. Therefore it is very important to get a proper plasma initiation, by proper triggering. For the convenience and expedience, the test cavity did not contain end plates and the predominant rays coupling the energy from the plasma into the crystal were the primary reflections and a few skew rays.

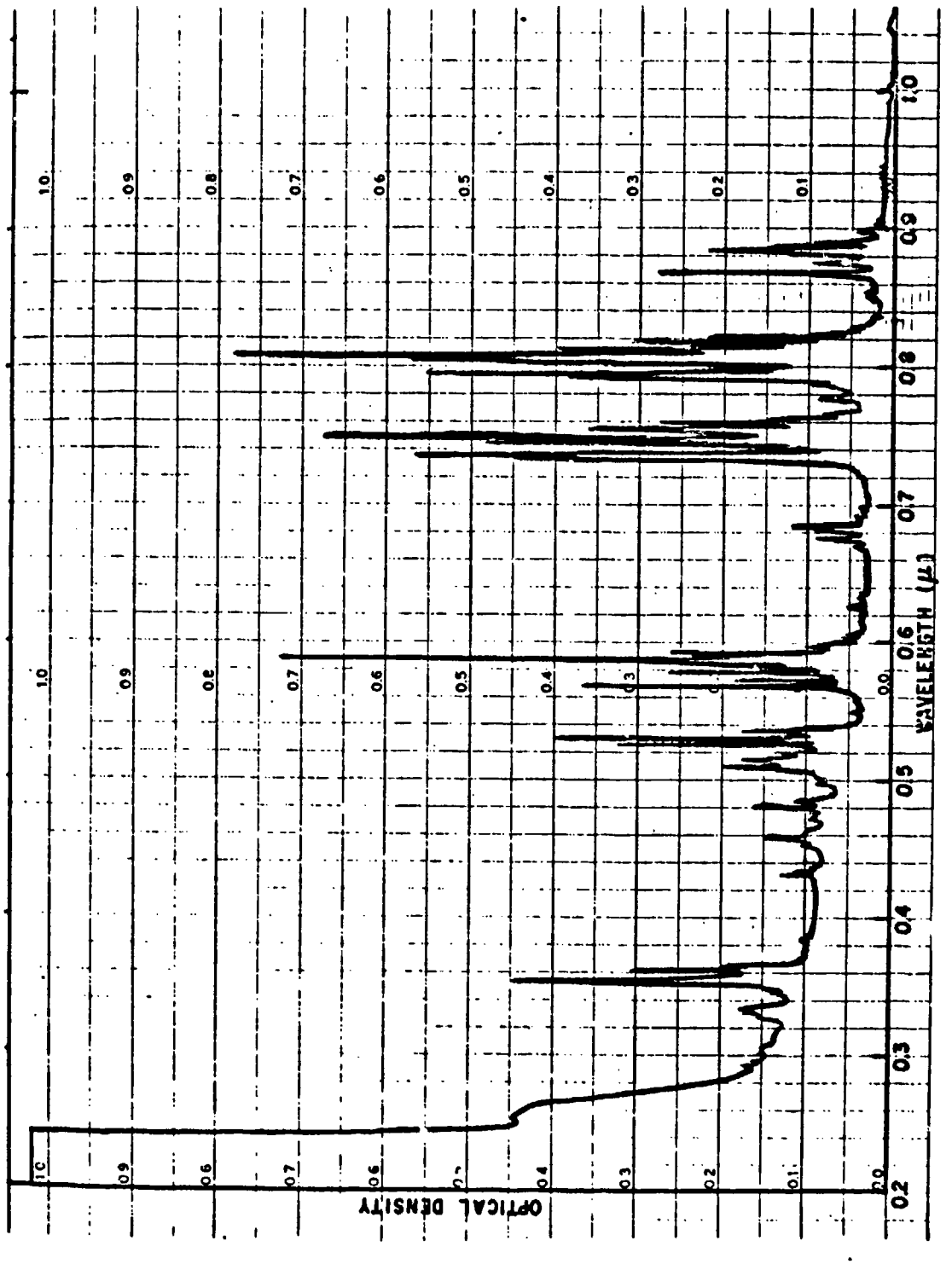

Room temperature absorption spectrum of $Nd^{3+}:Y_3Al_5O_{12}$ from 0.2 to 1.0 μ.

Picture #7

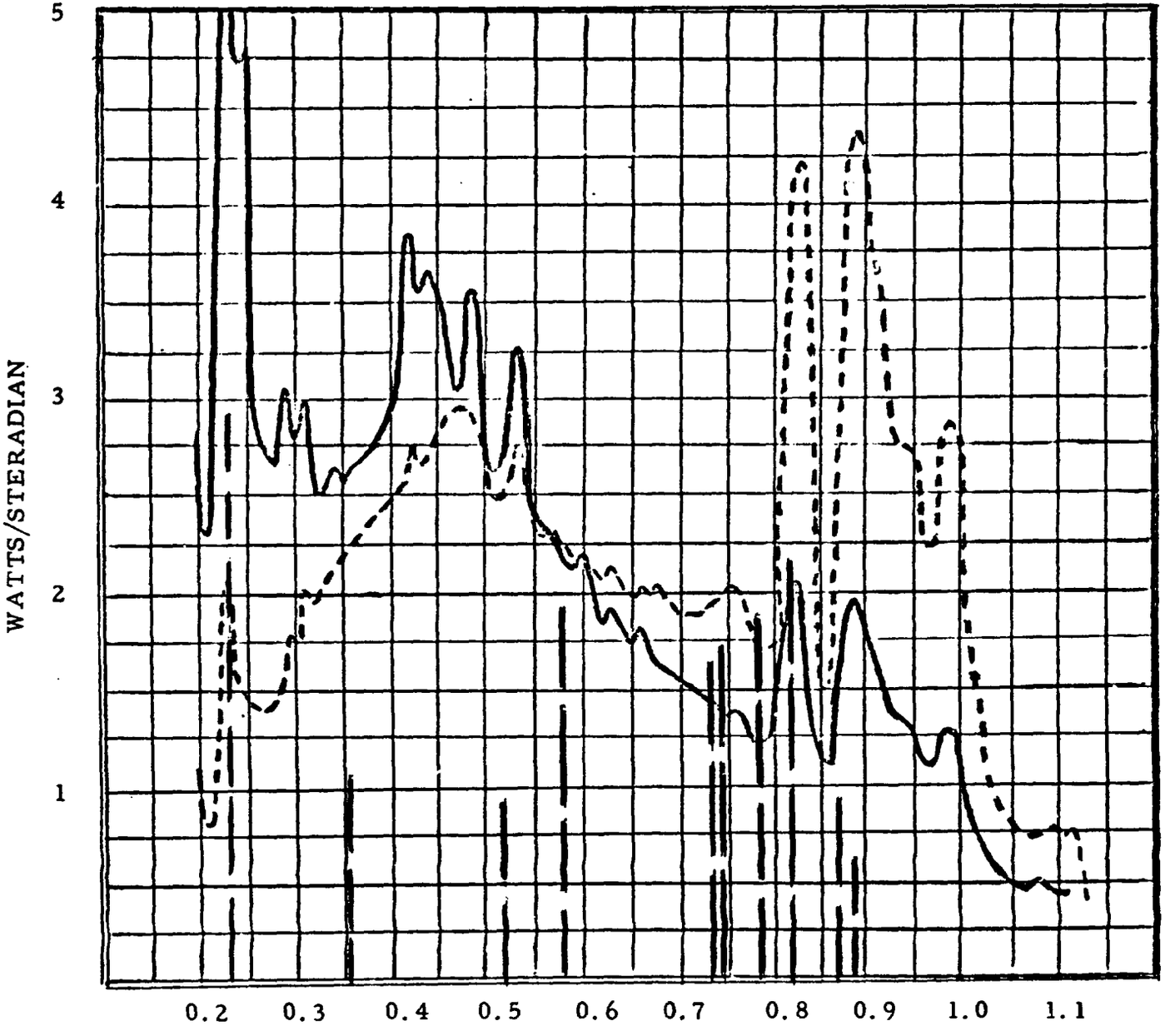

Plasma:

Dia.: 4 mm
Length: 76 mm

Input Energy:

50 joules for both traces

Storage Capacitor:

Solid line: 51.4 MF
Charged to: 1400 VDC
Dotted line: 204.6 MF
Charged to: 700 VDC

Note: The vertical broken bars indicate the location of the major absorption bands in Nd^{+3} YAG. The relative height indicates the relative absorption.

Picture #8 Spectral emission distribution shift due to plasma excitation current in xenon filled flash tube.

The tests revealed the influence of the plasma size, gas fill and excitation currents, upon the pumping efficiency. It was confirmed that the plasma temperature (a function of the pulse current density amp/cm^2) plays a key role in the pump band matching and the efficiency of the laser optical pumping. Lower plasma current density shifts more energy into .75 and .8 micron bands (see Picture #8).

2.8 The Role of Reflectivity

The optical pump energy, generated in the plasma, must reach the crystal to produce the necessary excitation and population inversion. Since a compact laser invariably uses linear flashlamps, the plasma generated energy must be reflected from the walls of the pumping cavity in such a way as to transverse the crystal and produce excitation. The choice of this reflective surface will directly influence efficiency.

The reflectivity of various materials is well known. (see picture no. 9)

The choice of a diffusive or imaging cavity is governed by the design of the pump cavity and the crystal surface finish.

An imaging cavity utilizes a metal film of reflective material. Such metals are silver, gold, aluminum, etc. In a diffusive cavity such substances as Aluminum Oxides, Magnesium Oxides, Titanium Oxides, etc. are used. These oxides are spray deposited and baked at elevated temperatures, to bond to the metal pump cavity surfaces. Some pumping cavities are made of alumina, mullite and other ceramics. The metallized surfaces are polished to a high degree of surface uniformity and reflectivity. The mirror surface of these walls must be protected against atmospheric corrosion. The metallization process is a very exacting science and requires extreme care. (The Raytheon proprietary process control specification for plating contains over twenty-six steps.)

The mirror surface contains several layers of different metals, each individually finished and controlled to a fraction of a thousandth of an inch.

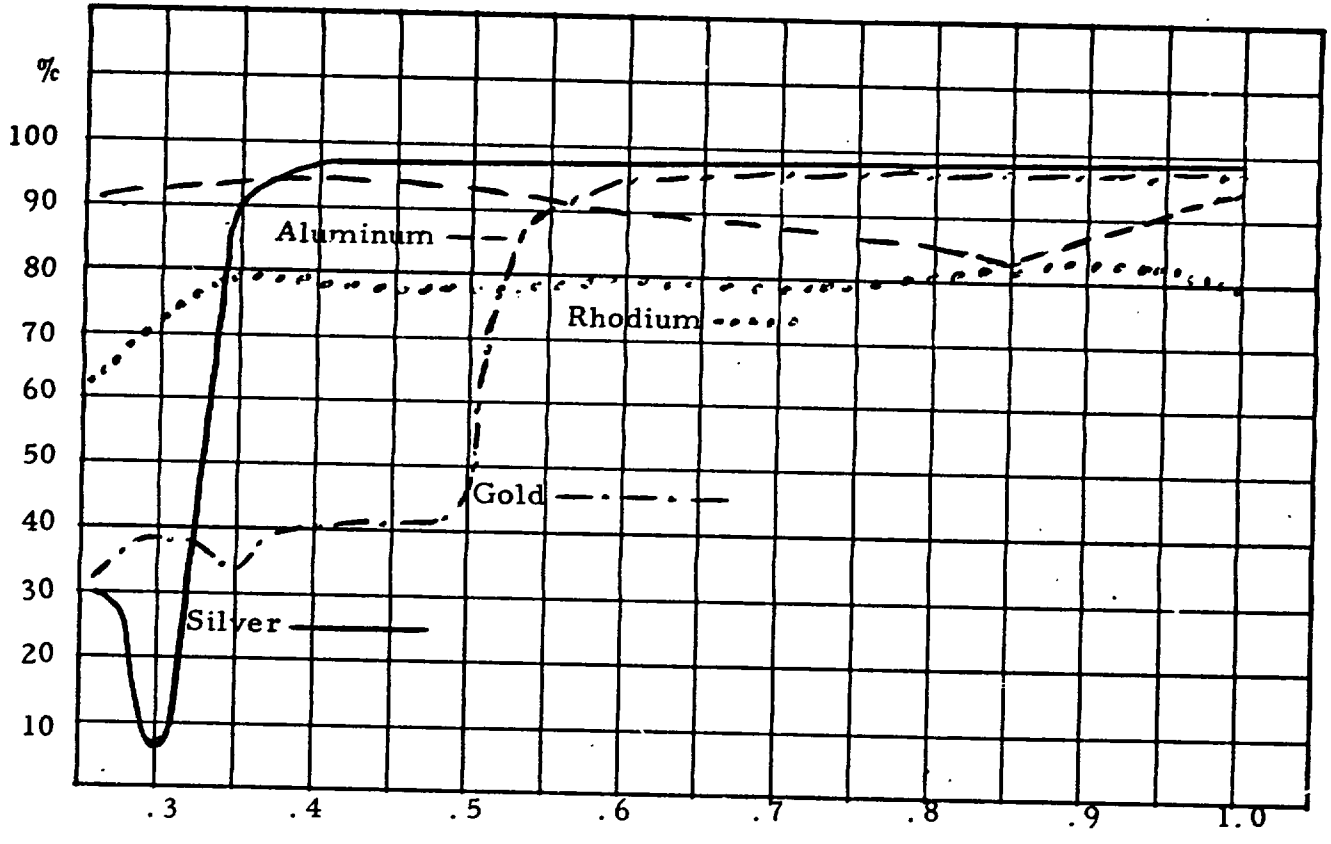

Spectral Reflectance of Optically Polished Metal Surfaces

Picture #9

An improperly applied finish on any of the interface surfaces, can trap impurities, which during the acoustical excitation, and the accompanying ultraviolet radiation and thermal shock produced by the flash tube will absorb radiated energy and explode under the thin layer of the finished surface. The exploding impurities rupture the surface layer and pop out forming little craters and deposit debris over the inside optical surfaces. The miriads of small craters with the exploded impurity around them, form a non-reflecting (and highly absorbing) layer on the inner reflecting surfaces. This effect was observed in connection with silver, gold, aluminum and all the diffusive coatings used today since all are deposited in multiple layers (exceptions are the total ceramic envelopes).

The only way to avoid this catastrophic degradation is to observe rigid standard of quality control. Contact with the surfaces in manufacture must be avoided. The entire process must be performed under clean room conditions.

The optimum reflectivity obtainable in compact lasers follows pretty much the theoretical work. The diagram (Picture #10) indicates the relative efficiency of the same cavity, lamp and crystal tested, with various reflective surfaces. The reflectivity is highest for silver, followed by aluminum, gold and finally magnesium oxide.

Current density of about 500-700 amperes in a 3 mm bore and one to two atmospheres pressure of xenon, will shift the major part of the pumping energy into the lines located near red. Higher currents, 1000 amperes and over, will shift the pumping energy into the blue end. The shift in the blue causes a less efficient matching of the pump bands. (See Picture #5)

2.9 Pumping Geometry and Coupling

The size of the crystal and the related flashlamp determine the basic size of the pumping cavity. The theoretical size of the crystal required to deliver the approximate 50 millijoules is about the volume of a 5 millimeter diameter, 54 millimeter long crystal. Several conditions demand such volume. First, the laser must be Q-switched in order to obtain the 15 ns long pulses. Performance of the Nd^{+3} YAG laser in the

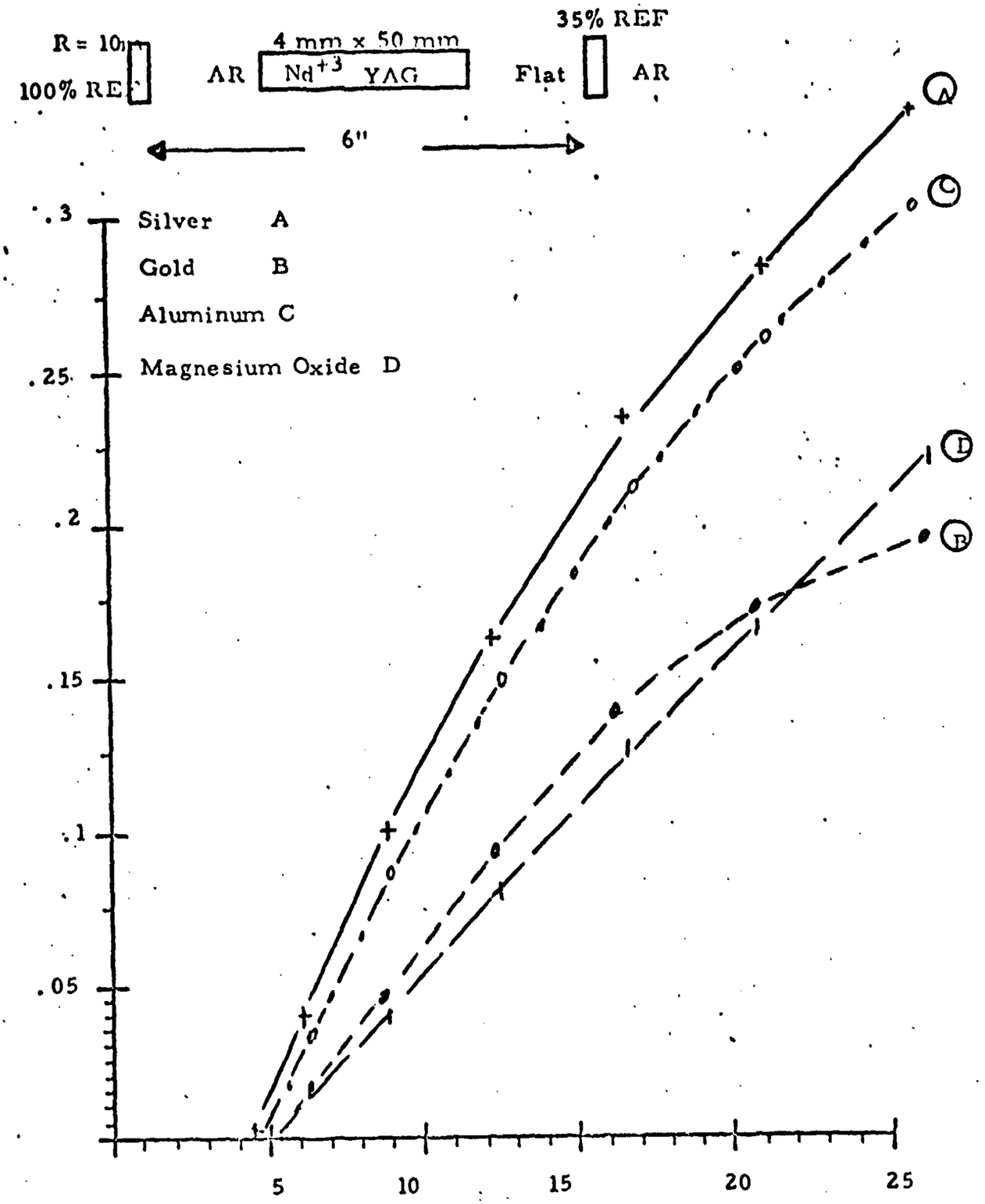

Energy Transfer Graph
reflectivity vs. Efficiency

PICTURE #10

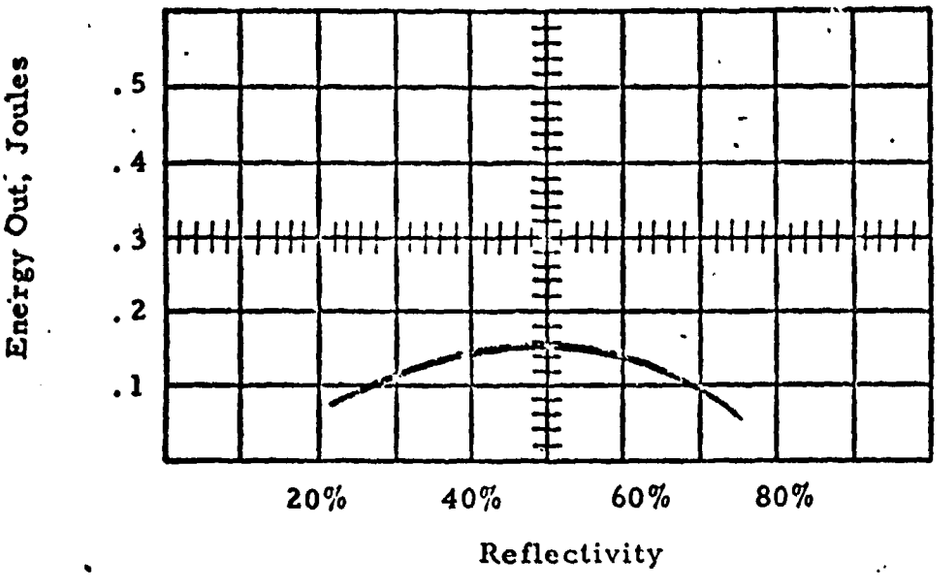

Output coupling reflection versus output of laser at constant input of 9 Joules

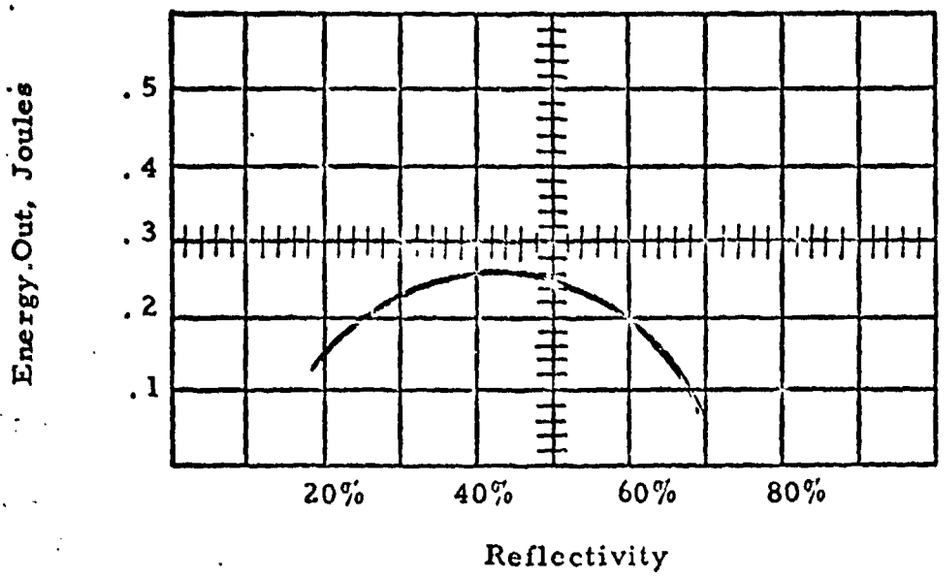

16 Joules

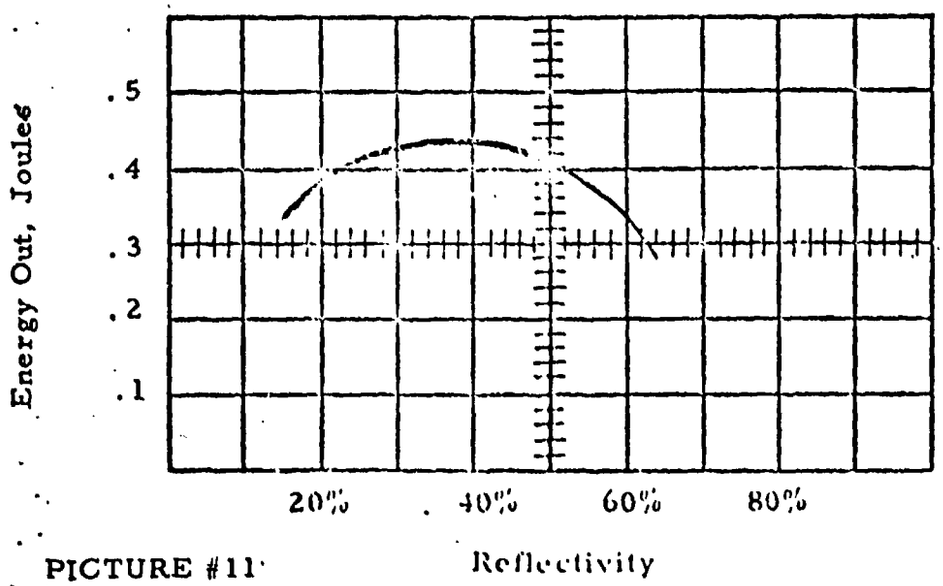

25 Joules

All curves taken at 100 u laser output pulse

PICTURE #11

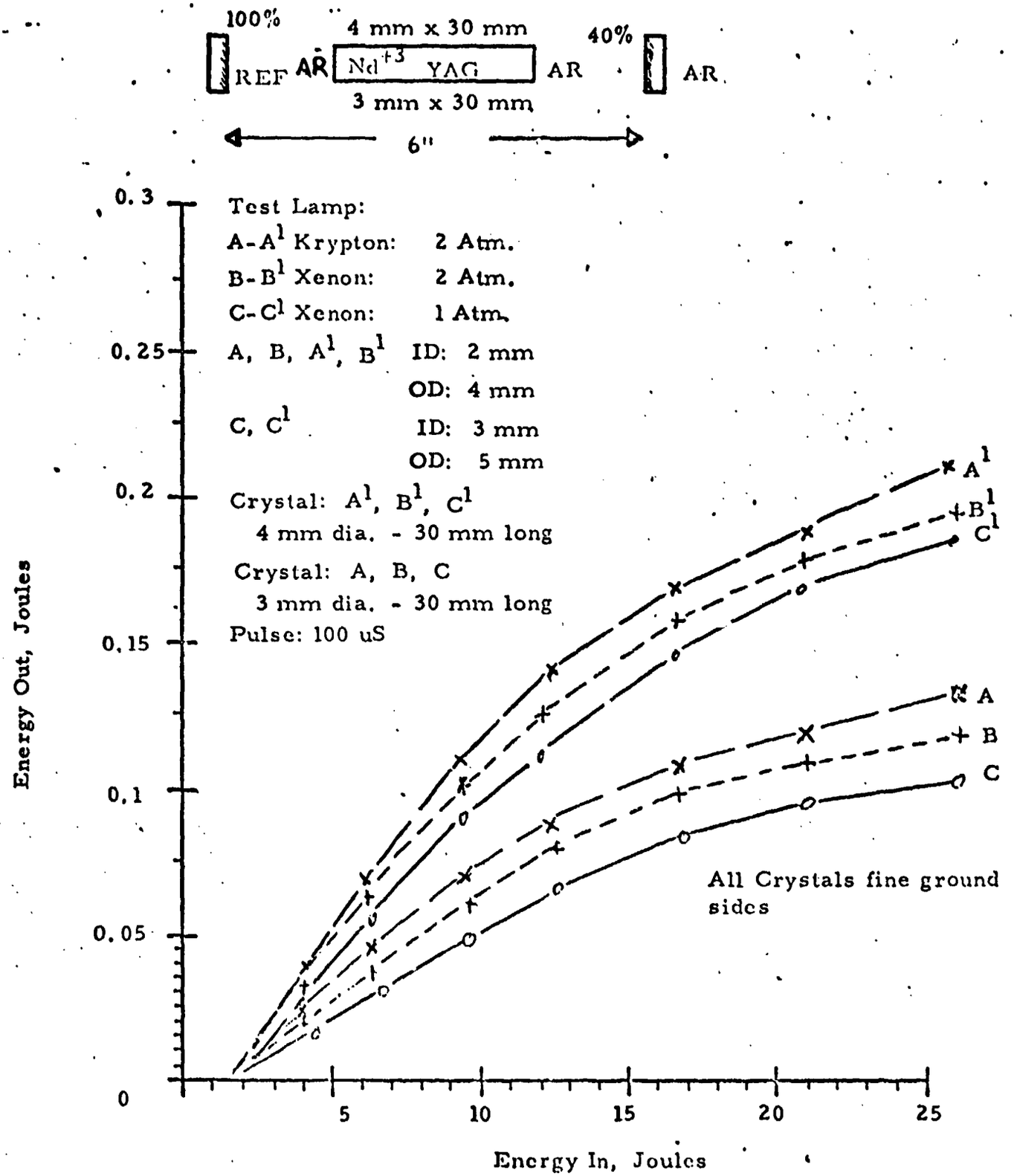

Energy Transfer Graph
2 and 3 mm: Krypton and Xenon
Plasma pumping 3 and 4 mm dia. crystal

PICTURE # 12

Q-switched mode is severely limited by super radiance and self-pumping saturation. This saturation is volume restricted and follows a well-known relationship between the output coupling reflectivity and the crystal volume. (See Picture #11). Increased front reflectivity yields lower level of saturation, because of the increased effect of super-radiance. Typically, at 35% to 40% output coupling reflectivity, a 1/4" by 2" crystal saturates at 180-200 millijoules, a 5 mm by 50 mm crystal at about 90-110 millijoules a 4 mm by 50 mm at about 50-70 millijoules and a 3 mm by 30 mm crystal at about 30-50 millijoules. Once the length of the crystal and the lamp have been determined, the length of the pumping cavity is fixed; the remaining choice is then the cross sectional geometry of the cavity.

The geometry of the pumping cavity may well be one of the most controversial issues in the laser state of the art. Due to the large variety of geometrical configurations a vast amount of data is available on the performance of different pumping cavities.

To select the most suitable pumping cavity configuration for the space hardened laser transmitter, the work of C. Bowness; T.H. Maiman; M. Ciftan et al; K. Kamiryo et al ; J.L. Walsh et al and K. Hamal was reviewed.

From all the studies, C. Bowness' work is related directly to the requirements of our space hardened cavity. The selected cavity must have as basic characteristics, efficiency compactness, light weight and high mechanical stability. C. Bowness' analysis clearly defines the expected efficiency in terms of the true energy transfer from the plasma into the crystal by the imaging of the true optical cross section of the flashlamp into the lasing crystal, treating the finite sizes and the applied corrections of such sizes in terms of pumping cavity dimensions.

The configuration of an elliptical cylinder was chosen above the other configurations because of the ease of manufacturing and finishing a cylindrical surface and the minimal amount of metal required to produce a cylinder of great rigidity, so important for the stability of the space hardened laser. Another reason for the choice of the elliptical cavity

is the ease of generation of symmetrical duality, to accommodate a second pump lamp. Generally a dual elliptical cavity is recommended, if higher power (or energy) is desired, and a single lamp cannot deliver the brightness desired. In our case the dual lamp approach has a different reason. In the orbit-borne satellite, there is no possibility of maintenance, therefore a cavity and the flashlamp must survive the number of flashes that correspond to the life of the satellite. The two lamps are fired alternately, and therefore they are able to extend by a factor of two, the expected life of the laser transmitter (compared with a single ellipse, single lamp cavity).

In the previous paragraphs we indicated the reasons for a choice of a 5 millimeter diameter crystal.

Therefore, C = 5

Choosing a lamp of 3 millimeters plasma image diameter, the $\frac{c}{d} = 1.66$. From the graph for $\frac{c}{d}$ of 1.66 and a $\frac{b}{a} = 80$ we can see that the expected pumping efficiency will be about 60% for simultaneous firing of two lamps. In our case it will be less, because the lamps are fired alternately and only one lamp will pump optically at a time. This is the penalty for the trade-off of double laser life.

Once the dimensions of the cavity are established and the dual lamp configuration is accepted, the choice between a diffusively pumped or an imaging cavity approach must be made.

If one chooses a true focusing pump system, one must use metal film reflectors as described in the previous paragraph. In such a case the outer surface of the crystal should be fine ground to prevent filamentary lasing. If a diffusive pump system or a focal reflective system is chosen, the crystal surface may be polished. For a truly imaging reflective cavity, the best results may be obtained by elliptical focusing of the plasma into the crystal. The placement of the optical elements in a circular cavity as compared with the efficiency of an elliptical cavity of comparable size and the offset of the elements within the circular cavity were studied. Picture # 14 presents graphs

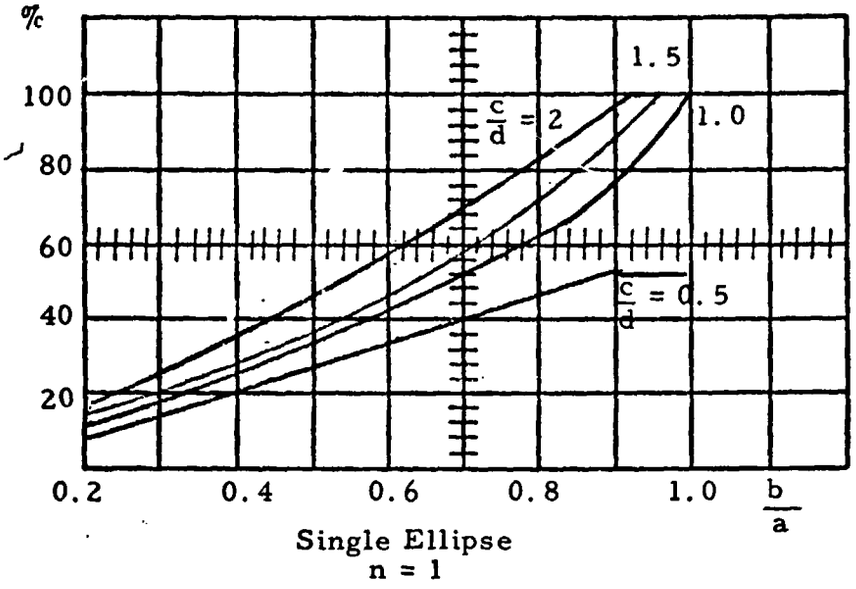

Single Ellipse
n = 1

Efficiency curve for a single ellipse cavity.

a = semimajor axis
b = semiminor axis
c = crystal diameter
d = lamp diameter
e = ellipticity = $\left[1-\left(\frac{b^2}{a^2}\right)\right]^{\frac{1}{2}}$

n = number of elliptical sections

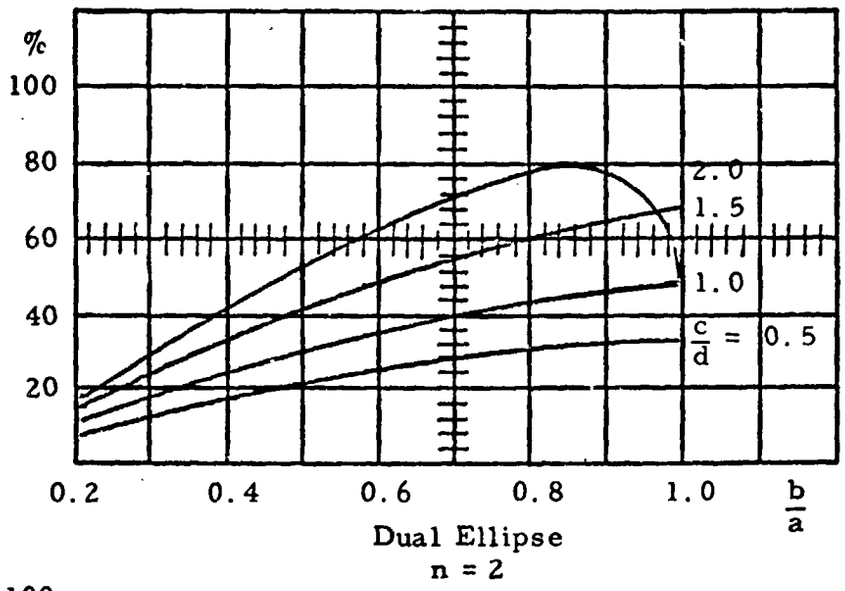

Dual Ellipse
n = 2

Efficiency curve of a dual ellipse with one common focus located at the crystal axis. The other two focii are located at the axis of each lamp.

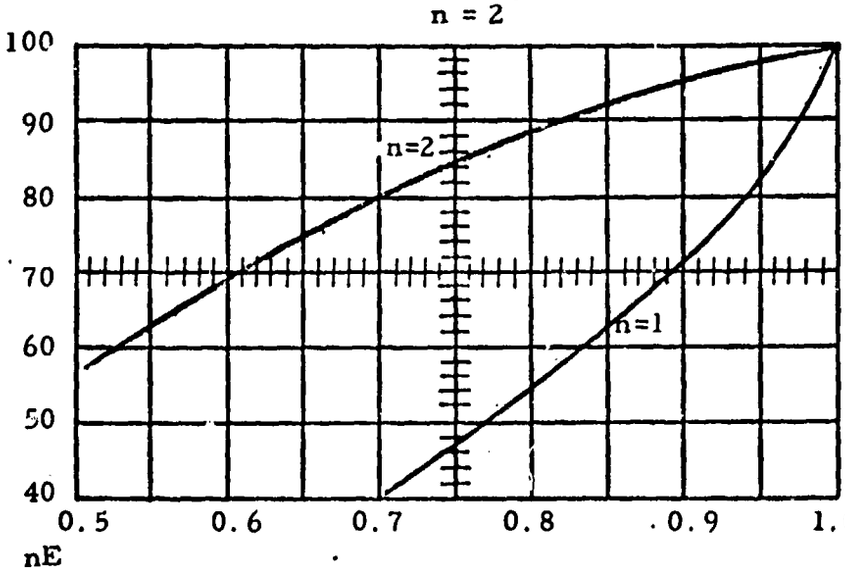

Comparison of single lamp pump brightness with two lamp pump brightness.

(Curves after C. Bowness)

Picture #13

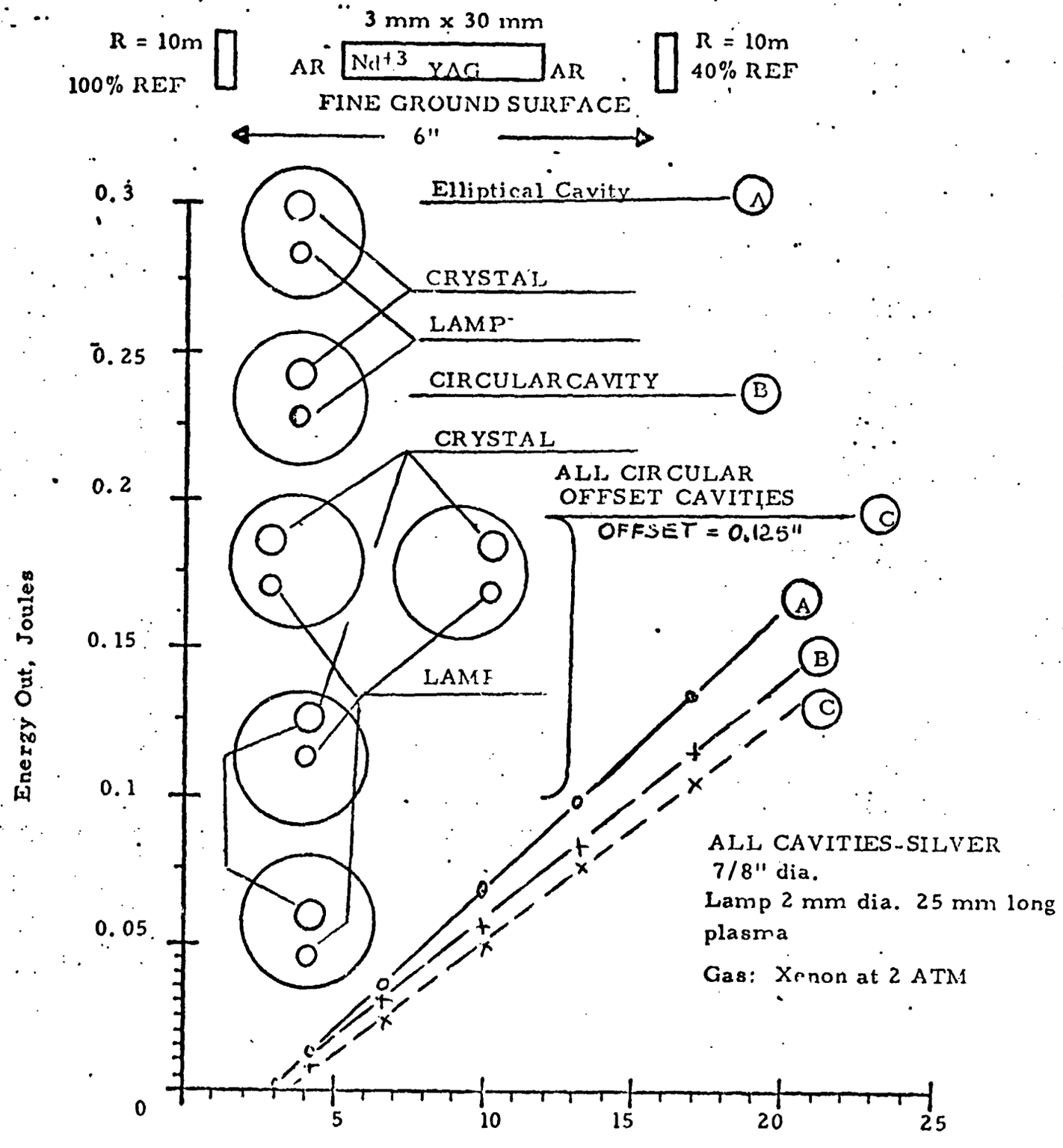

Comparison Graphs - Elliptical versus Cylindrical Cavity - Aligned and Offset

Picture #14

of the behavior of a typical 3 mm by 30 mm crystal, pumped by a 2 mm diameter by 25 mm long plasma in silver coated cylinders of elliptical and circular cross section. First the circular cross section is centered in relation to the crystal and the flashlamp and also in this figure the graphs present the effects of the offset in various directions. The graphs indicate that even at these small dimensions the ratio of the diameters of the lamp and crystal to the major axis in the case of our elliptical cavity or diameter of a circular cavity is still significant enough to produce a substantial difference in efficiency. In the case of the ellipse, the ratio of the major and minor axis is also a significant factor (ellipticity).

The curves indicate that at a fixed minimal separation between the crystal and the plasma, excentricity of these elements in the circular cylinder does not introduce significant changes in the efficiency.

By diminishing the distance between the crystal and flashlamp to the minimum possible and cutting down the size of the envelope to a "close-wrapped" configuration, one expects to obtain comparable performance between elliptical circular or slotted configurations.

2.10 Output Reflectivity

The choice of reflectivity of the output mirror is closely related to two important factors, to the saturation level of the Q-switched laser output and to the gain of the cavity. Well-known gain curves indicate that there is an optimum reflectivity for the specific cavity gain and pulse length conditions.

Let us accept for optimum reflectivity for the idealized cavity a value of 40%.

At higher values of reflectivity, the pulse length dependency on the resonator length becomes small. But at low values, the shorter cavity (5" long) produces a narrow pulse of 10 ns, whereas a longer cavity (12" long) produces a pulse of 20 ns as shown in Picture #15 In the low reflective cavity, mode beating patterns are detected that

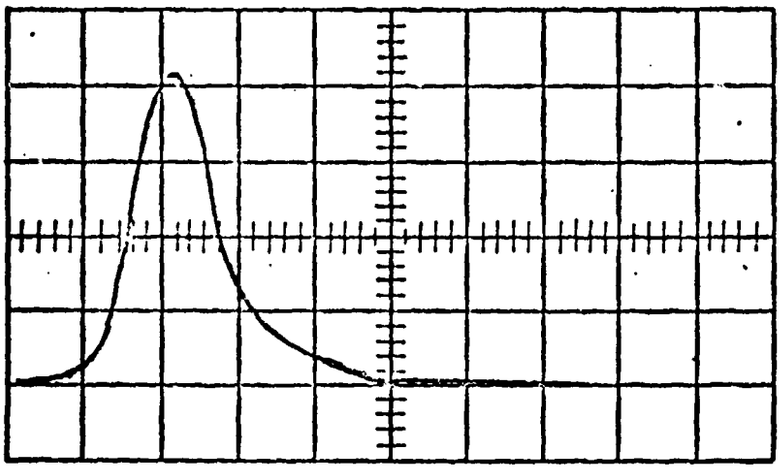

5" long resonator 10 nS/cm

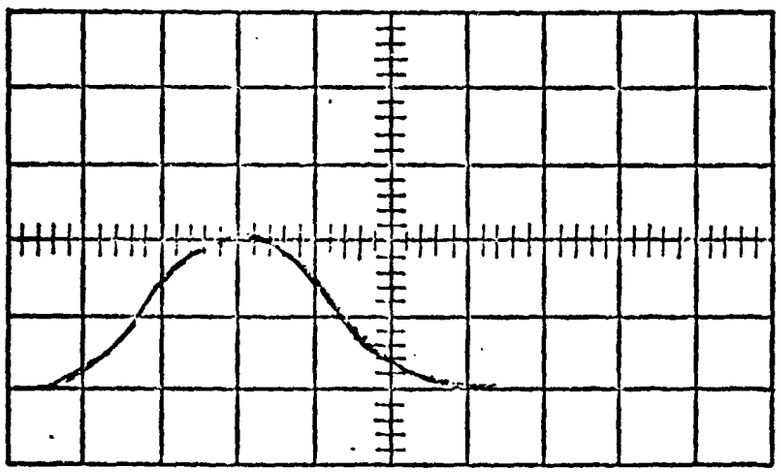

12" long resonator 10 nS/cm

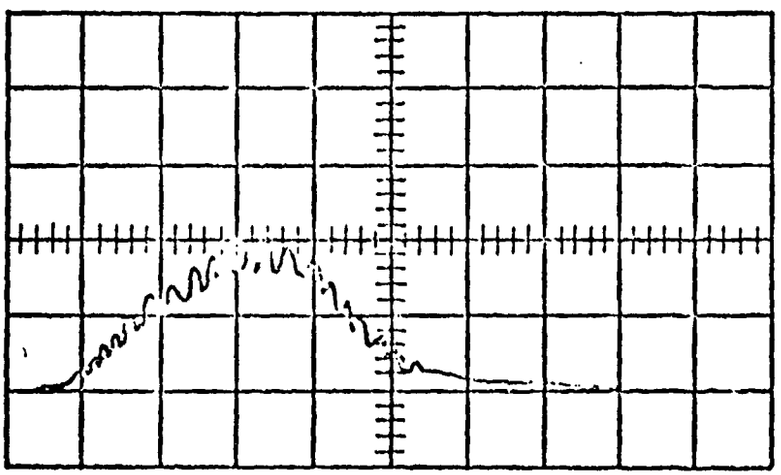

12" long resonator with mode beat 10nS/cm

Output reflectivity constant 20% on all graphs

1" long silver elliptical cavity with 3 mm by 30 mm Nd^{+3} YAG crystal and passive dye ce (B4-DN)

Flashlamp EG&G XFX-163
2 ATM. XENON gas fill

Plasma bore: 2 mm
Lamp od: 4 mm
Arc Length: 25 mm

may be detrimental in the detection of the pulse-echo in the receiver. Since this phenomenon (quasi-mode locking and mode beating) is dependent of the length variations of the cavity, one can expect that thermal and stress induced dimensional changes in the length of the interferometer housing, may transitionally sweep through such a condition. This will happen when λ becomes an integral multiple of the resonant cavity length. Mode beating will occur during the pulse buildup (as indicated in Picture # 15). This length modulation may occur even with extremely stable structure, simply due to the thermal and acoustical shock to the crystal, which can "ring" from this dual impact. Since the propagation coefficient in YAG is different from the surrounding air, the effective path length of the laser pulse can be modulated by longitudinal vibration of the crystal. The mode perturbation is partially the result of the choice of the Fresnel number of the cavity. This relationship is described in the paragraph treating the optical design considerations of the space hardened laser transmitter. Mode beating and other pulse shape distortions were observed often during our tests.

The attached graphs were obtained during our study of the role of reflectivity in miniature cavity design.

2.11 The Stabilization of the Optical Laser Resonator

The reasons for the elaborate design characteristics of the oscillator is to counteract the described causes of the instability.

The high efficiency of the resonator permits low input energy operation and therefore minimizes the thermal perturbance of the crystal geometry. The low input energy also permits efficient removal of the absorbed and unused heat from the crystal.

Minimizing the thermal gradients, in axial and radial directions the lensing and wedging effects are negligible for the specified input energy.

The laser interferometer operates at near saturation, far above the threshold. The benefits of this operation are: an exceptionally good plasma fill in the flashlamp; good diffused imaging of the plasma into the crystal; a stable beam output and divergence; high efficiency in the

pumping cavity. At high pumping levels, the placement of a mode selecting aperture into the resonator, produces highly stable and repeatable performance at high output power levels and low order of transverse modes.

The output level of the oscillator is about 5 megawatts peak power in multimode. The beam diameter is about 5 millimeters.

To obtain mode stability in the resonator we must consider the nature of mode forming. The ideal output would be, of course, pure Gaussian TEM_{oo} output. Because of the complexity, size and the cost, a second best choice is multimode operation with low order modes, but higher than TEM_{01}, TEM_{10} or TEM_{11}. The very low order modes cause constant mode competition in an aperture and result in beam wandering and path modulation. Performance comparison of efficiency is treated in the following paragraphs.

2.12 Mode Formation and Size in the Laser Resonator

The choice of the Fabry-Perrott resonator configuration is dictated by several requisites of the laser cavity. Virtually any stable resonator configuration will do the job, but certain elements within the oscillator will determine the most favored choice of resonator. It is known, that the TEM_{oo} mode size (beam diameter) is not constant within the resonator. Therefore it is reasonable to place optical elements such as polarizers, Q-switches and the lasing crystal in the segment of the resonator, where the beam diameter (mode size) is the largest. This allows the optical element to operate at the lowest damage density levels. Choosing a stable resonator configuration of a flat front mirror and a curved rear mirror (R = 10 meters) 100% reflective and a length of 200 millimeters for the resonant length (L), the TEM_{oo} mode will grow as indicated on Picture # 16

$$W_0^2 = \frac{\lambda}{2\pi} \sqrt{d\,(2R - d)}$$

To measure the TEM_{oo} output, an aperture is placed between the front mirror and the laser crystal. The aperture is slightly larger than the

Diagram of a Laser Resonator with Half Symmetric Geometry

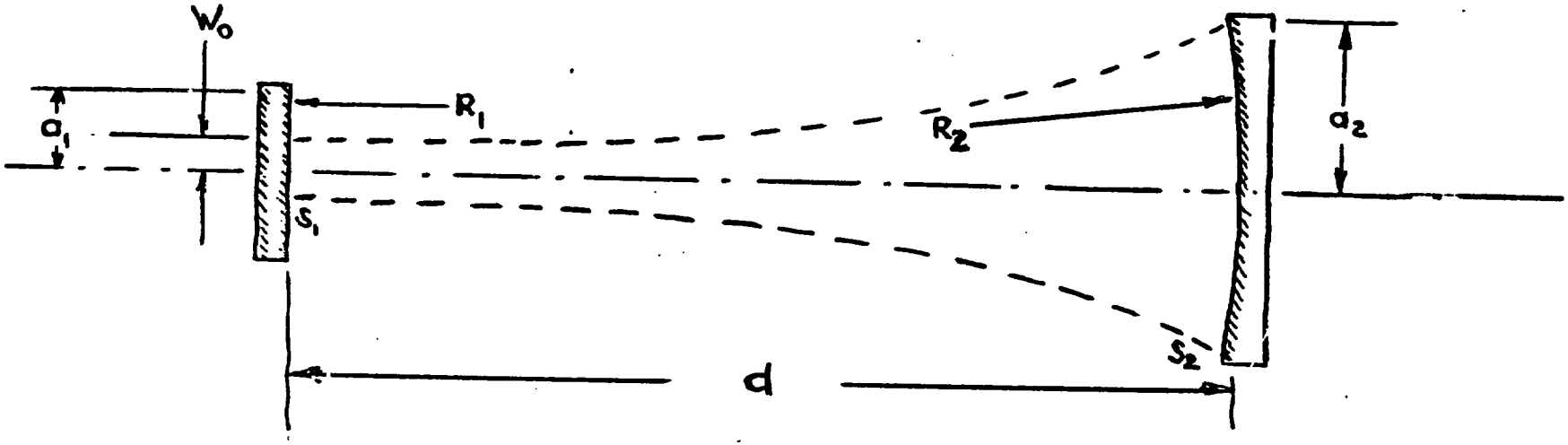

If $W_0 < a_1$

and $R_1 = \infty$

$d = 2f$

and $f = \frac{R}{2}$

$k = \frac{2\pi}{\lambda}$

where $G_1 = g_1 \frac{a_1}{a_2}$

$G_2 = g_2 \frac{a_1}{a_2}$

and $g_1 = 1 - \frac{d}{R_1}$ $g_2 = 1 - \frac{d}{R_2}$

The Fresnel Number $N_F = \frac{a_1 a_2}{\lambda d}$

and the lowest diffraction loss for this N_F is when $R_1 = R_2 = d$

The stability criteria are:

$$0 < G_1 G_2 < 1$$

or

$$0 < g_1 g_2 < 1$$

Picture # 16

actual diameter of the mode to prevent truncation and the formation of undesired side lobes. The function of the aperture is to prevent higher order modes from buildup and amplification.

The output of such an oscillator has a Gaussian profile of energy (or power) distribution. To obtain stable operation, several electrical and mechanical parameters must be satisfied in the design of the resonator. This of course applies on either single or multi-mode operation.

The thermal and mechanical stability of the suspension of the optical elements is a basic prerequisite. In the space hardened oscillator this will be accomplished by the specially designed thermally stabilized optical suspension. The stability of the optical elements is guaranteed by the special Ball-Socket optical holders and locking devices.

The design of the oscillator provides for ideal coaxial and concentric placement of the laser beam in respect to the mechanical axis of the system. This provides for correct interception of the TEM_{oo} beam by the aperture, forming a gap, uniformly spaced between the aperture and the beam. It is important to note that the aperture does not form the TEM_{oo} mode and it does not determine its size or location. The aperture only suppresses the higher order modes, prevents their oscillation and amplification.

Generally, the behavior of the TEM_{oo} and other low order mode wave fronts was studied by the Raytheon-LADC staff and by others, yet very little is known about certain unstable conditions during the formation of Q-switched "giant" pulses. These unstable conditions lead to a distorted formation of the wave front of the laser output, and contribute to the generation of multiple peaks on the top of a giant pulse, where the peak power density exceeds the permitted levels and destruction of optical materials results. These "hot spots" and "filamentary lasings" induce material damage, such as craters and bubbles in the optical elements like mirrors, prisms, crystals, etc.

The space hardened laser cavity must be designed to satisfy the requirements of an optimized resonator. Length, curvature of the mirrors, apertures, etc. are theoretically determined to obtain the maximum freedom from temporal distortion and "spike" generation in the output beam profile.

2.13 The Temporal Stability of the Beam

The low level of the awareness of the peculiar behavior of the Q-switched giant pulses can be attributed to the speed of the beam formation. Realizing that a Q-switched pulse is average 10 nanoseconds in duration, and even this time represents several passes through the resonator, the distortion will last only a few nanoseconds. The basic available instrumentation in the present state of the art, does not lend itself for observations of such fast events.

The observation of the temporal distortion is even more difficult, because of the variance of the phenomenon, from pulse to pulse, does not permit the use of sampling methods.

The gain saturation induced perturbations in the resonator containing gain mediamay or may not dampen out during the pulse. This will cause distortion of the wave front, and the emitted portion of the laser pulse may have a severely distorted profile.

Photographs taken by a profile storing method (imaging the beam profile on an image inverting phosphor and then scanning the secondary emission) show that the amount of the perturbance is directly related to the Fresnel number of the resonator.

The Fresnel number $N_F = \frac{a^2}{L_\lambda}$ for single rectangular apertures

or $N_F = \frac{a_1 a_2}{\lambda d}$ for curved mirror radius and apertures

where
a^2 = area of the aperture (rect)
$a_1 a_2$ = radii of the mirror apertures
$L = 2d$ (dual pass distance)
d = mirror separation
λ = wave length of the radiation

Reproduction of the pictures taken from an Invar Stabilized Resonator

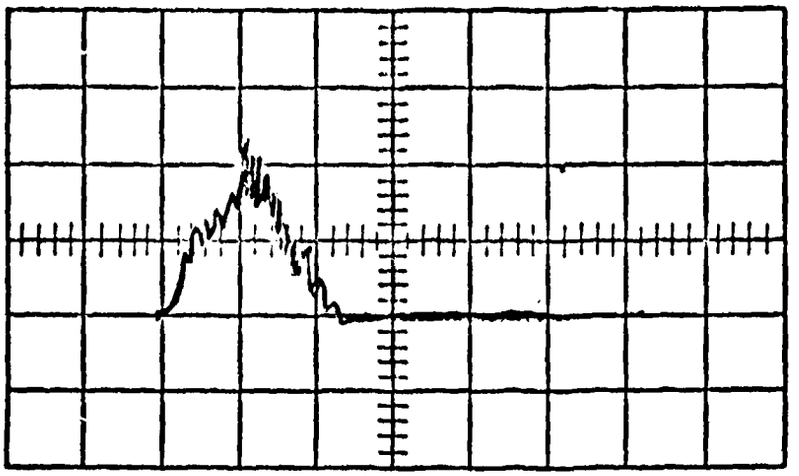

20ns/cm

The Q-switched pulse with high Fresnel Number (80-100) shows high distortion of the pulse and large mode competition instability.

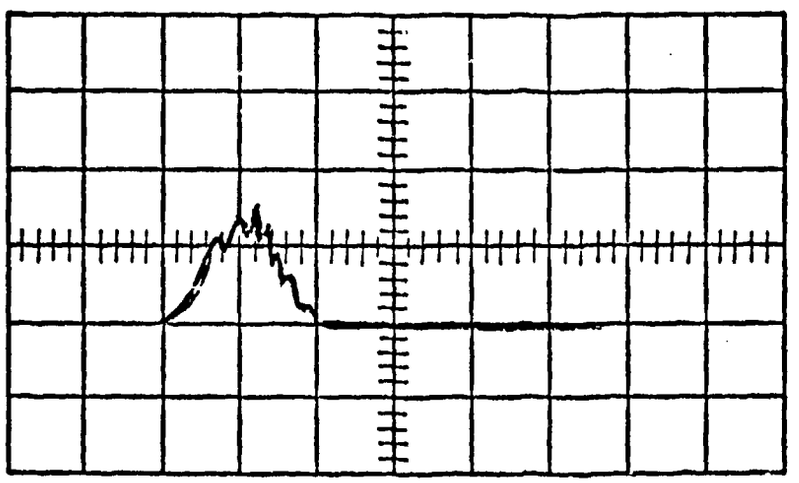

Medium Fresnel Number shows stability improvement. The N_F changes wer made by changing the aperture diameter and lengthening the resonator.

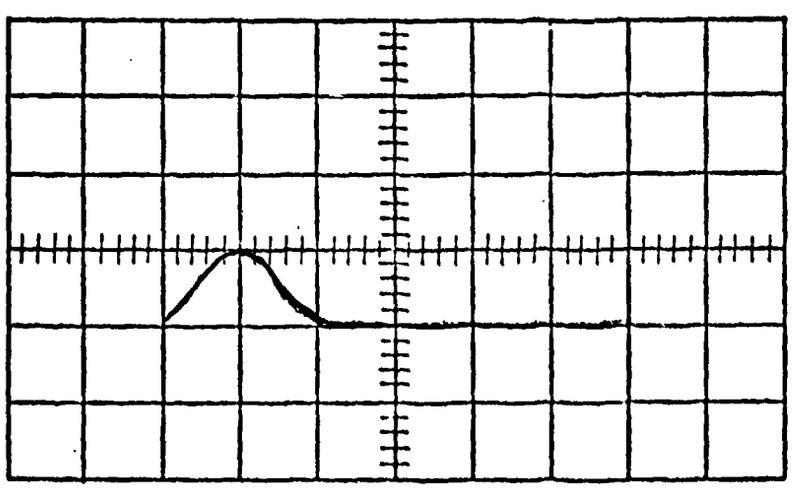

Small Fresnel Number (N_F = 1) shows excellent pulse shape and no "spikes". Pictures taken with external pinhole and LA-31 detector and Tektronix #519 scope.

PICTURE # 17

In resonators with large Fresnel numbers this perturbation is excessive and quite visible on the photographs as temporal distortion and high peak power spiking.

With low Fresnel numbers such as unity or less, the perturbation is absent and the spiking is minimal.

2.14 The Optically Stable Resonator

Setting aside all the thermal mechanical and other structural and environmental stability requirements, an oscillator must be optically stable.

For an optical resonator to be stable, it must fulfill the basic stability criteria

$$0 < G_1 G_2 < 1$$

or

$$0 < g_1 g_2 < 1$$

because, under such conditions the optical resonators are stable. Otherwise they are unstable.

Special cases, when $R_1 = R_2 = d$ (confocal) or $R_1 = R_2 = \frac{d}{2}$ (concentric) or $R_1 = R_2 = \infty$ (plano parallel) deserve special attention and care since they are borderline cases, and with small deviations, they can become unstable.

Also special considerations should be given for the eigenvalue and the geometrical phase shift in the resonator, defined as

$$\delta = \frac{2\pi d}{\lambda}$$ and the Q of the cavity $$Q = \frac{2\pi d}{\lambda d_t}$$

where d_t is the total resonator loss due to diffraction, output couplings absorption, scatter, etc., become all these conditions will determine the mode growth and distribution at the modes and the stability of the resonator.

Between the numerous possible variations of the positive and negative and infinite radii and different lengths and distances of the center of curvatures, we have selected the plano-concave mirror resonator. T s type of resonator has the advantage of containing the

minimum W_o on the front coupling mirror reflective surface. This makes the placement of the TEM_{oo} aperture very convenient. The beam size inside the resonator fans-out and the hyperboloid of the beam is intercepted by the rear mirror curve (10 mR). The wave front at the W_o is truly single plane and an aperture in this plane has an ideal location, for the control of the TEM_{oo} output.

Based on the described studies, a laboratory oscillator was designed and fabricated. Its output characteristics are indicated on Picture numbers 16, 17, 18.

The measured Gaussian profile matched the theoretical Gaussian profile (within $\pm$ 5%), as measured with a scanning detector and displayed on an oscilloscope. The oscillator provided up to 10 mJ output in TEM_{oo} in Q-switched mode. The stability of the unit was tested for several million pulses during a full month period, without a single realignment of the resonator.

2.15 The Multimode Laser Oscillator

The basic stability, repeatability and optical design of the resonator apply to both the single mode and the multimode master oscillator. By removing the aperture from the resonator, the laser becomes a multimode oscillator. The original design of the Laser Oscillator intended to obtain, basically, a low order mode resonator, since the lower the number of the higher order modes in design parameters, the more output the TEM_{oo} oscillator yields after the insertion of the aperture.

The multimode design goal was to obtain a relative low beam divergence and simultaneously good mode stability.

Since the uncorrected beam divergence is determined by the curvatures of the mirrors and the length of the resonator and the limiting apertures, the number of modes and mode sizes should be determined for a given resonator geometry. In our laser oscillator the size of the crystal is fixed because of the predetermined output require-

ment of 0.05 joule minimum. Previous studies indicate that a 5 mm diameter crystal of 54 mm in length yields a maximum of .1 joule output. The volume of this crystal can store .10 joule of retrievable energy in multimode and Q-switched operation. The defining aperture of the resonator is the end face of the crystal, since no other smaller apertures are in the resonator.

Assuming that the waist of the hyperboloid of all the modes W_o is generally near the crystal, the far field beam divergence can be calculated from the crystal aperture - d - and the empirical number - m - of the highest order number of modes, that will fill the aperture without truncation - TEM_{moq}

Defining θ as the full angle divergence

$$\theta = (1 + 2m) \frac{4}{\pi} \frac{\lambda}{D}$$

and accepting the restriction that the highest order mode TEM_{moq} will fit into the aperture D

the size of fundamental TEM_{ooq} must be

$$2 W_o = \frac{D}{(1 + 2m)^{1/2}}$$

If we choose m = 0, the output divergence will be diffraction limited.

The choice of numbers between 0 and 3 is not advisable, because the low order of modes cause instability in the aperture when the thermal or mechanical perturbations cause nonsymmetrical distribution of the modes, especially if there is a lateral off-axis displacement of modes due to the perturbation.

Checking for D = 5

and m = 4

We obtain:

$$\theta = (1 + 2m) \frac{4}{\pi} \frac{\lambda}{D} =$$

$$= 9 \times \frac{4}{\pi} \frac{1.06 \times 10^{-3}}{5} =$$

$$= 2.4293 \times 10^{-3} \simeq \underline{2.4 \text{ milliradians}}$$

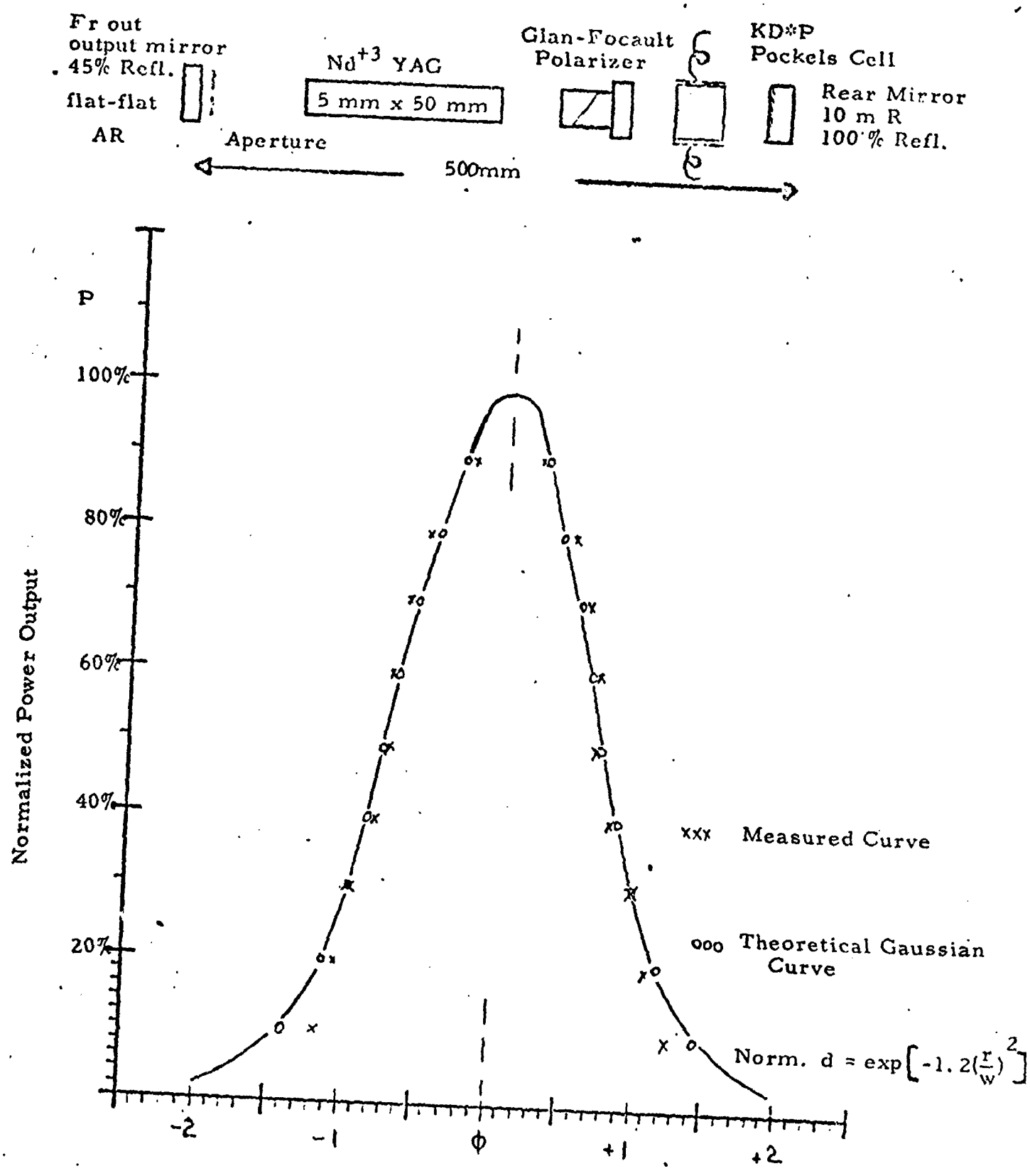

Normalized Radius - d

Master Oscillator Beam Profile 6 mJ Energy Output

Picture # 17

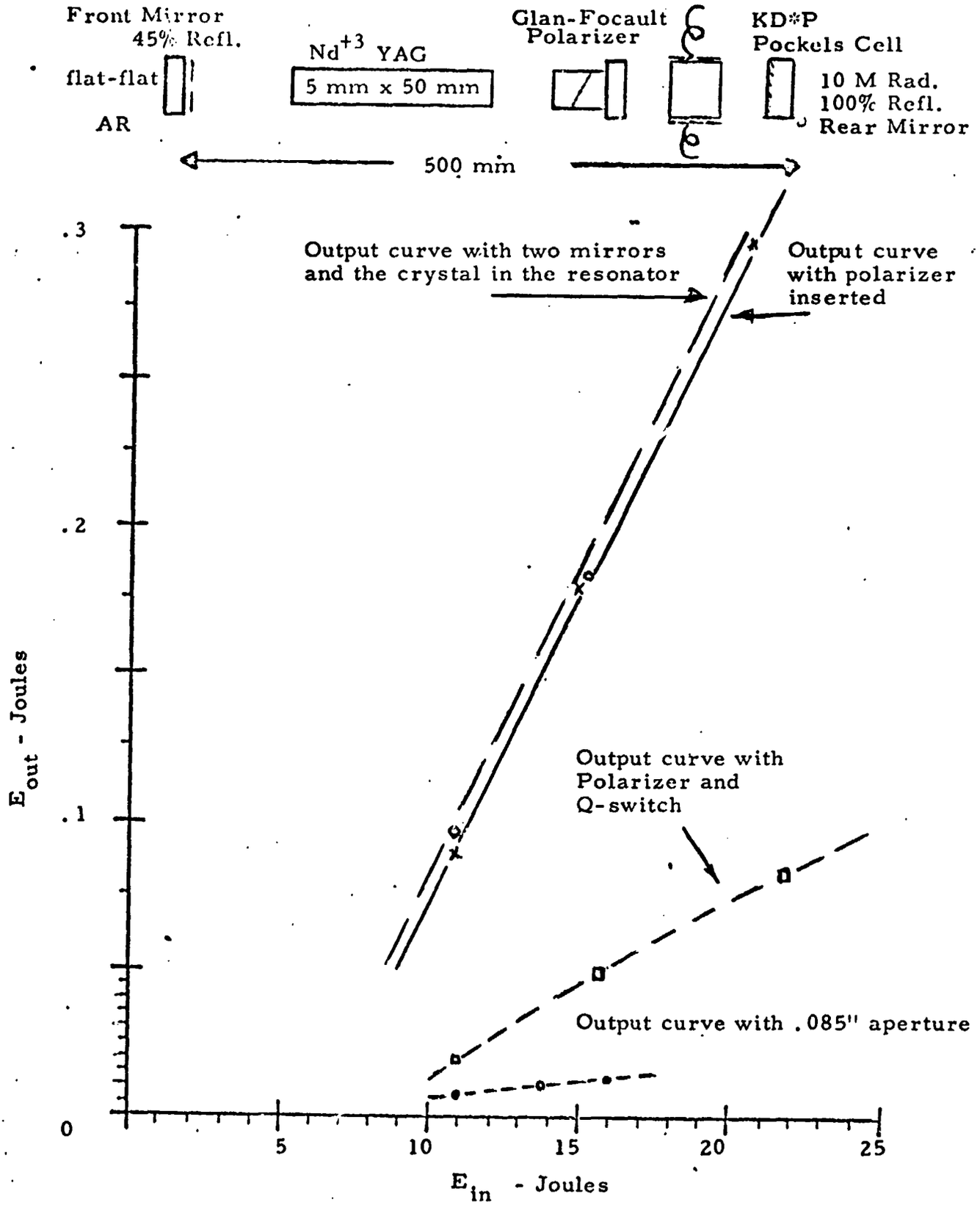

Energy Transfer Curves of the Master Oscillator

Picture # 18

which is the uncorrected beam divergence, and the size of the fundamental

W_o from the equation

$$2W_o = \frac{D}{(1 + 2m)^{1/2}} =$$

$$= \frac{6.35}{9^{1/2}} = 1.66$$

$$W_o = \underline{0.83 \text{ mm}}$$

2.16 Summary of the Study

The study of the parameters of the optimization of the space hardened laser oscillator reveals the following recommendations:

1. The resonator should have a dual lamp, dual ellipse cavity.
2. The active crystal shall be 5 mm x 52 mm Nd^{+3} YAG crystal with 0.95 to 1.1% doping level.
3. The flat ends of the crystal should be AR coated flat within $\lambda/10$ and parallel within 5 sec.
4. The body of the crystal shall be fine ground.
5. The flashlamps shall have a 3 mm plasma bore and a plasma length of 44.44 mm.
6. The dual ellipse pumping cavity shall have a high reflectivity, with polished silver coating, chromate protected per MILL-QQ-S-365-a GRADE - A
7. The resonator shall be 200 millimeters long.
8. The rear mirror shall have a 10 meter radius of curvature and shall be coated for 100% reflectivity at 1.06 micrometers.
9. The front mirror shall have 45% reflectivity on one of the flat surfaces and antireflection coated on the other flat surface. The material of the mirrors shall be shlieren-free fused silica.
10. The polarizer shall be Glan-Focault calcite prism with all four windows antireflection coated at 1.06 micrometers
11. The Pockels Cell should have a Lithium Niobate crystal, cut for transverse field excitation. The crystal shall have a 1.5 KV to 2 KV $\lambda/2$ retardation of polarization with an extinction ratio of

500 :1 min. Theaperture shall be a min. 8mm and shall be AR coated (both ends).

12. The resonator shall operate in multimode (4 orders of modes) and shall have an uncorrected beam divergence of 2.5 mR max.
13. The resonator shall be of rugged design, stable, mechanical, resonance free, to minimize all possible perturbances.

3.0 THE DESIGN OF THE FINAL TRANSMITTER

3.1 The Conversion of SS-219 into SS-223

Since the size, weight, and optical properties of the major components were firmed up, the first layout of the transmitter was drawn up. The location of the major components was established and the design effort was divided into two major groups:
The opto-mechanical group reviewed the original SS-219 optical layout and analyzed properties of the subassemblies from the standpoint of vibrational shock, and vacuum operational effects on the stability and also the thermal considerations of the transmitter.

The SS-219 transmitter was designed for terestrial use in hand held mode. Obviously, most of the subassemblies are not directly suitable for space hardened environment. The main components of the SS-219 are:

The Dust Cover
The Resonator
The "Q" Switch
The LPS-100 Charging Supply
The Trigger Electronics
The "Q" Switch Electronics

(See Pictures #19through 24)
The pictures reveal the modular buildup of the resonator and the sheet metal structure of the laser transmitter. The structures are described in the following paragraph.

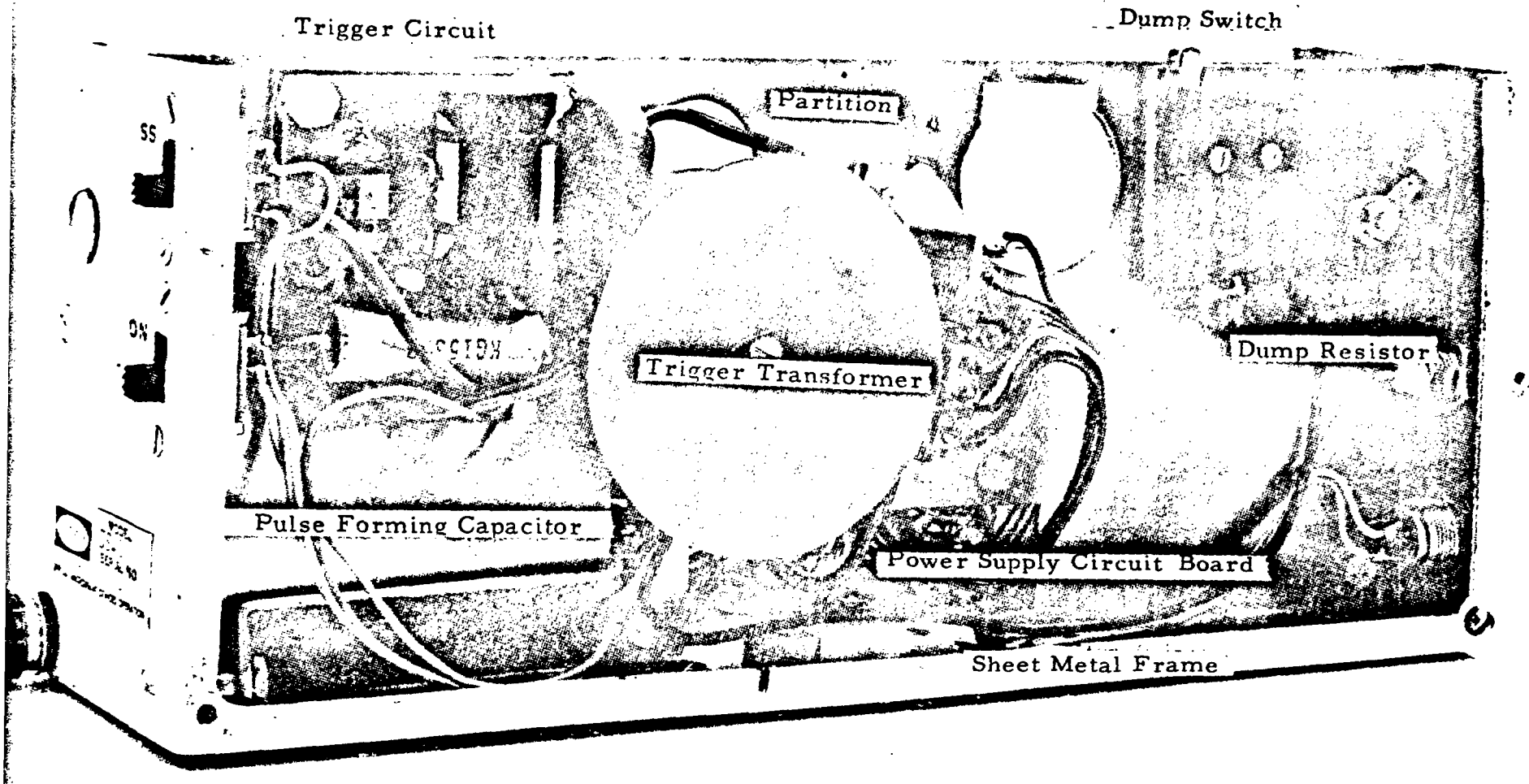

Picture #19

Sheet Metal Housing

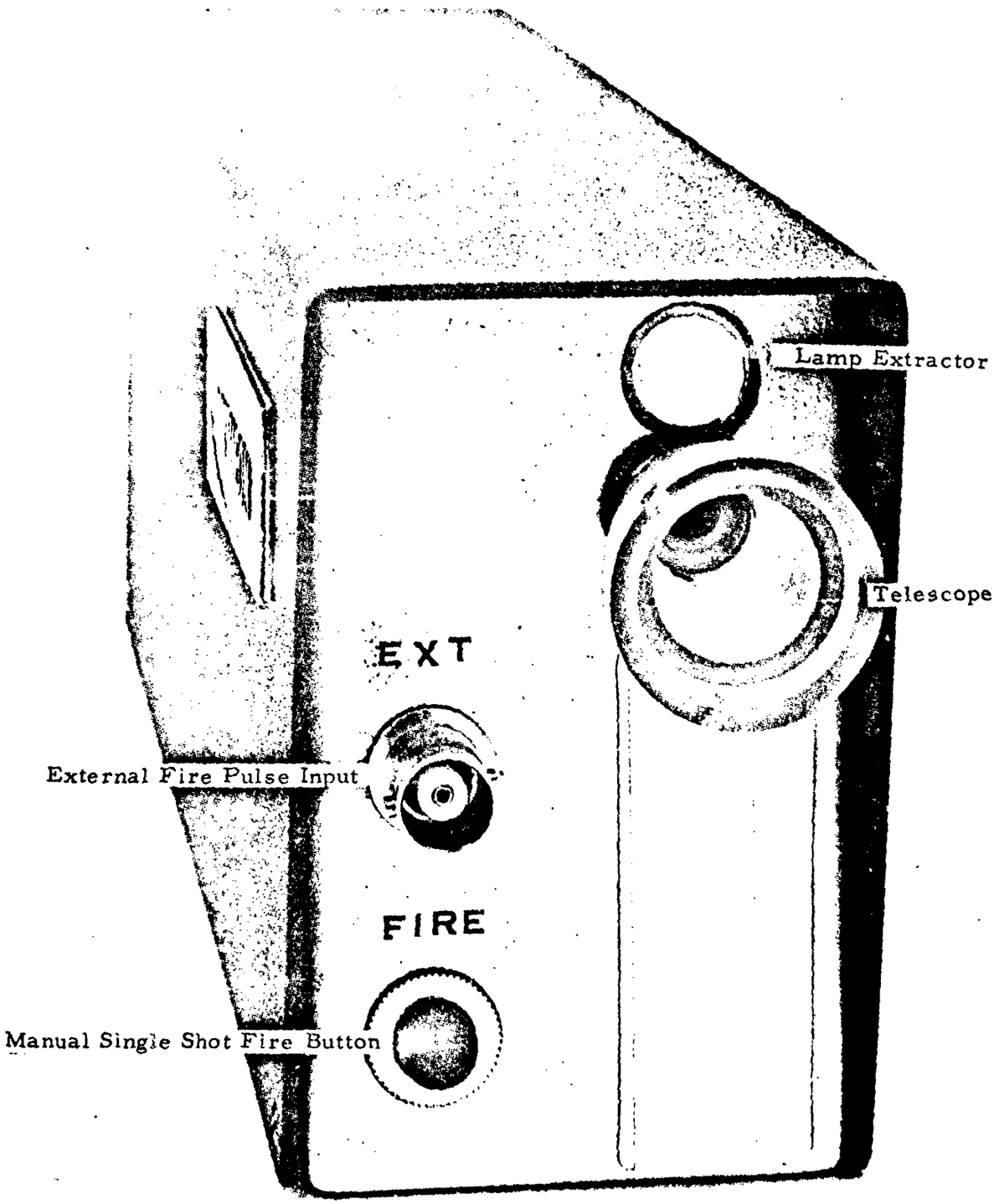

Picture #20 - Front Controls of SS-219 Laser Transmitter

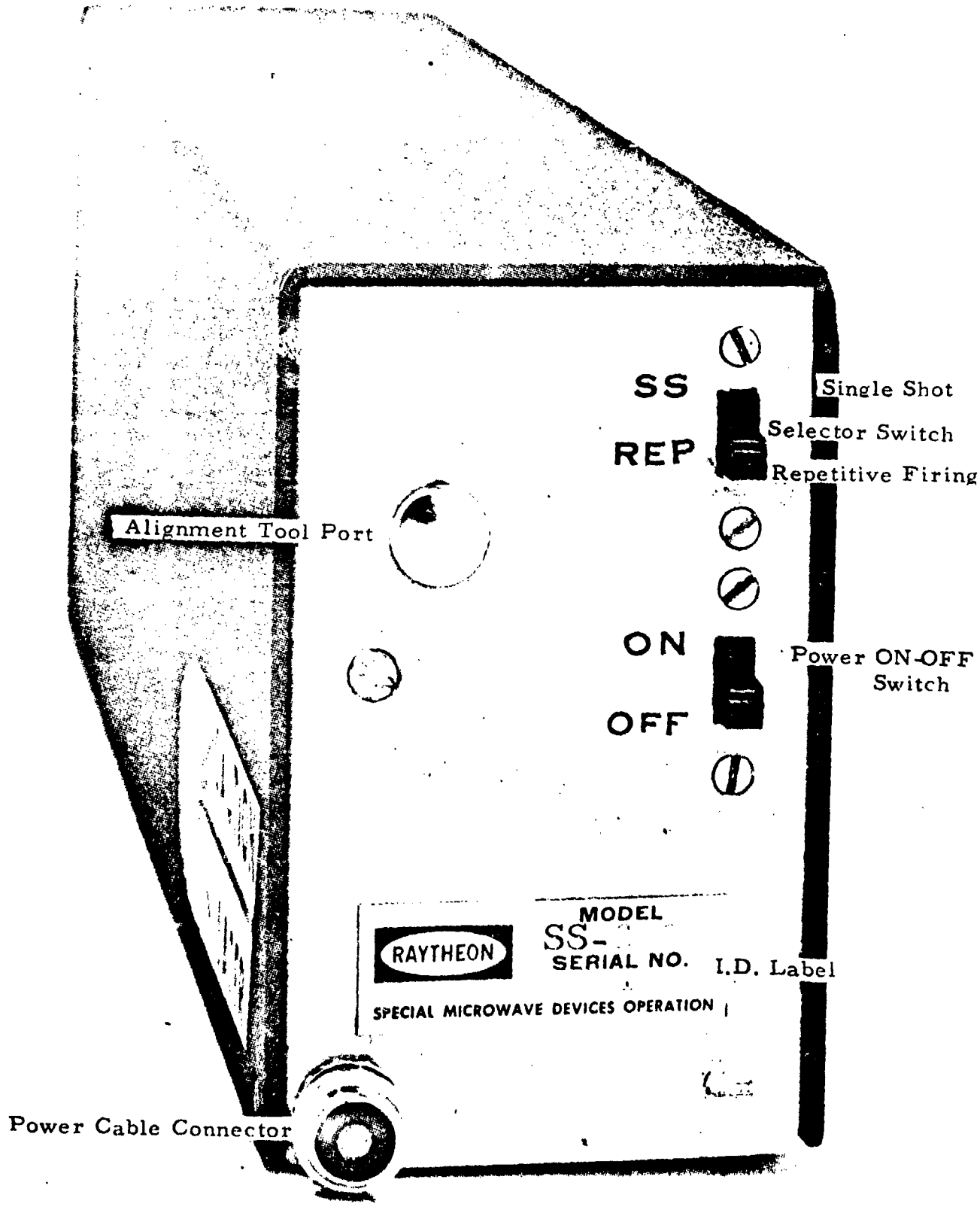

Picture #21 - Rear View of Controls of SS-219 Laser Transmitter

3.2. Laser Head - Technical Description

3.2.1 Laser Head Design SS-219

3.2.1.1 Laser Cavity (See Pictures #25 26 and27)

The laser cavity incorporates the optical pump cavity, the flashlamp, lamp cooling electrodes, the laser crystal and its thermally conductive crystal holders, and finally, the fixed coupling optics and adjustable rear optics into a single modular unit.

The principal purpose of this interferomter is the generation of a laser pulse of a specific duration and energy content at a specific spectral wavelength.

The interferometer, also known as laser resonator or resonant cavity (a descendant of the masers and excited microwave devices) is basically two mirrors, a crystal, and a flashlamp in a reflective enclosure.

The process of the generation of the pulse can be summarized as follows. A flashlamp filled with a rare gas (Xenon, Krypton) receives a current pulse from a pulse forming network composed of storage capacitors and inductors. The gas is ionized into conduction by a high voltage trigger pulse (15-20 Kv). The current passing through the flashlamp, forms a plasma discharge. This plasma emits photon energy at various wavelengths. Some of these wavelengths are directed (focused) by the reflective housing toward the laser crystal. In our case the active crystal is Neodymium doped Yttrium Aluminum Garnet, for short Nd^{+3} YAG. Some of this photon energy is absorbed by the crystal and it causes the impurity atoms to be excited in a higher state. When the population inversion occurs and the excited atoms return back to the initial state, fluorescent emission occurs at the typical wavelengths of the impurity (dopant).

Right-Hand "X-Ray" View of SS-219 and SS-359 Units

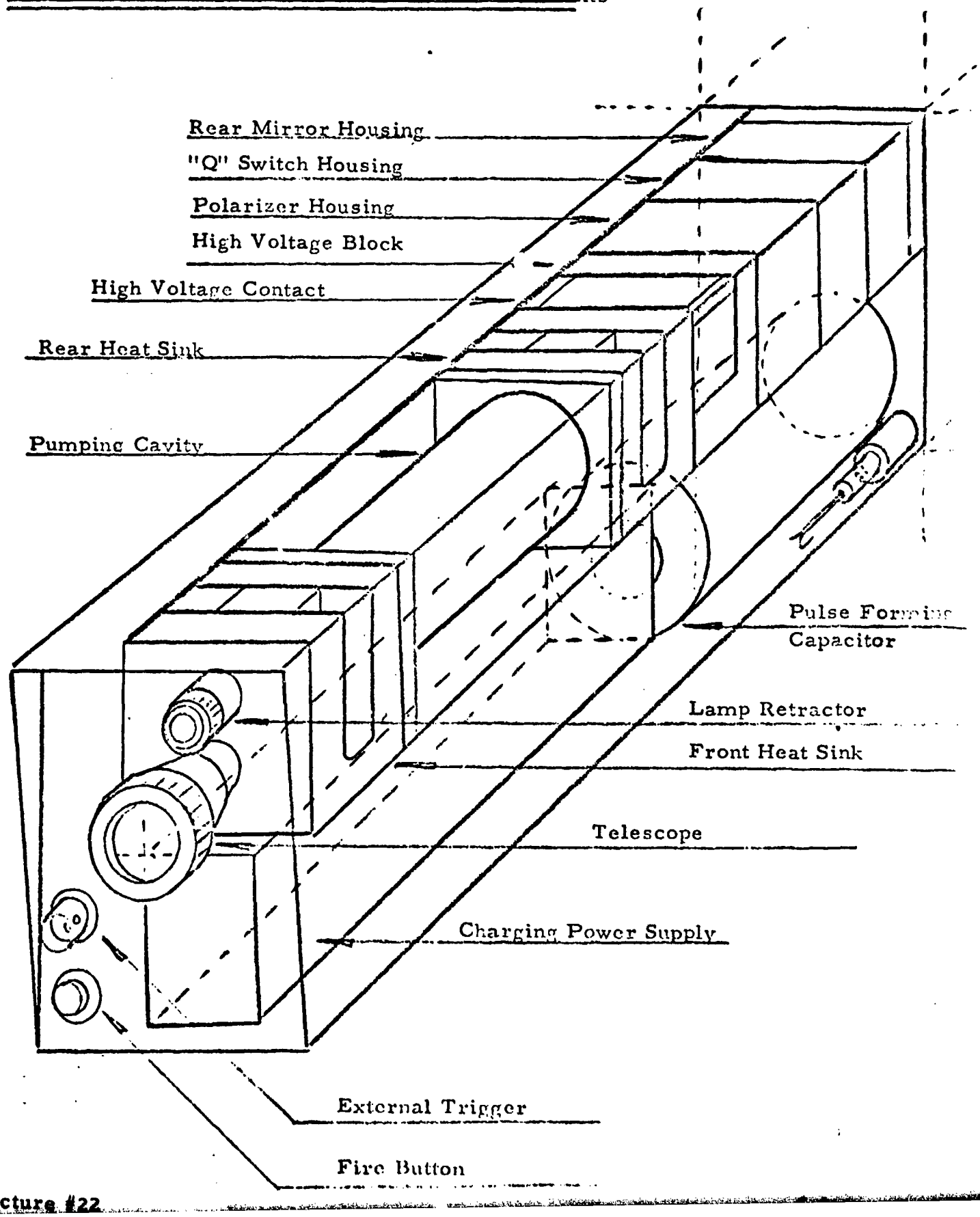

Picture #22

Left-Hand "X-Ray" View of SS-219 and SS-359 Units

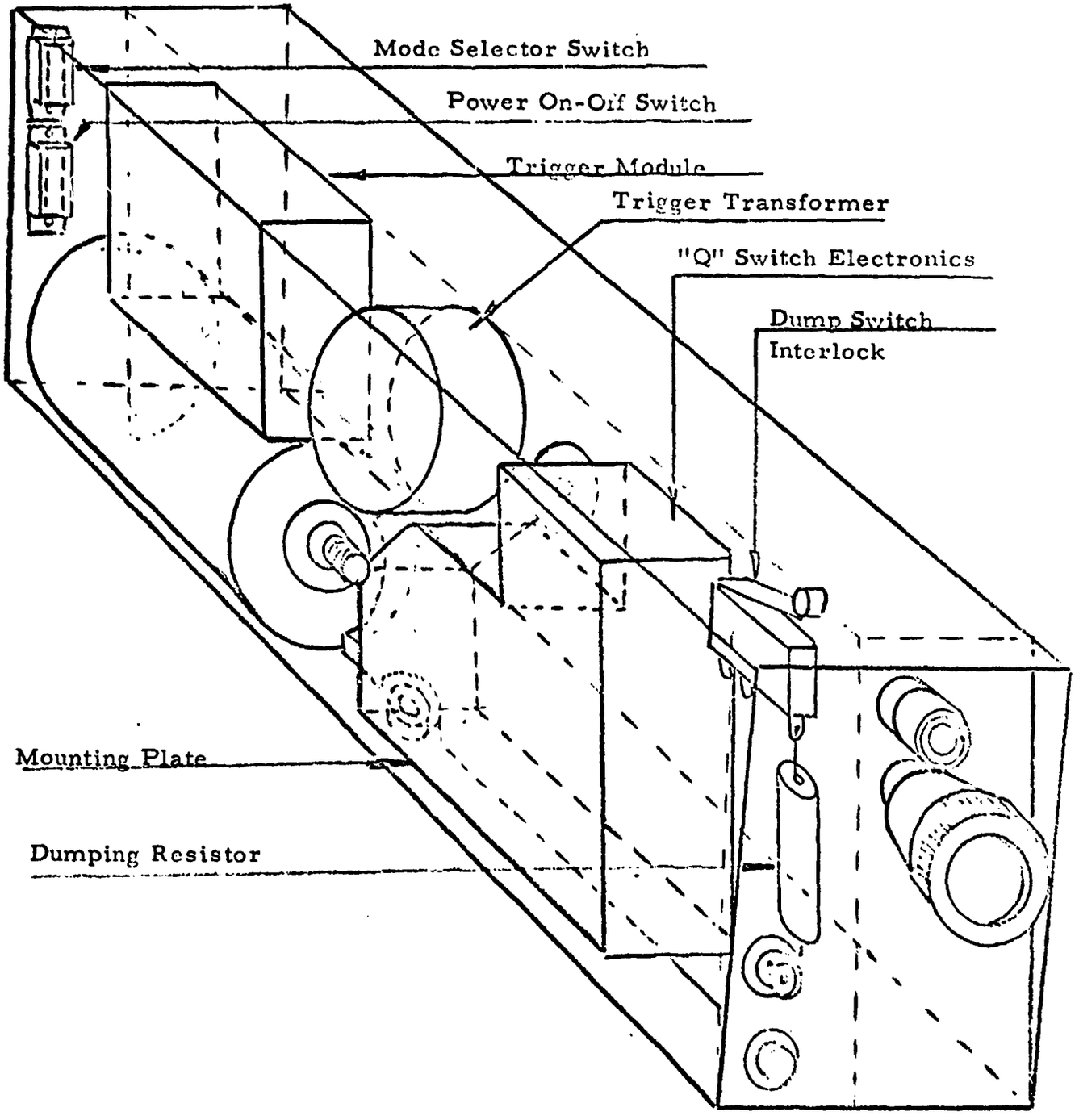

Picture #23

WSIO

The two mirrors at the two ends of the laser crystal are aligned normal to the axis of the cylindrical crystal and are plano parallel with each other to form a resonator. The excited crystal in the middle of the resonator acts as the supporting source of oscillation at the wavelength selected by the gain-preferential coating of the optics, in our case 1.06 microns.

If the two mirrors were 100% reflective, this oscillation would proceed until the entire energy would be consumed by the losses of the resonator. In order to extract a part of the energy from the resonator one of the mirrors is coated for only partial reflectivity. We refer to this mirror as the output coupling mirror. Any or both mirrors could be deposited on the end surfaces of the crystal, but that would hinder the insertion of other elements into the interferometer and the alignment would depend solely on the surface alignment of the crystal, with no flexibility of alignment corrections.

The partially reflecting mirror reflectivity may vary depending on the application of the interferometer betwen 20% and in some cases as high as 90%. This reflectivity will largely influence the amount of the output energy and therefore the efficiency of the interferometer.

3.2.1.2 Optical Pump Cavity

A cylindrical section of a metal tubing (6) is properly cut down at the two extremes to form two reference shoulders at the ends of the cylinder. Two rectangular flanges with elliptical center holes are pressed on the two reference shoulders of the tubing. After proper polishing and buffing, the assembly is coated with multiple layers of electrolytical plating with the last layer being pure silver with optically polished surface. Each end of this central section mates with a heat sink block.

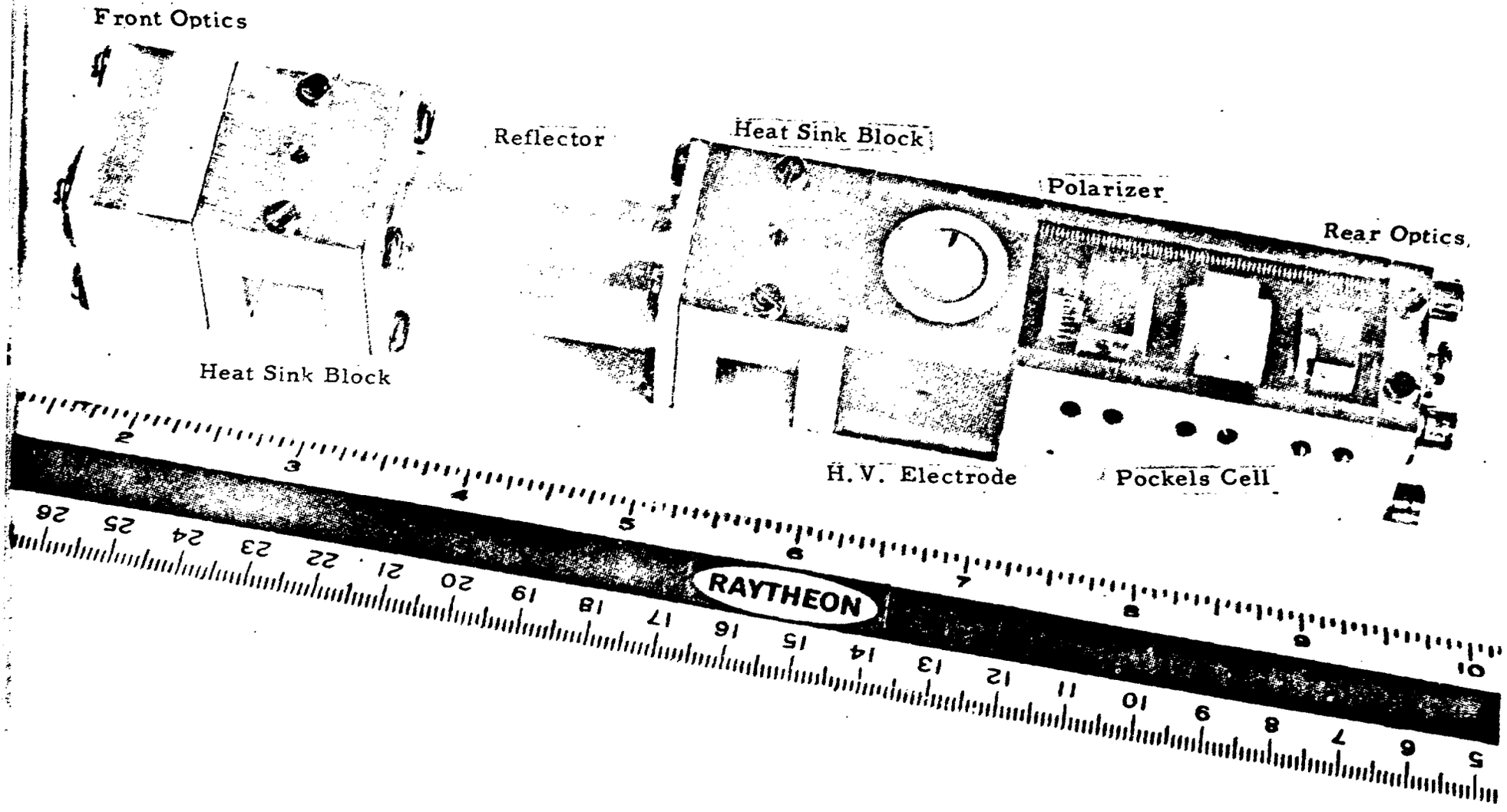

LC-42 Laser Cavity in the SS-219 System

Picture #24

3.2.1.3 Heat Sink Blocks

The front end heat sink block (transmitting end) of the assembly (1) is used as a common heat sink for the crystal holder (10) and the lamp electrode holder (23). The crystal holders (10-11) are aluminum mandrels with four, segment preloaded, grips. The two ends of the laser crystal (19) have two metallized 2 millimeter wide bands where the grips interface with the crystal and provide an excellent thermal path and mechanical support. One each of such cylindrical mandrels is attached to each of the two ends of the crystal.

The rear heat sink block of the assembly (2) is used as crystal heat sink only, because the rear end of the flashlamp is at high electrical potential. This end of the flashlamp (18) is the cathode (negative). The opposite grounded end of the lamp is the anode (positive). This end is equipped with a knurled button and a cylindrical shank (23). This cylindrical shank serves as electrical connection for grounding of the lamp electrode and simultaneously as a thermal interface between the lamp electrode and the heat sink block. This lamp extracting button is locked in place by a set screw (34), located in the heat sink block.

The heat sink blocks are attached to the flanges of the central section of the pumping cavity with four screws on each flange. The side of the heat sink blocks that faces the central section is also polished and buffed and plated the same as the cylinder. The crystal holder mandrels are locked into position by set screws, one in each sink block.

3.2.2 Cooling System

The rear heat sink block (2) provides the thermal path for the rear, antireflection coated end of the crystal. The back end of the flashlamp unfortunately cannot be cooled directly by heatsinking it to the blocks because this end (cathode) is under high voltage (up to 2000 VDC) and it receives a pulse of 17 to 20 kilovolts upon triggering. The cathode end cap of the flashlamp mates with an aluminum pole piece holder (15). This holder is provided with a mating hole for the lamp cap. The holder is slit in a plane through the axis of the lamp cap mating hole. The slit does not go all the way to the end of the cylinder and therefore

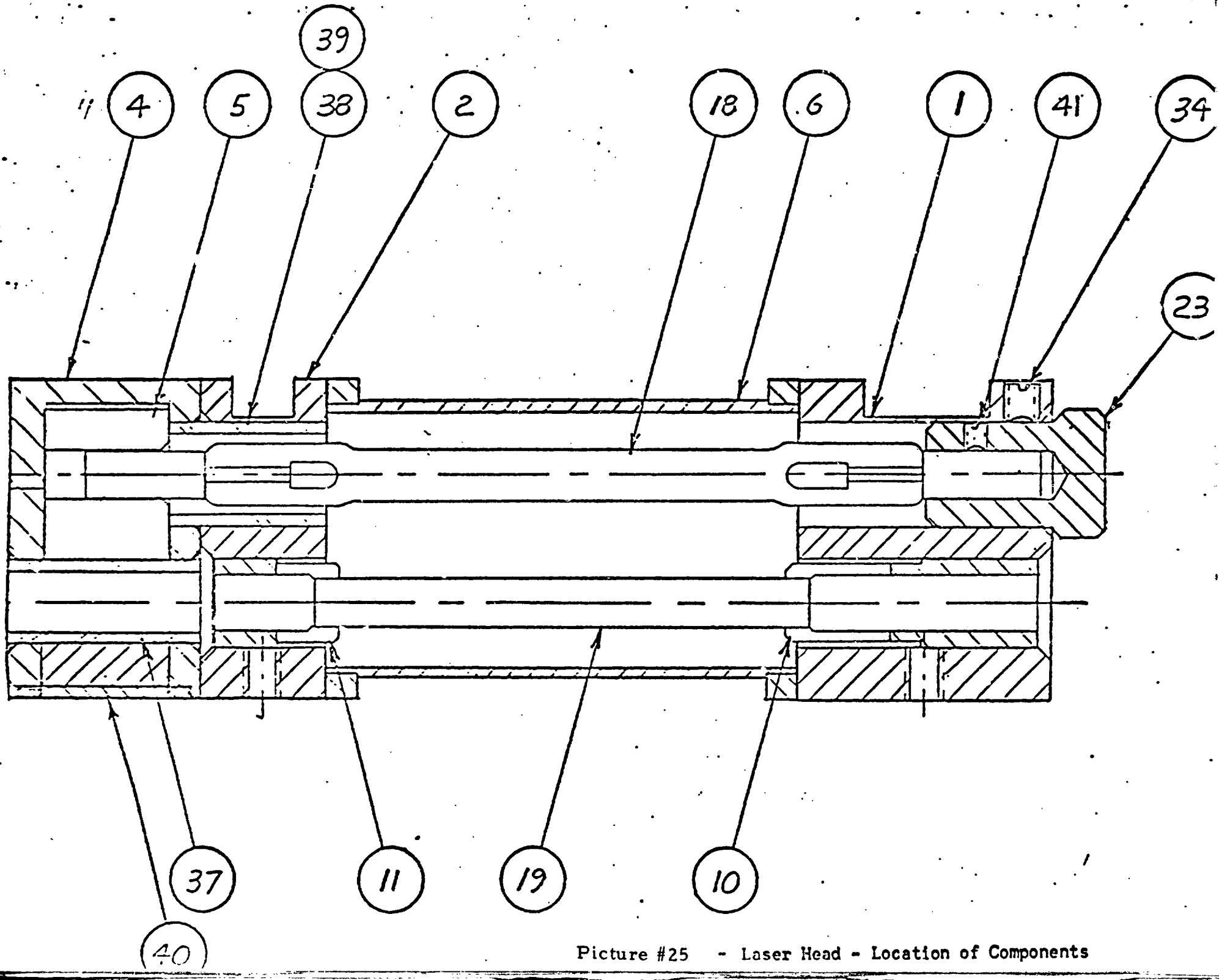

Picture #25 - Laser Head - Location of Components

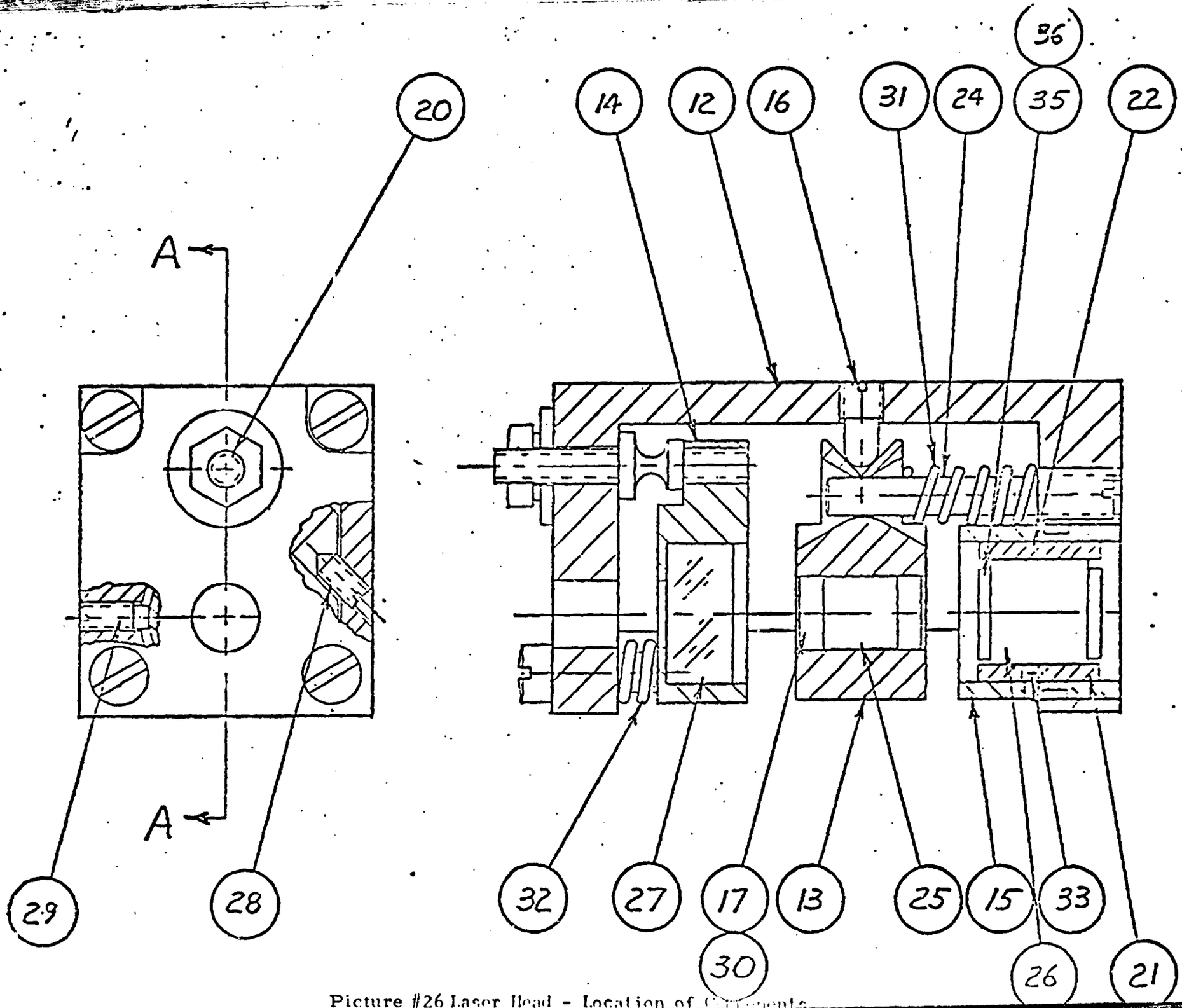

Picture #26 Laser Head - Location of Components

it forms a pincer-like form. The two arms of the pincer are preloaded, and thus exert pressure on the lamp cap, inserted in the mating hole. A quartz (or sapphire) disc (40) is bonded to this holder with a high thermal conductivity epoxy to provide cooling.

The entire contact assembly is placed in a epoxy-glass block of matching dimensions of the heat sink block and the remainder of the laser cavity. Four mounting holes in the epoxy-glass block provide mounting clearance for four feedthrough screws between the rear optics assembly and the pump cavity.

The electrical contact to the lamp holder is made via a #4-40 screw, fed through an opening in the side of the insulator block. Two quartz corona guard tubes are epoxied into this block. One (37) is placed into the bore through the bottom part of the aluminum cylinder to provide clearance for the laser beam path between the crystal and rear optics and the second (38) is epoxied into the block at the cathode end of the flashlamp. Both serve as insulators between the lamp holder-cylinder and adjacent metal housings.

The lamp holder-cylinder is constantly under pressure against the heat sink due to a spring washer located at the top of the assembly. The quartz washer - insulating block gap is filled with epoxy to prevent high voltage corona breakdown to the heat sink.

3.2.3 Polarizer and Q-Switch (Electro-Optical)

The polarizer Q-switch and retro-optics are a single subassembly. An aluminum channel (12) serves as housing for the three adjustable optical elements. The nearest to the laser crystal is the polarizer (26) assembly. The polarizer windows are antireflection coated for 1.06 micron radiation. This polarizer is mounted inside an aluminum barrel (21). This barrel inserts into the opening of the retro-optics housing. The barrel has a knurled collar to facilitate its fingertip rotation in the opening. A set screw inserted in the housing can lock the barrel into permanent position (33). The rotation of the polarizer is essential to align the plane of the polarization with the plane of the Q-switch mechanism.

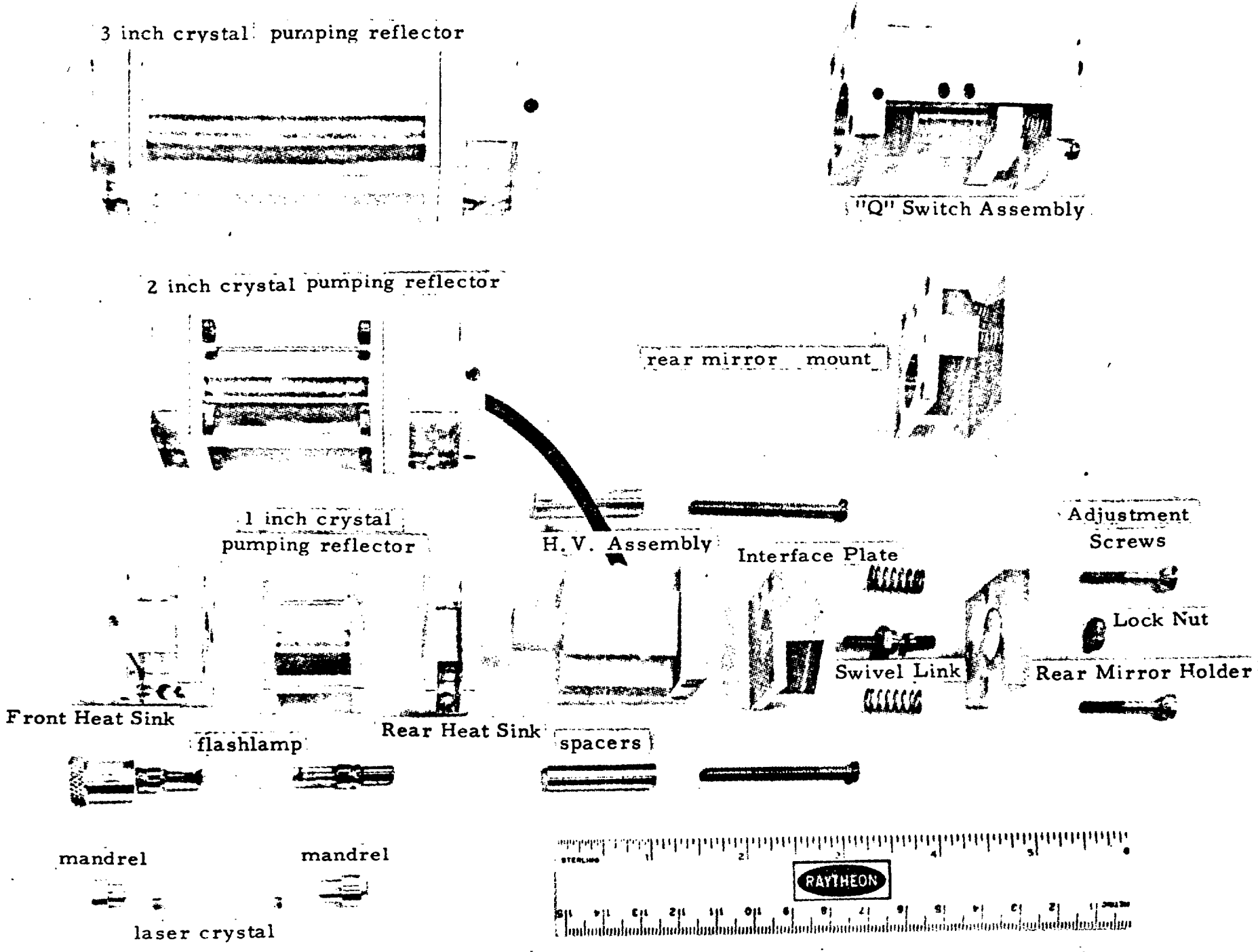

Picture #27 Exploded view of the LC-42 cavity in 1 inch, 2 inch, 3 inch long crystal configurations

The retro-optics is a 100% reflective coated mirror (27). It has a 10 meter radius of curvature on the coated side. This mirror is epoxy-bonded into the rear mirror adjusting plate (14). This plate is mounted to the back end of the retro-optics housing via a flexible linkage and two adjusting, spring loaded screws (32). The screws permit independent orthogonal alignment of the rear mirror with the optical axis of the laser. When the proper alignment is obtained, a third locking screw locks the mirror in permanent position.

The Q-switch assembly (13) is located between the polarizer and the retro mirror. This assembly is housed in an epoxy-glass swivel holder. The holder is suspended on a sliding pin and swivels about a ball joint (16) on the top of the assembly. The holder is spring loaded on the pin against two taper tipped adjustment screws (28). These screws work against two inclined planes on the Q-switch o holder and provide orthogonal adjustment for the Pockels Cell. The faces normal to the "A" axis are metal coated and serve as electrodes. The Q-switch pulse is applied to these electrodes.

3.2.4 Evaluation of the System for Conversion

The cooling method of the laser crystal used in the SS-219 system can be used directly in the space hardened laser transmitter. The heat transfer from the crystal was studied and tested to be about 10 times more efficient than needed in the space laser. The input energy into the laser pumping cavity is 10 Watts maximum in the SS-219 and it is 1 Watt maximum in the space laser, SS-223. Neglecting the lack of radiational and air-convection heat transfer, the 10 times smaller power input indicates reliable performance in the SS-223 system. The single flashlamp cavity in the SS-219 is not recommended for the SS-223 because the single lamp failure would mean total loss of transmission, therefore two lamps will be fired alternately in a dual ellipse cavity. This extends twice the expected length of the life of the laser transmitter. In addition, the reliability of the laser is increased, because in case of a lamp failure, the second lamp will still work and the transmitter will still transmit at one half of the repetition rate, at full power output. The optical mounts of the SS-219 system are not suitable

for conversion and a new approach was recommended. The use of the LINOBATE "Q" switch and Calcite polarizer is advisable, but new mechanical alignment systems for these elements is mandatory. The overall layout consideration should be changed to a rigid framework, from the present sheet metal structure.

3.2.4.1 Mechanical Space Hardening

Virtually all parts of the SS-219 laser head had to be modified or redesigned. The central pumping cavity in the SS-219 system is a single lamp single ellipse cylinder. The space hardened concept requires a dual elliptical cylinder to accommodate the two flashlamps and the single crystal located in the center of the cavity. The heat sink blocks were redesigned to accommodate the dual lamp geometry. A new generation of optical holders was developed and designed. The basic design philosophy of terestrial use of a laser was totally discarded since such design is service oriented. The space hardened laser does not have need for "easy access" to adjustments or flashlamp exchange etc. Once in orbit, the laser cannot be serviced. The cooling considerations are also different from terestrial lasers, mainly due to lack of "air cooling" provisions. The entire heat load must be conducted away from the heat absorbing components to the heat sinks provided inside the satellite.

The final design concept of the resonator optics went along the lines of a previously developed Raytheon concept of super-stable optical holders. This concept incorporates the rigidity and ease of the initial alignment of resonator. The mechanical rigidity and stability is achieved through a special concept of non-beam-translating optical suspension, perfectly balanced and locked into permanent position after the proper alignment.

3.2.4.2 Problems of "Standard" Optical Mounts

In the previous paragraphs, we have pinpointed the most predominant causes of perturbation induced instability in laser interferometers. In fact, the same conditions apply to amplifiers and other optical

systems too. The response of the optical suspensions to the perturbations is measure of the quality of the optical mount.

Several stringent requirements regulate the quality of such suspensions. The best of such suspensions must have mechanical rigidity, fine adjustment, reliable repeatability, stepless advanced, fine resolution, locking provisions and preferably no translation.

The simplest suspension is a pivot and two adjustment screws on a mounting plate. The screws are spring loaded against the plate.

Such suspension is simple and inexpensive, but it does not provide protection against translation and stepped motion and therefore the repeatability is not too good in such a suspension (see Picture #28).

The next more sophisticated suspension is the cross-cut optical holder. This system provides high compliance for the adjustment of the optical element, but it suffers from vibrational instability, poor repeatability and bad motion (see Picture #29). The closest to the ideal suspension is the "Cardan" or "Gimbal" suspension. This suspension features three concentric rings of diminishing diameters. The outer ring serves as base, the second and third ring move in the X-Y planes. The center ring serves as the optical holder. This is the favorite optical suspension supplied by most of the manufacturers. The "Cardan" technique permits true independent X and Y adjustment with no cross translation, but the rings are invariably magnetically coupled to the adjusting screws. This technique is very poor for vibration, and even worse for resetting the stepless motion (see Picture #30).

Since the adjustment screws or micrometers are not spring loaded, during the alignment procedure considerable blind travel occurs due to the backlash on the threads; and since there is no locking provision on the units, during the operation in a vibrating environment, the alignment constantly changes. Other weak features of this system are the pin bearings, interconnecting the concentric rings, and the off-plane mounting of the optics.

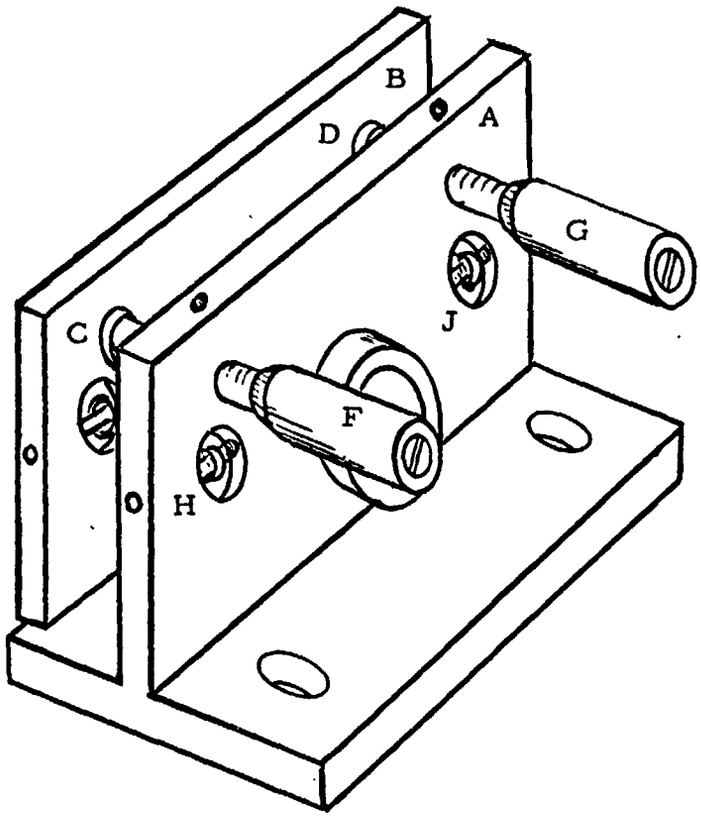

Plate "A" is rigidly mounted against the optical reference bench. Plate "B" is supported in three points, "C", "D", "E". Points "C" and "D" are spherical tips of two micrometers "F" and "G". The third point is a ball or pivot "E". The plate "B" is pressed against the points via springs "H" and "J". When adjusting micrometer "F", plate "B" moves in a plane defined by the connecting line of points "E" and "D". Similarly, adjustment on micrometer "G" causes plate "B" to move in a plane defined by rotational line connecting points "C" and "E".

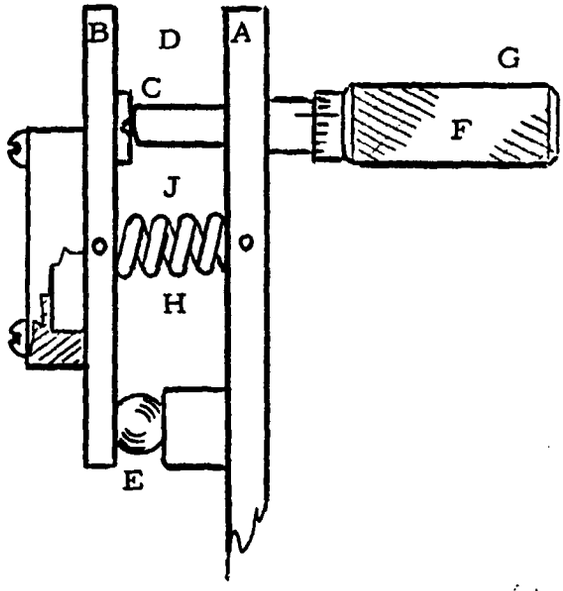

To prevent plate "B" from turning around the point "E", two "V" grooves are provided at points "C" and "D". The groove in pad "C" is parallel with the base of plate "A" and the groove in the pad "D" is perpendicular to the base plate. Therefore the two grooves are normal at each other. The rounded tips of the micrometers should slide in the grooves, but instead they "step" on the opposite edges of the grooves.

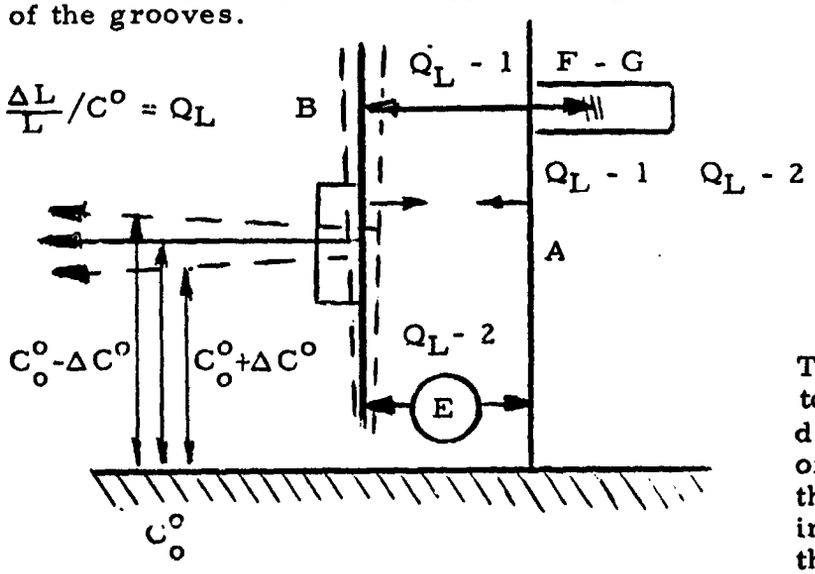

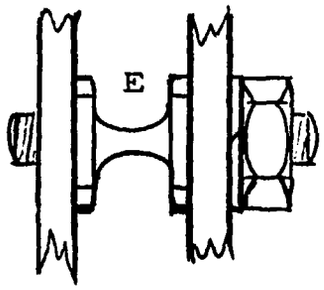

Thermally the mount is sensitive to variations, because of the different materials and lengths of these materials, connecting the plate "A" with "B". Changes in ambient temperature detune the laser.

Picture #28 Parallel Plate Optical Mount

The cross-cut optical mounts feature a thin wall, high compliance tube "A" with two sturdy flanges at the ends "B" and "C". The thin wall tube is provided with slots, two each, across each other on the opposite sides of the tube. Each successive pair of slots is rotated 90° to obtain a cross-cut pattern. Sometimes the thin wall cross-cut tubing is substituted by three springs. Flange "B" is mounted on a plate perpendicular to the optical base plate. Three screws are screwed into three taped holes in the base flange "B" passing through three clearance holes in the flange "C". The optical element is mounted in the recess "E" of the flange "C".

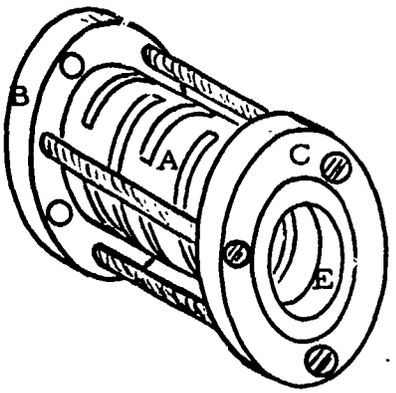

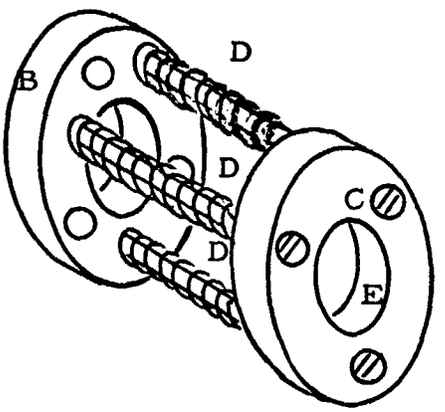

Initially the three screws are tightened, compressing and prestressing the cross-cut tubing "A" or the springs "D". Individual loosening of any screw will permit the flange "C" to rotate in the plane containing the connecting line determined by the other two screws. Note that the alignment system is not orthogonal! The temperature immunity of these mounts is superior to the parallel plate mount, but the shock and vibrational stability is inferior.

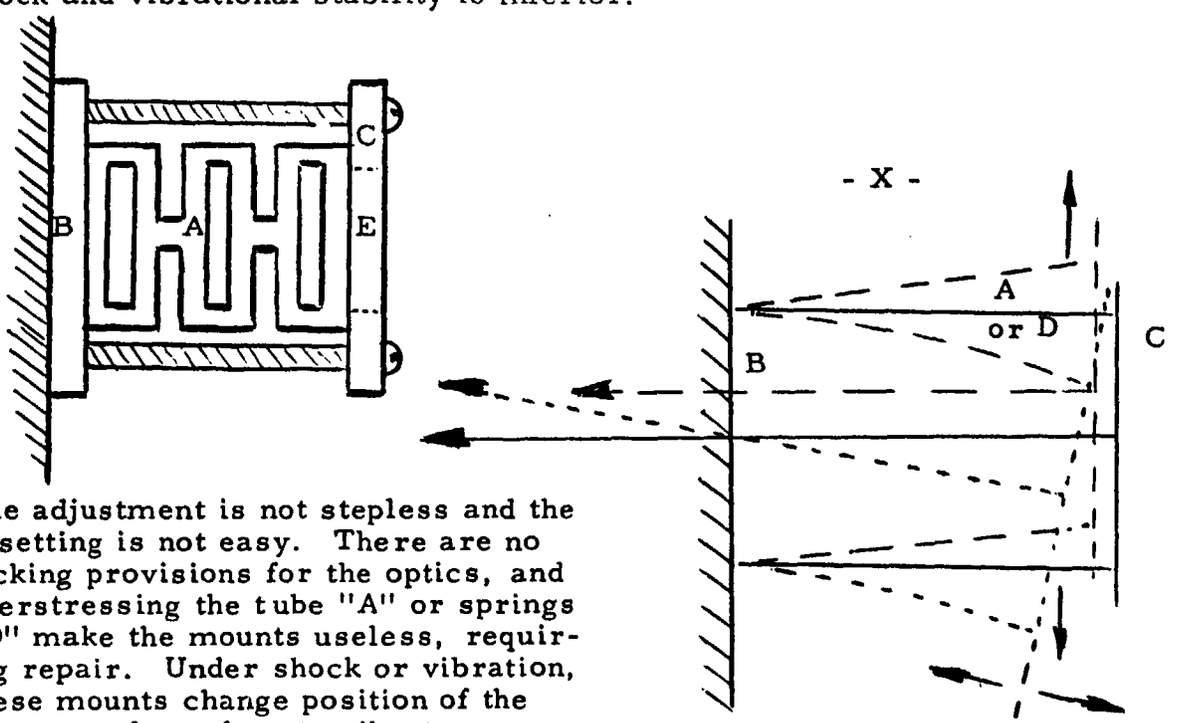

The adjustment is not stepless and the resetting is not easy. There are no locking provisions for the optics, and overstressing the tube "A" or springs "D" make the mounts useless, requiring repair. Under shock or vibration, these mounts change position of the flanges and are free to vibrate (as shown on detail "X") introducing material fatigue and failure.

Picture #29 The Cross-Cut and Spring Mounted Optical Mounts

The Cardan or Gimbal mounted optics is the most widely used optical suspension for laboratory or limited field use in lasers and other optical systems. They more sophisticated optically and more complex mechanically than all the other systems described. Unfortunately, they were designed for laboratory use with controlled environment in mind. No large temperature variations or shock & vibrations are allowable in use. Compared with the parallel plate or the cross-cut or spring mounts, this complex and sophisticated mount, suffers from all the ills of the previous mounts combined.

The mount features three concentric rings as the linkage between the optical reference base and the suspended optical element. The outermost segment "A" is mounted to the base and contains pivots "B" and micrometer "C".

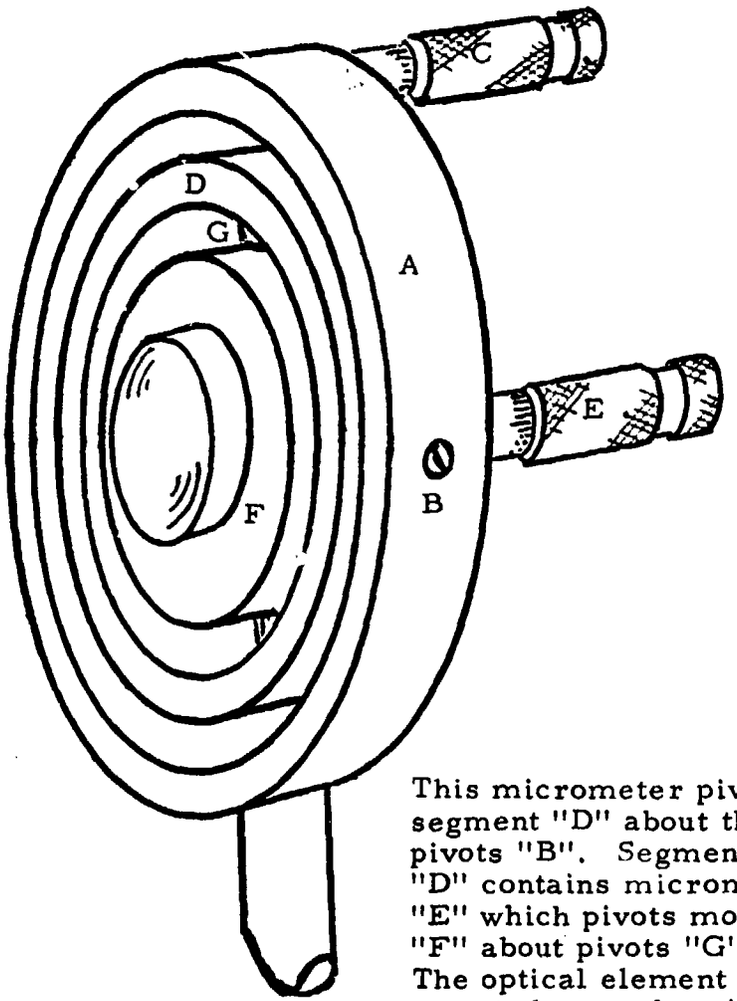

This micrometer pivots segment "D" about the pivots "B". Segment "D" contains micrometer "E" which pivots mount "F" about pivots "G". The optical element is mounted to surface "H".

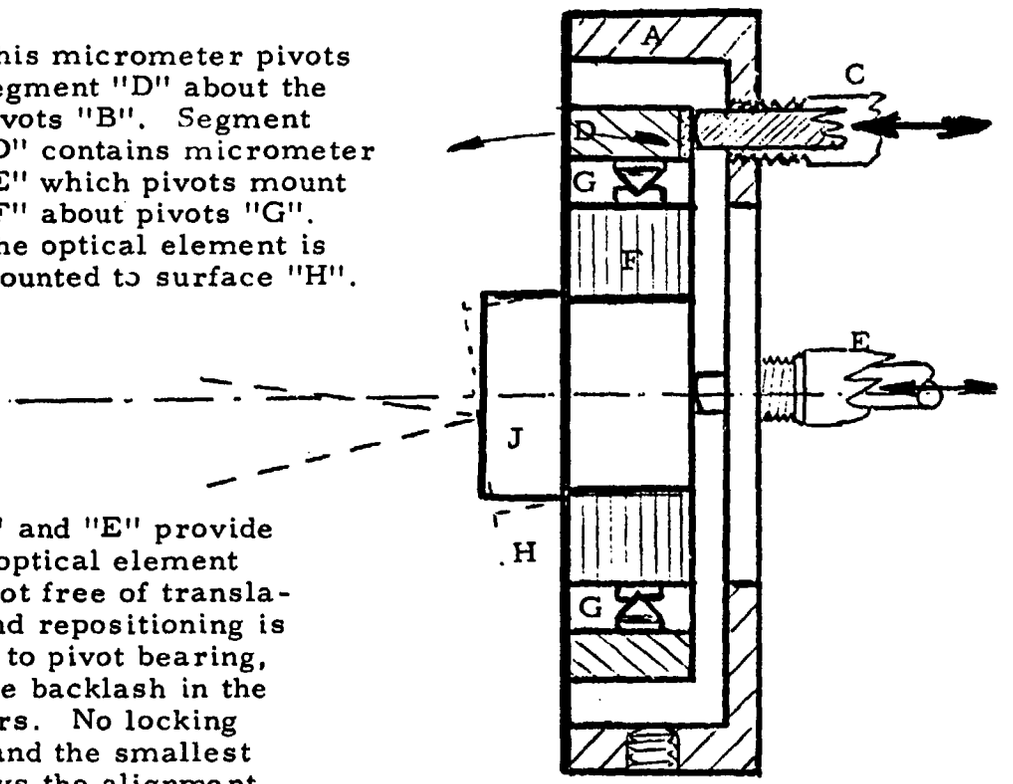

The two micrometers "C" and "E" provide orthogonal adjustment to optical element "J". The adjustment is not free of translation and is not stepless and repositioning is not accurate, largely due to pivot bearing, magnetic walk-off and free backlash in the threads of the micrometers. No locking provisions are available and the smallest shock or vibration destroys the alignment.

Picture #30 Cardan or Gimbaled Optical Mount

A large variety of optical mounts presently existing on the market can be traced to the four basic configurations, studied and presented herein. All the variations on the four basic concepts feature, primarily, changes in the details that do not influence the basic problems of each one of the basic design. Some feature increased radius on the bolt-circle of the adjustment screws or micrometers. Some apply differential micrometers to improve the adjustment resolution. Some use prisms instead of mirrors and others apply compound spring action to increase the rigidity of the mount. None of these refinements improve the stability or the immunity to shock, vibration and thermal perturbances of the optical mount.

Another area of the defficiency in the optical mounts is the method of fixing the optical element to the adjustable mount itself.

The optical element, usually glass, quartz or some optical crystal, is of a considerably different coefficient of expansion than the material of the mount, which is usually metal. The interface of the two represent a serious problem area and an ideal solution would be a grated transition similar to the grated seals between glass and metal, where the transition from the metal to the glass follows step with consecutively small differentials from one step to the next.

3.2.5 The New Ball-Socket Optical Suspension System

After years of study of the problem areas of the optical mounts, Raytheon LADC has developed an optical suspension, which is free of all the mentioned problems.

The basic principle of this suspension is a locking ball joint, with the center of the optical surface in the center of the ball.

This arrangement permits independent X-Y motion, by the sliding of the ball in the ball-socket. Once the alignment is achieved, a locking ring presses the ball against the socket and no further motion of the ball is possible.

During the adjustment the ball is spring loaded against the socket and this provides a smooth, stepless sliding motion. Due to the nature of the ball-joint, no translation is possible, and the beam does not "travel" on the surface of the optical element. The locked ball in the ball socket guarantees the highest possible resistance against shock and vibration.

The ball-socket optical suspension concept has other distinctive characteristics besides the mechanical rigidity and optical stability. The design of the supporting mechanical members was accomplished with perfect dynamic balancing for immunity from rotational and temperature variational perturbations. Complete axial symmetry of the elements guarantees immunity against dynamic unbalance at high "g" loadings and the thermal cross sectional symmetry permits large temperature variations without the danger of optical misalignment (see pictures

During the study, we have measured in our laboratory, the thermal effects on the largest selling laboratory precision mounts, of the type described in Picture #30. After mounting a mirror on the mount, a helium-neon laser was pointed at the mirror and reflected back on a meter scale on the wall. A precision thermocouple was mounted on the optical mount. The optical mount was aligned to a spot on the meter scale. The mount was heated by hot air to a temperature $50^{\circ}F$ above the ambient ($70^{\circ}F$). The spot traveled 3 mm, at a distance of 6 meters, indicating 10 microradians per degree (F) thermal drift.

3.2.5.1 Development of the Ball-Socket Optical Suspension

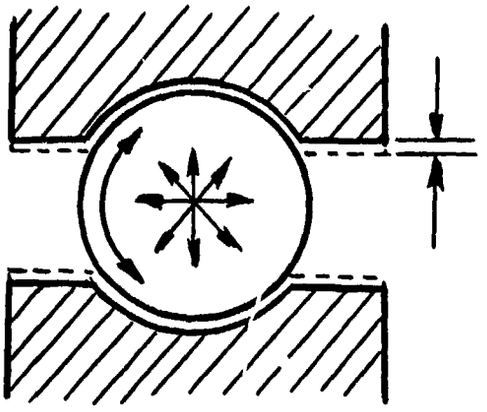

A sphere, located between two hemispherical sockets, and provided with a gap, has complete freedom of rotation in all directions. Applying pressure on the hemispherical sockets, the sphere is locked into a position, and will not be able to move, unless the moving force overcomes the resistance presented by the friction of the mating surfaces.

Addition of clamping screws to the ball sockets, a sphere located in between the sockets can be positioned in any orientation and then by tightening the screws, the sphere can be locked into alignment. A mirror mounted in the center of the sphere will reflect, but not translate any impinging beam of light.

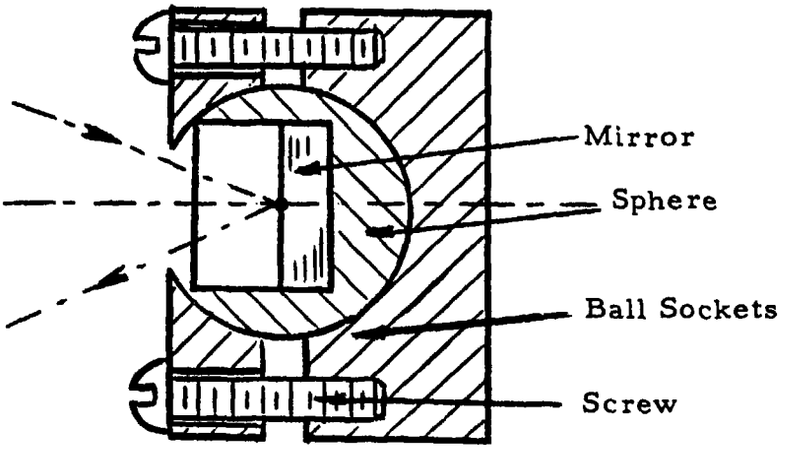

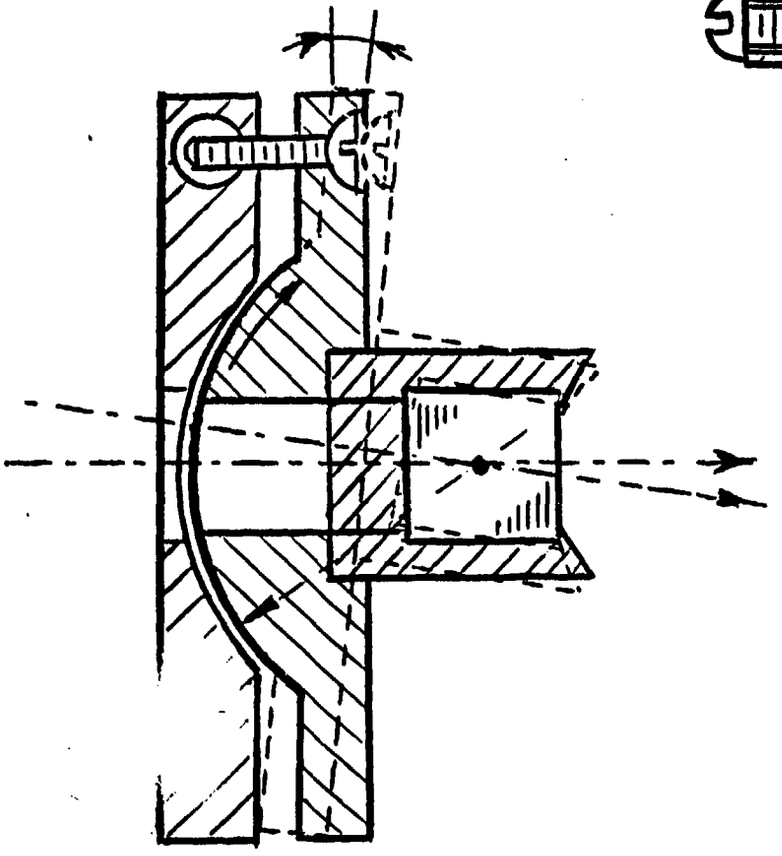

Cutting down the volume of the sphere to a segment of a sphere and placing the segment into a single spherical socket, we obtain the same freedom of movement and the locking capability. The radius of the curvature of the spherical mount is determined by the size and location of the optical element. To use a segment instead of a complete sphere is sufficient, because the required alignments of the optical elements seldom exceed $\pm 5^{\circ}$. The screws in this case serve not only for locking, but also alignment function.

Picture #31

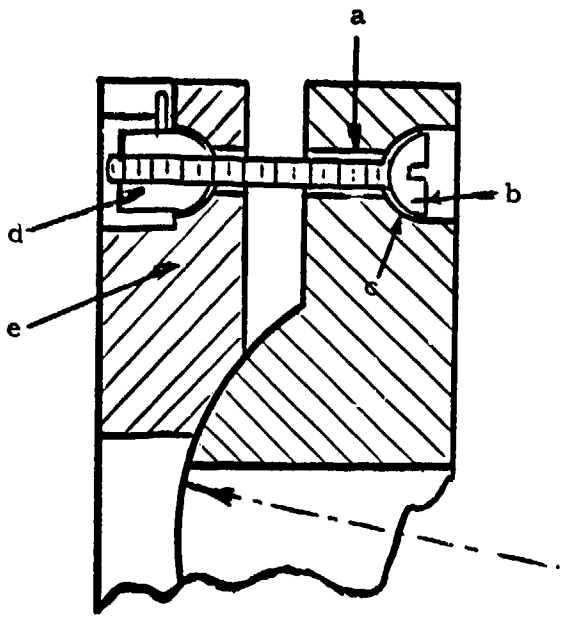

In practice a ball socket combination does not require contact on the entire surface of its members, the socket is reduced from a hemisphere to a countersink. The slanted contact surface of the socket is tangential to the surface of the sphere.

Since the clearance hole "a" describes a radial path during the adjustment of the screw "b" the head of the screw is hemispherical and rides in the spherical socket "c". To prevent the stress in the screw "b", a floating ball and socket type captive nut "d" is inserted into the socket "e".

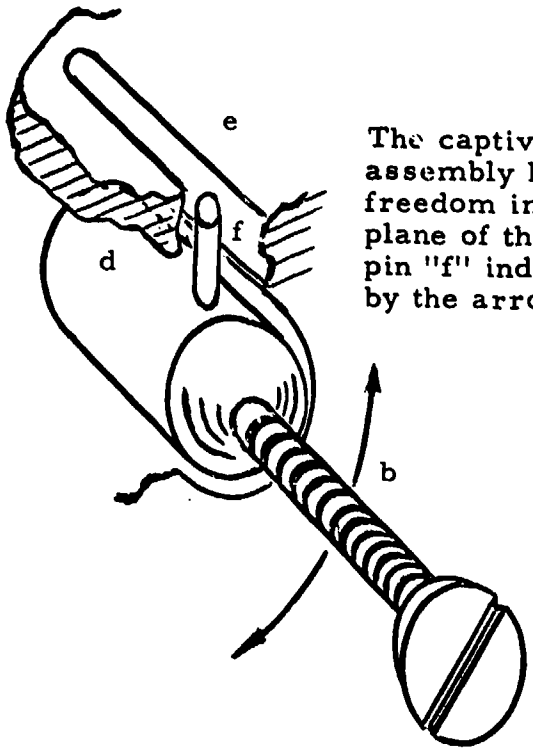

The captive nut assembly has freedom in the plane of the guide pin "f" indicated by the arrows.

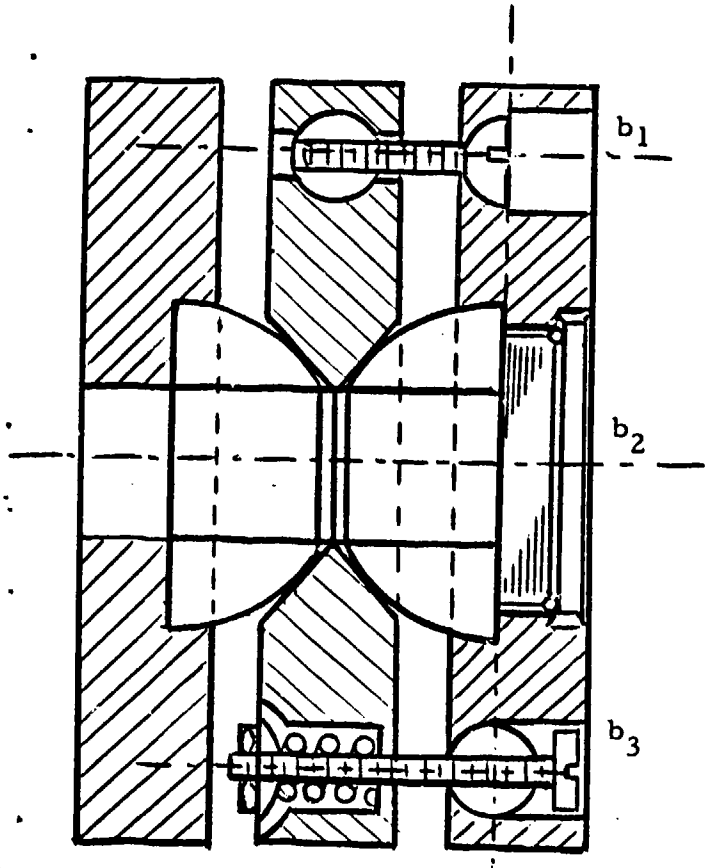

Picture #32

Two optical holders can be accommodated on the two sides of a common socket plate. The adjustment screws are located orthogonally (b_1 - b_2). The locking screw, b_3, is located opposite centered on the same bolt circle. The alignment begins with loosening of the screw b_3 and the optical holder is aligned with b_1 and b_2. Then b_3 is tightened locking the alignment permanently.

The two independent orthogonal adjustment screws b_1 and b_2 can position the centrally located mirror "m" into any position within a cone angle of 10°.

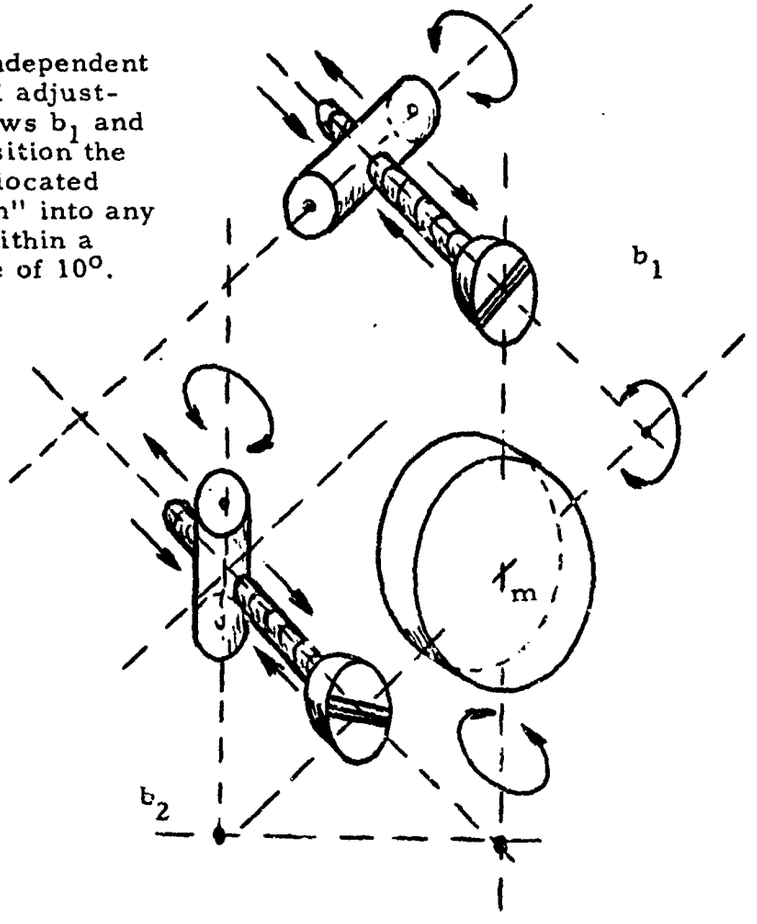

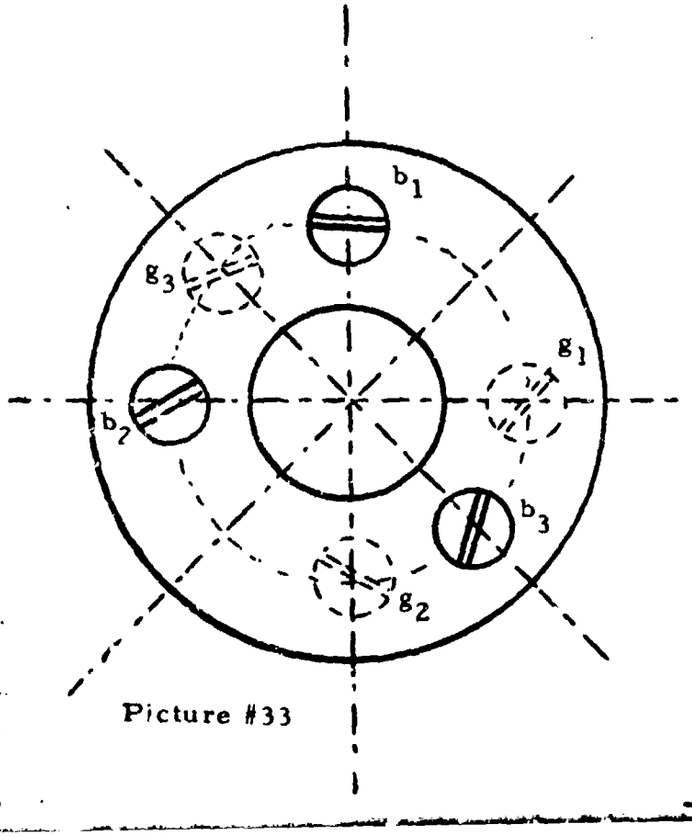

Picture #33

A typical rear view of a dual mount. Screws b_1 and b_2 provide for X and Y adjustments of the rear mirror. Screw b_3 is the corresponding locking screw for the rear mirror system. The "g_1" and "g_2" adjustment screws adjust the Pockels Cell located on the opposite side of the socket plate. This arrangement permits the alignment of the rear mirror and the Pockels Cell from the same location.

The permanent locking of the aligned optical mount is accomplished by the locking mechanism. The locking mechanism is comprised of, the locking screw "A", the universal joint "B", the return spring "C" and locking disk "D".

Drawing -X- indicates the relative location and the possible freedoms of motion for the key components of the locking mechanism.

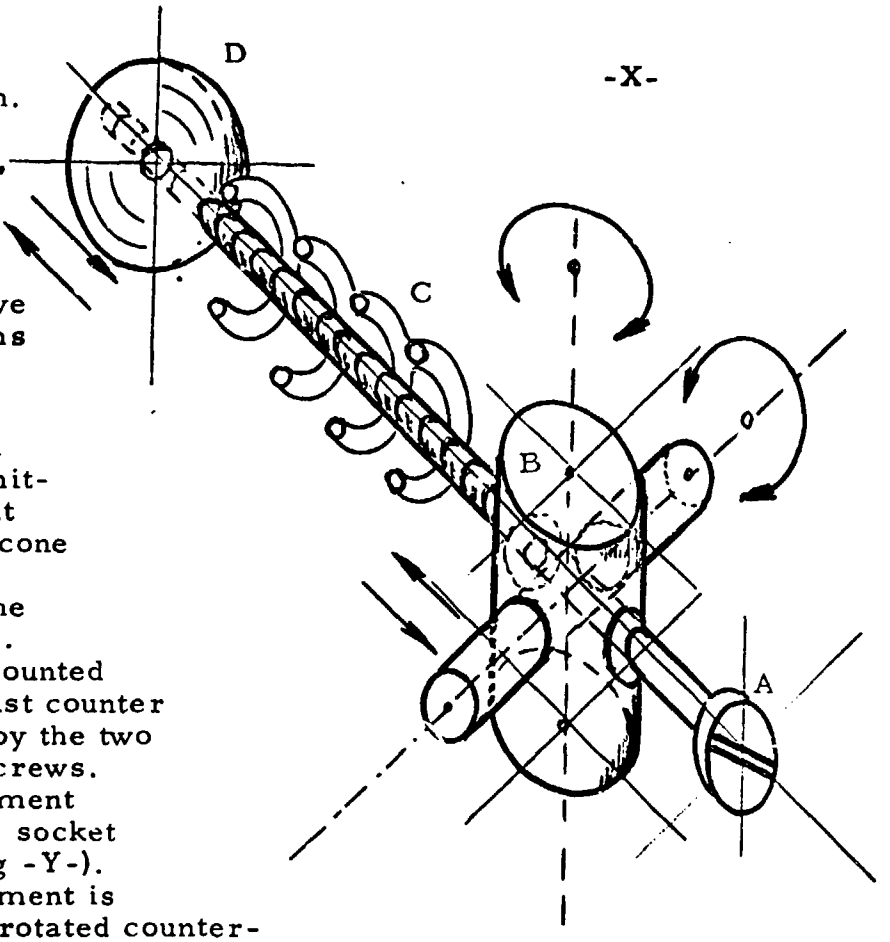

The universal joint "B" is seated in the stationary plate "E", permitting the screw "A" to rotate about its longitudinal axis limited to a cone of freedom of 10 degrees. This freedom is necessary to follow the deflection of adjustable plate "F". Spring "C" loads the plate "F" mounted sphere "G" into socket "H" against counter points "K" and "L" represented by the two orthogonally located alignment screws. Loosening or tightening the alignment screws, sphere "G" slides in the socket "H" in any direction (see drawing -Y-). Once alignment of the optical element is accomplished, the screw "A" is rotated counter-clockwise (unscrewed). This motion brings the locking disk "D" into intimate contact with the plate "F". In this position, plate "F" has no freedom of movement any longer.

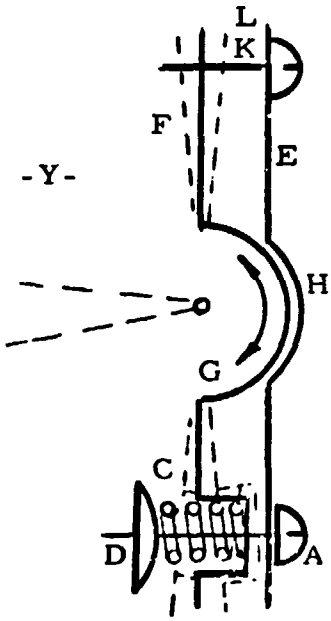

Picture #34

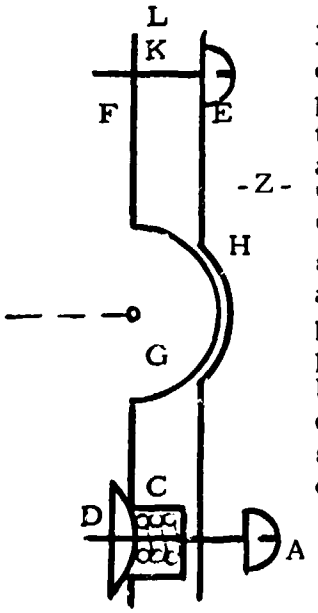

Drawing -Z- shows the optical mount in locked position. In this condition the orthogonally placed alignment screws "K" and "L" and the locking screw "A" are stressed in the same direction by the same amount of stress. The partial sphere "G" is pressed into the socket "H" by the sum of stress forces of "A", "K", "L" and it is stressed in the opposite direction.

Telescope Mount

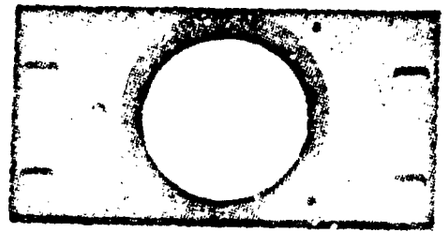

Socket Plate - Polarizer

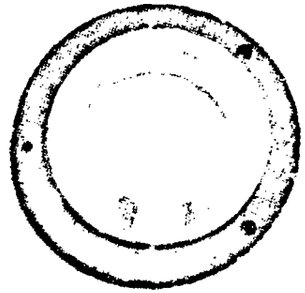

Mirror Mount

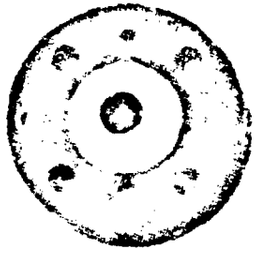

Socket Plate - Mirror

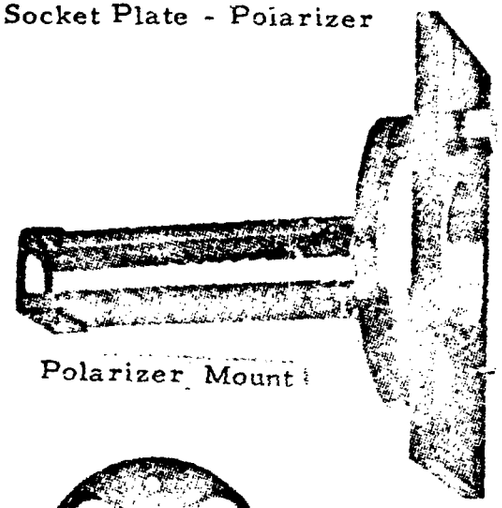

Polarizer Mount

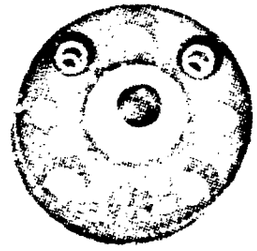

Prism Mount

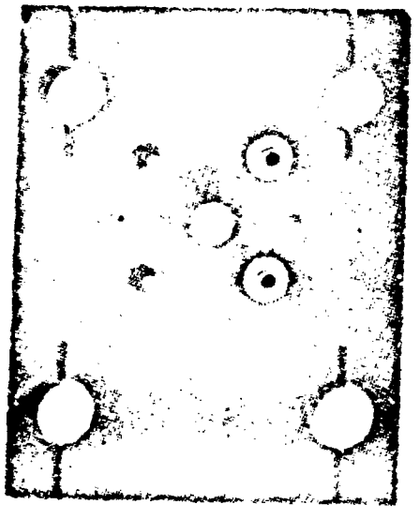

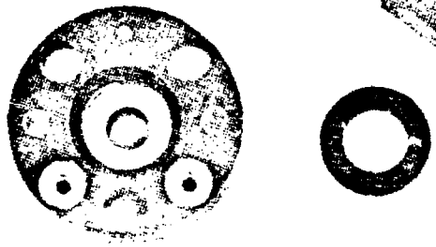

Mirror Mount

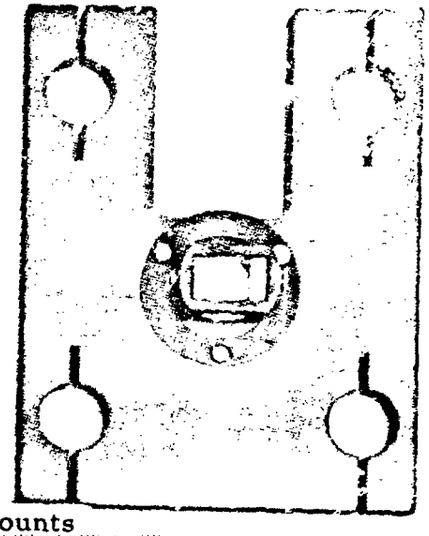

Raytheon Proprietary Ball-Suspension Optical Mounts

RAYTHEON

Picture #35

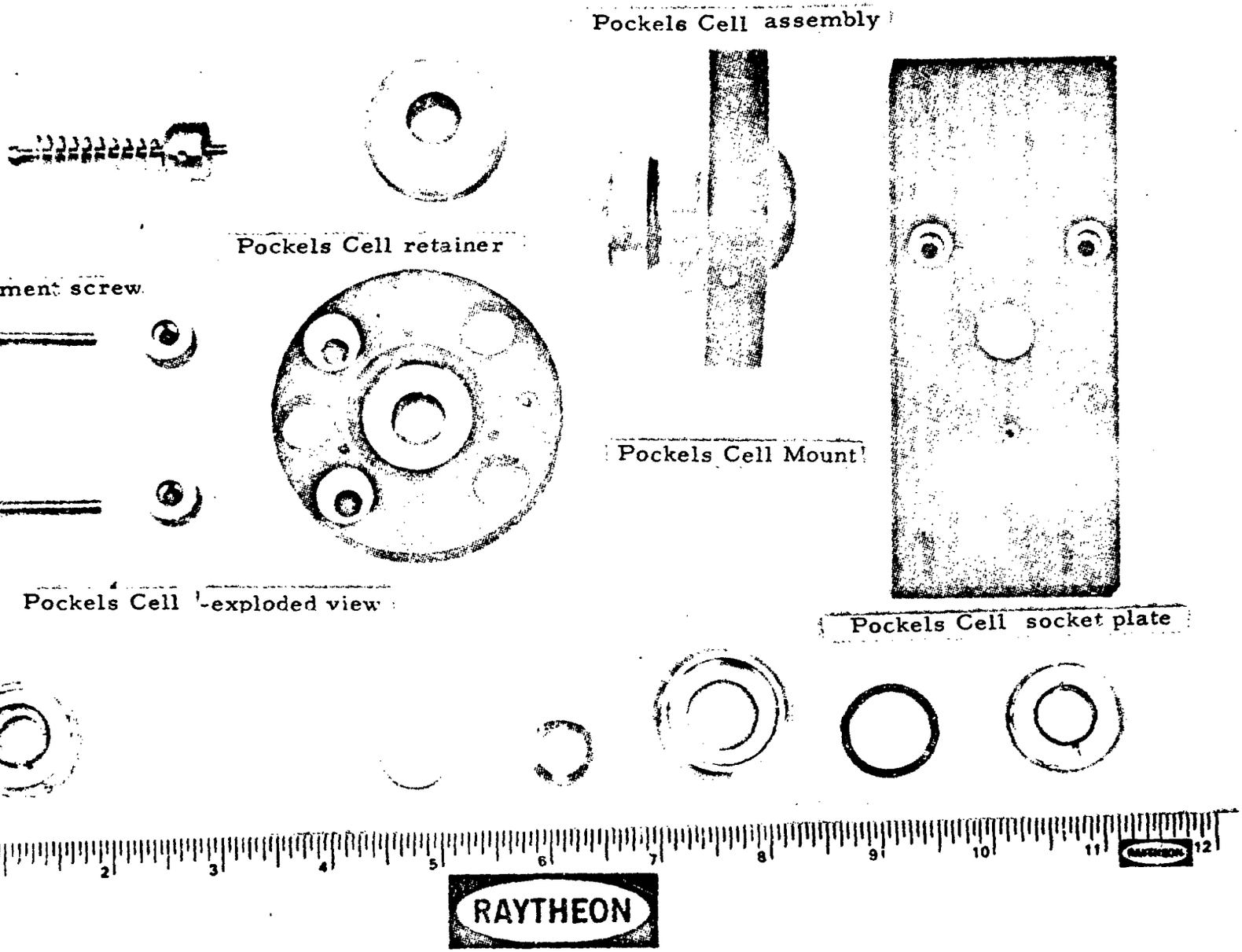

Raytheon Proprietary Ball-Suspension Optical Mounts

Picture #36

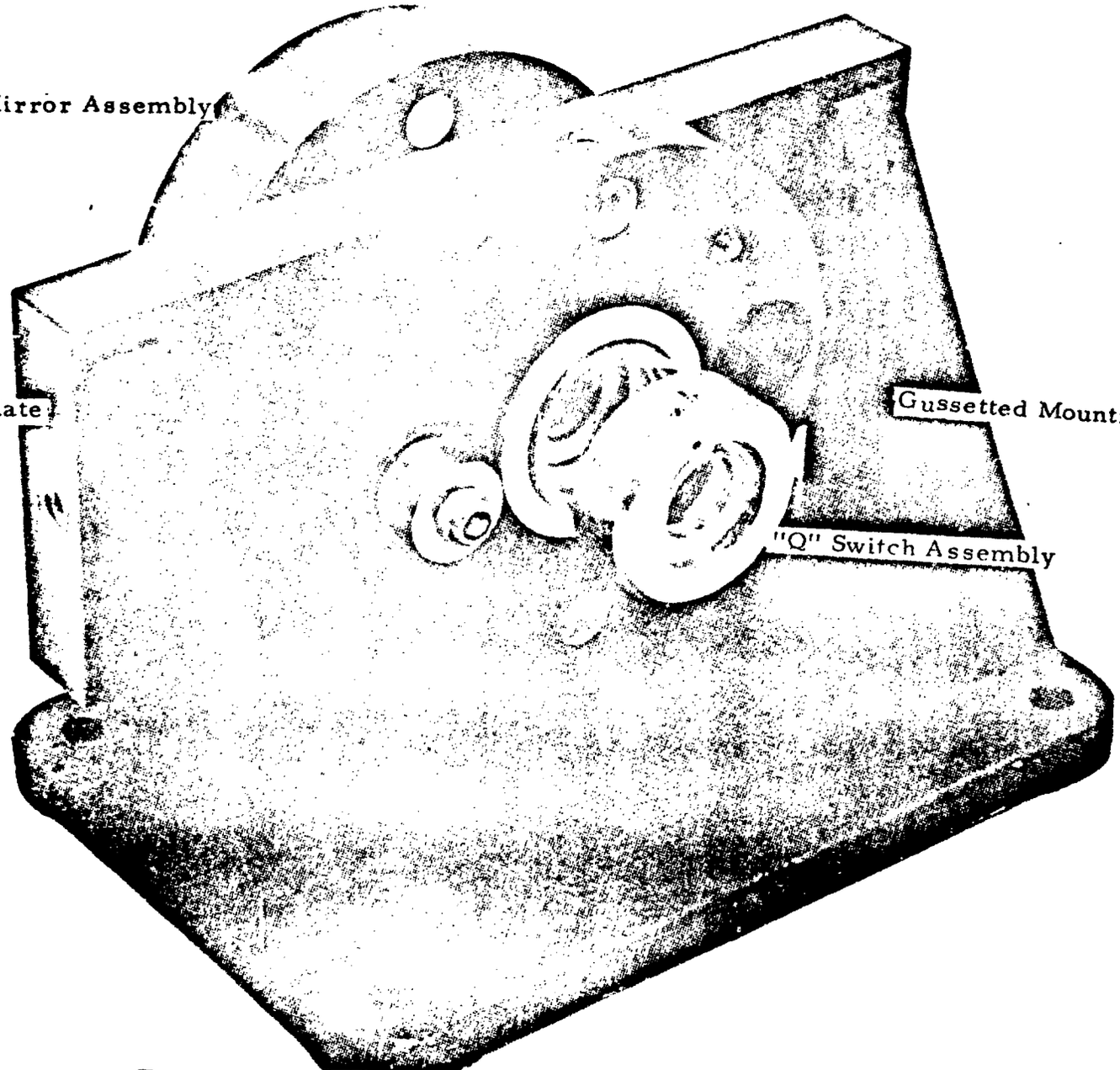

Picture #37

Typical Dual Ball-Socket Optical Assembly

3.2.5.2 The Ball-Socket Suspension in the SS-223 System

The Spaceborne SS-223 system requires a great deal of mechanical and thermal rigidity and stability. The extensive study of optical mounts convinced us to design the SS-223 laser system based on the ball-socket principle. The optical elements involved are; the front mirror assembly, the polarizer, Pockels Cell and the rear mirror assembly.

Since corrections of adjustments of the optical alignment are not possible during the lifetime of the laser, the simple clamping of the mounting sphere of the optical components was adopted.

Based on this clamping method, the necessary assemblies were designed and fabricated. After the fabrication, the components were assembled, the optical elements were installed and the first optical test of the laser cavity of the SS-223 system was conducted.

On the outset of the tests, two major areas of problems surfaced. One of the problem areas was the interface of the thermal contact from the flashlamp to the heat sink. The second area was the high voltage contact breakdown to the ground contact area.

The removal of the absorbed thermal energy from the flashlamp is accomplished by the electrical contacts interfacing the lamp electrodes with the heat sinks. The ground side of the lamp is thermally and electrically connected to the heat sink through a double cullet contact. The double cullet is formed from two independent finger-chucks, connected together at their bases. The larger diameter outer chuck is clamped into the ground side heat sink and provides thermal interface and electrical contact. The ground end of the flashlamp is inserted into the inner, smaller diameter finger chuck and provides the necessary electrical and thermal interface.

Since the two finger chucks are connected only at their common bases, the common base is floating and the inner finger chuck with the common foating base permits the inserted flashlamp axial, radial and nutating

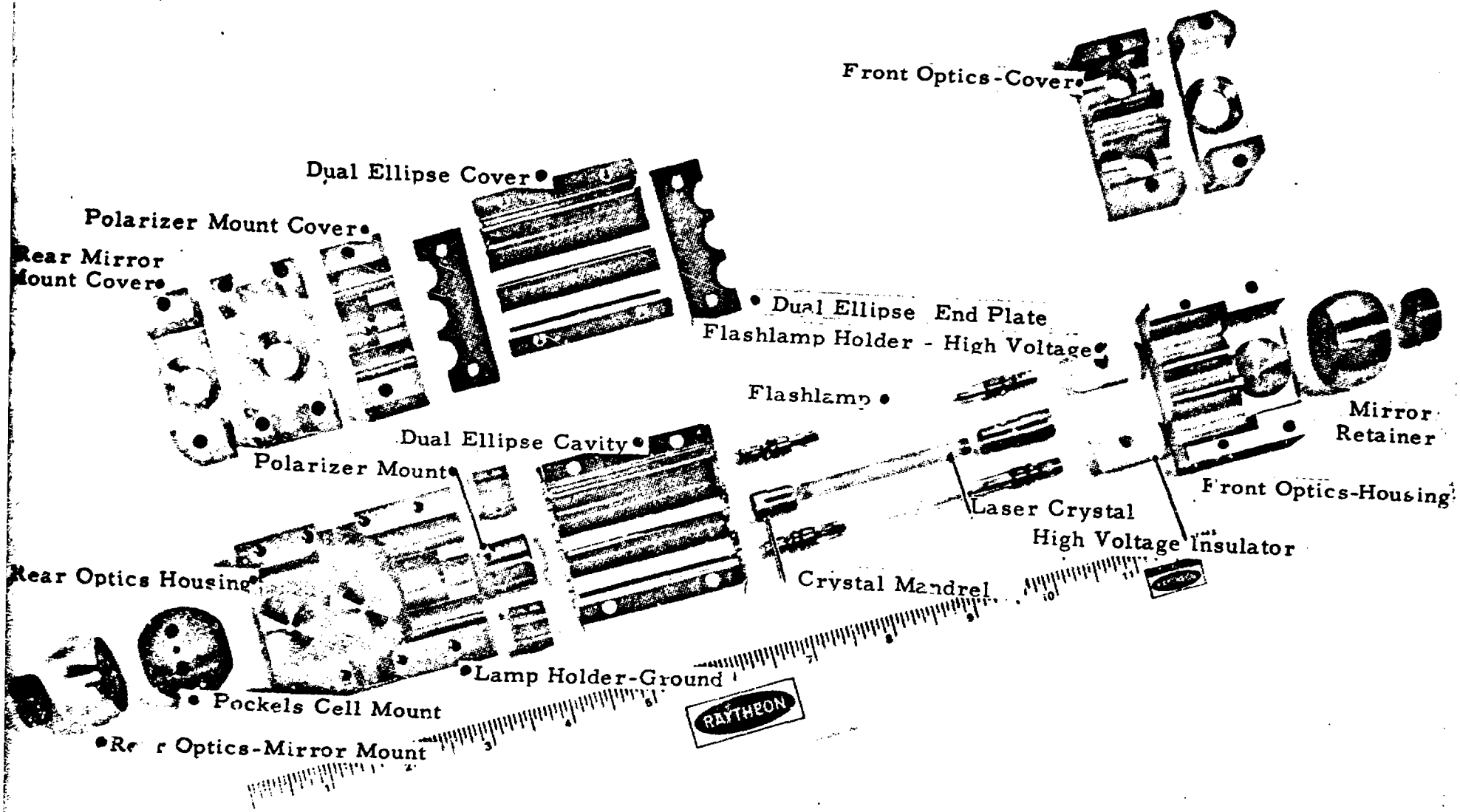

Picture #38 Space Hardened Laser Cavity - Exploded View

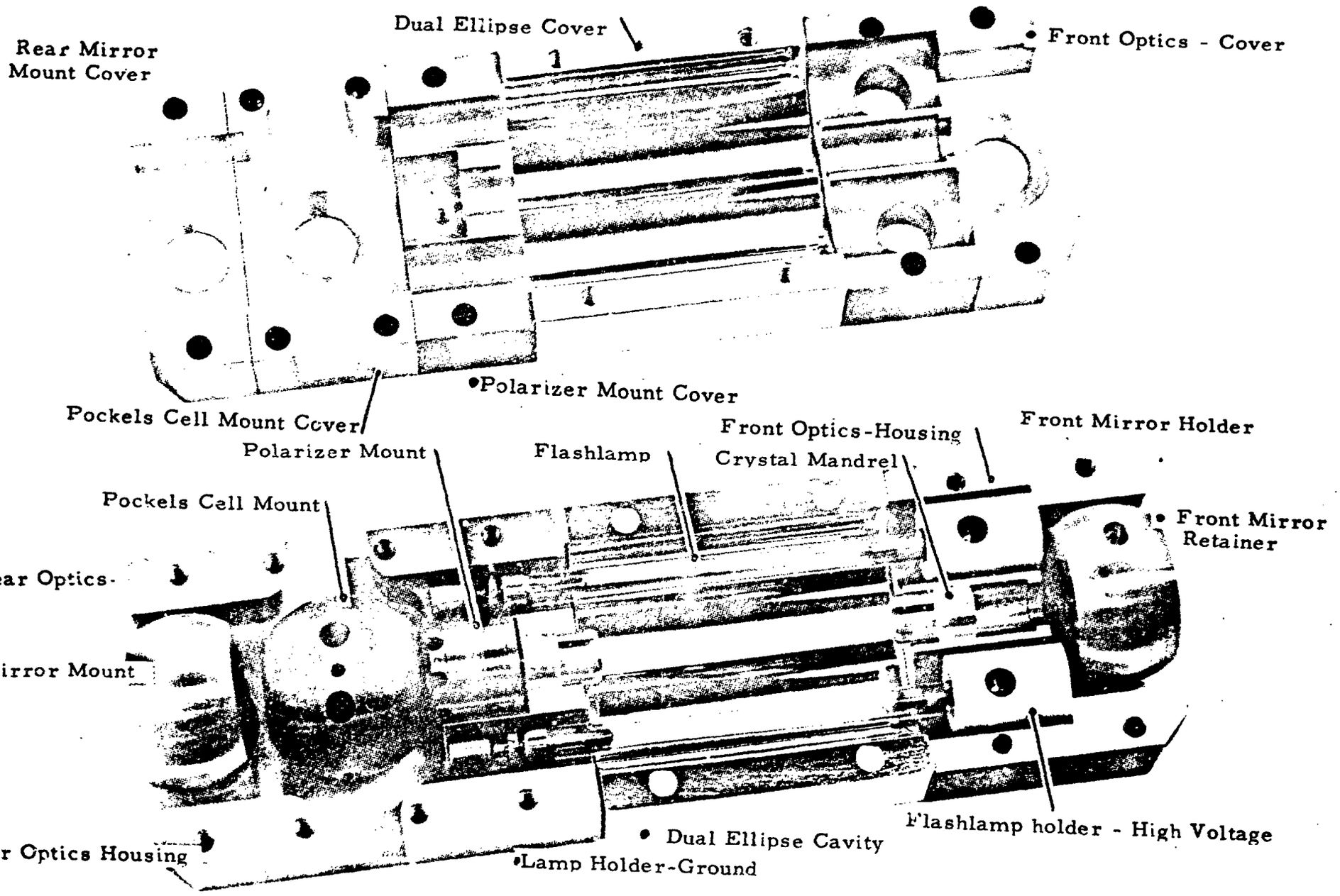

Picture #39

Space Hardened Laser Cavity and Cover

freedom. This freedom is necessary, because the large temperature differentials in the flashlamps produce considerable dimensional changes and introduce stresses and strain into the quartz or pyrex envelope of the flashlamps. The compliance of the double cullet, built up from the double coaxial finger chucks, protects the flashlamp against shock, vibration and thermal stress while providing good thermal and electrical conductivity.

The problem found with this interface was excessive brittleness of the dual cullet assembly. The defect was traced down to improper temper on the phosphor-bronze material used on the parts. Determining the proper annealing temperature, the newly fabricated parts were stable and no more catastrophic failures were recorded.

The high voltage end of the flashlamp has an identical dual cullet, except the high voltage end cannot be grounded and therefore an interface sleeving was developed to be used between the dual cullet and the heat sink assembly. The sleeving was fabricated from alumina and was metallized on the inner and outer surface for more uniform thermal loading. The metallization was not connecting the inner surface of the sleeving with the outer surface. A gap between the two metal bands provided high voltage hold-off of 20 KV in high vacuum and normal atmosphere.

The interface of the outer metallization to the thermal sink was accomplished by a special spring design, that provides simultaneously excellent thermal conduction and high mechanical compliance.

The breakdown of the high voltage end was traced to improper sealing techniques. The electrical seals were epoxy-bonded teflon and polyvinyl wire jackets. The bad adhering properties of several different brand epoxies eliminated the use of this sealing method. A redesign of the sleeving permitted an epoxyless seal and no more high voltage breakdowns were noticed. Solving the two main problem areas, we proceeded to test the resonator on the laboratory optical bench with external laboratory power supply. Alignment of the resonator was accomplished and normal mode (long pulse), lasing was obtained.

The polarizer and Pockels Cell were installed, and realigning the resonator, "Q" switched operation was obtained. The results are recorded on Picture #40.

3.2.6 The Mechanical Layout of the SS-223 Laser Transmitter

The satisfactory testing of the laser resonator led to the final layout design of the space hardened laser transmitter.

The temperature test series and simple laboratory induced shock and vibration (rubber mallet and mechanical vibrator) tests confirmed the soundness of the design. The size restriction of the available satellite space was determined as 8 inches of basic length and 4 inches by 4 inches as height and width, not including cable connectors, switches, mounting brackets and attachments.

Considering the rough 128 cu. inches of available space and subtracting 40 cu. inches for the housing, the remaining space of 88 cu. inches and estimated volume of 62 cu. inches of components determined a packing density of about 70%.

The layout was divided into three levels of cord wood type assembly. The lower level was reserved for the laser resonator and pulse forming storage capacitor.

The second level was reserved for the charging power supply and trigger circuits for the two flashlamps.

The third level was reserved for the timing generator, timing logic, multivibrators, "Q" switch logic and the T_o detector electronics. A Faraday shield was to be placed between the charging power supply and logic board. A fiber optics linkage is to carry the signal from the rear mirror to the T_o detector-amplifier on the logic board.

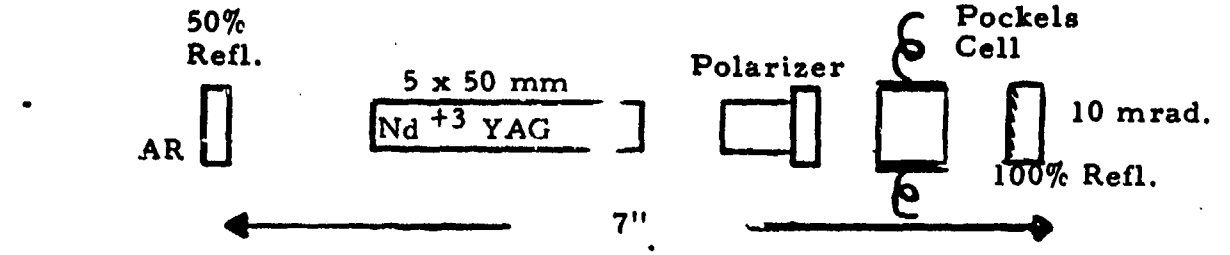

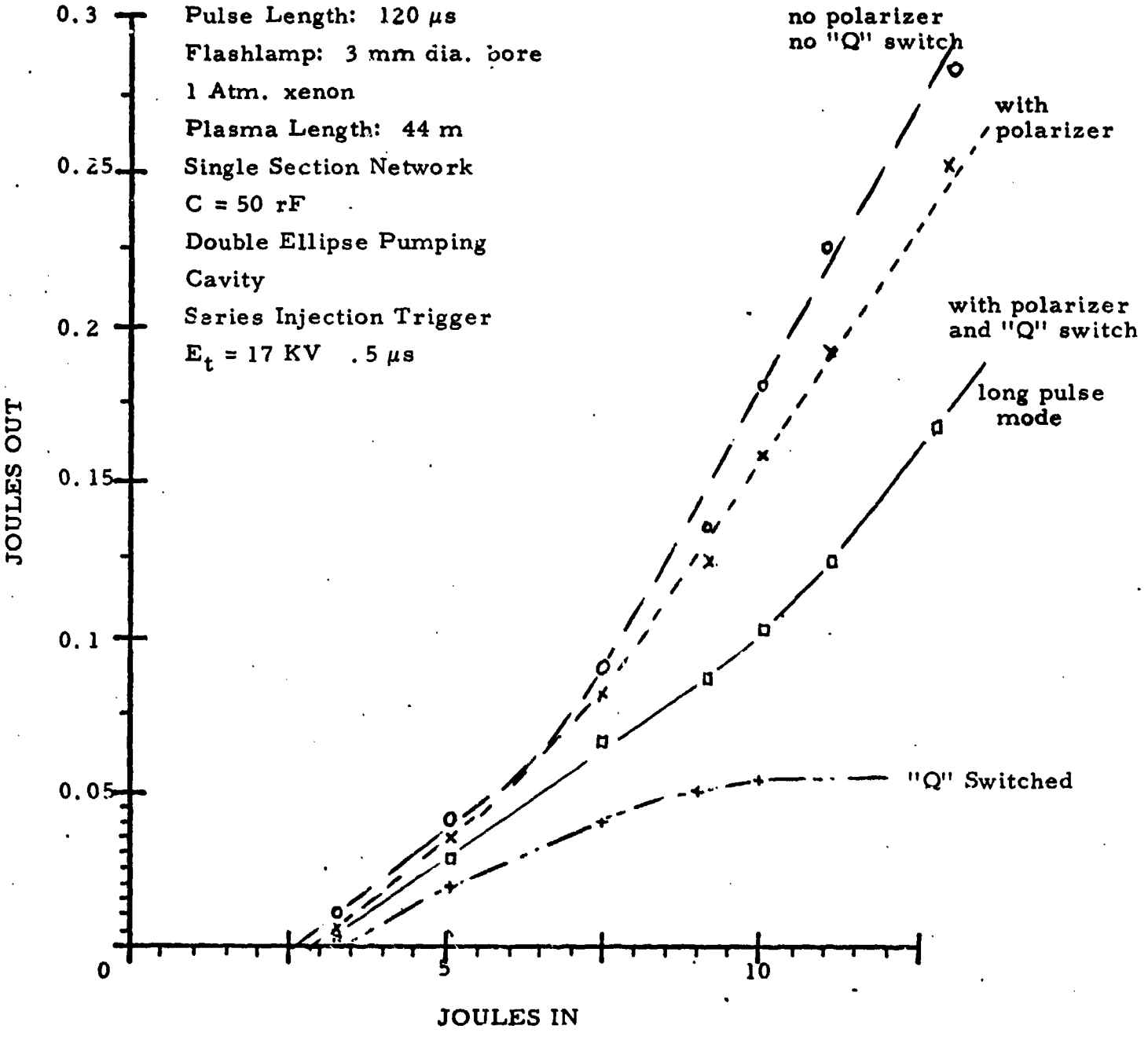

Input-Output Curves of the SS-223 System Operated from a Lab Power Supply at 1 PPS.

Picture #40

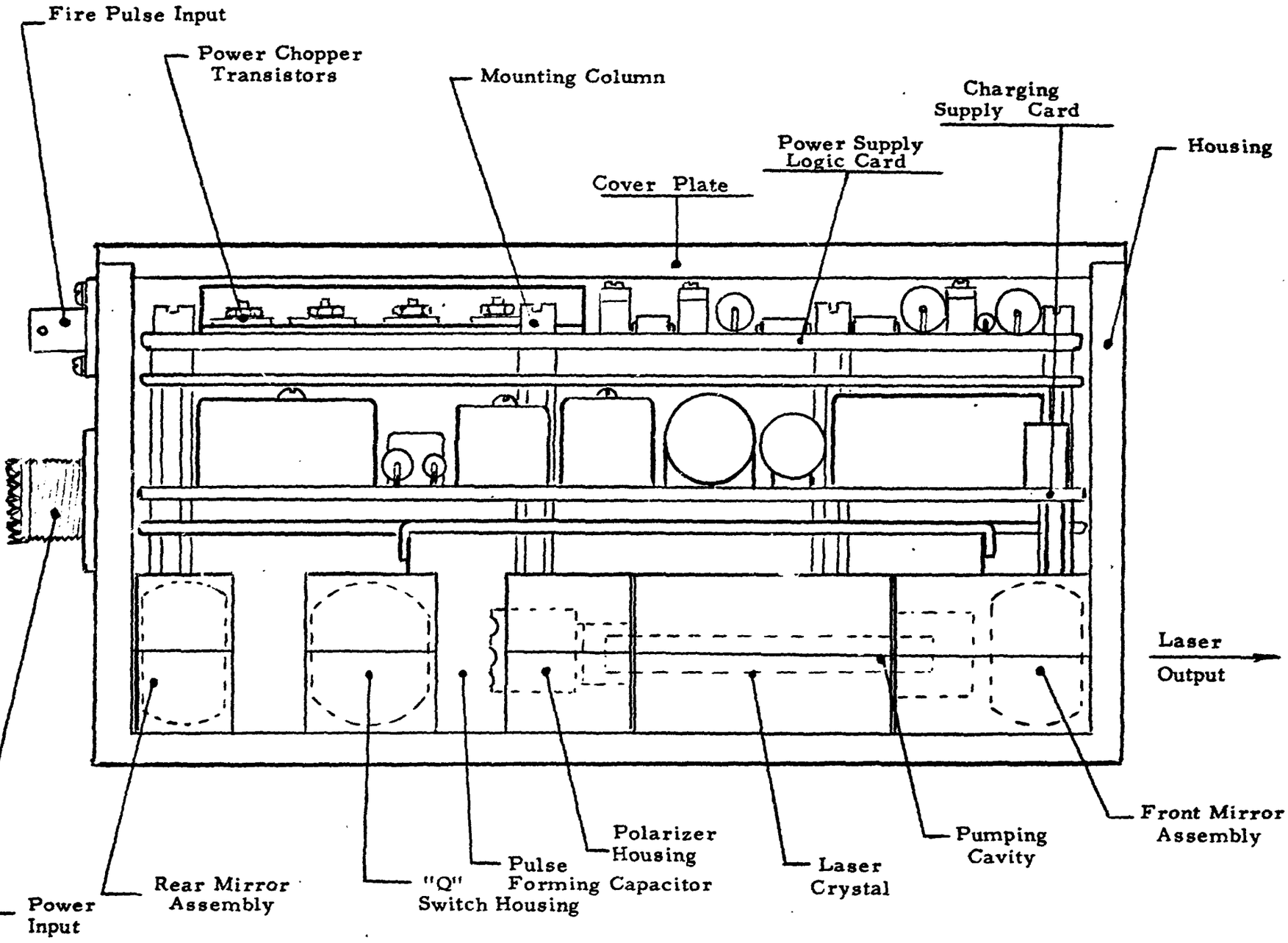

Picture #41 Side View of the Layout of the SS-223 Laser Transmitter

4.0 THE SPACE HARDENING OF THE ELECTRONICS

The space hardening of the electronics of the SS-219 ran parallel with the space hardening of the mechanics and optics. The first step covered the study of the existing SS-219 electronics comprised of the LPS-100AQ charging supply, the trigger supply and Q-switch supply. The charging supply bears the ESL-14871 PC board assembly number, the trigger supply is designated ESL-14885, and the Q-switch supply is ESL-14872.

4.1 Technical Description of the LPS-100AQ Power Supply

4.2 Inverter Power Supply and Logic

The driver and logic circuits for the LPS-100AQ power supply (see drawing ESL-51268) contain a variable frequency UJT clock operating at 20 KHz. This clock is an oscillator adjustable from 15 to 25 KHz. The master bystable oscillator operates at a rate of 10 KHz (one half of the clock frequency). The slave bistable is gated from an inverting AND gate, gated by the output level of the voltage sensing operational amplifier. When the voltage across the PFN capacitor is zero, the operational amplifier turns the inverting gate on and this turns the slave bistable oscillator on. The slave b.o. output drives a pair of buffer gates and they in turn drive the power transistor chopper. Through the power transformer and cascade doubler the PFN capacitor is charged up at a constant power rate up to 1000 VDC (adjustable). When the capacitor reaches the selected voltage, the voltage comparator operational amplifier turns the inverting gate off, which in turn shuts the slave off and it turns the buffers and the power transistor chopper off. This stops the charging process. After a certain time in single shot operation, the high voltage on the PFN capacitor will drop due to internal leakage and external bleed-off in the voltage sensing divider. This is sensed by the comparator, and the entire process starts up for a brief period of time. This replenishing rate oscurs at 100 millisecond intervals, in 20 millisecond bursts, at a voltage differential of 1% of the PFN voltage. The voltage comparator utilizes a reference Zener diode as comparative base.

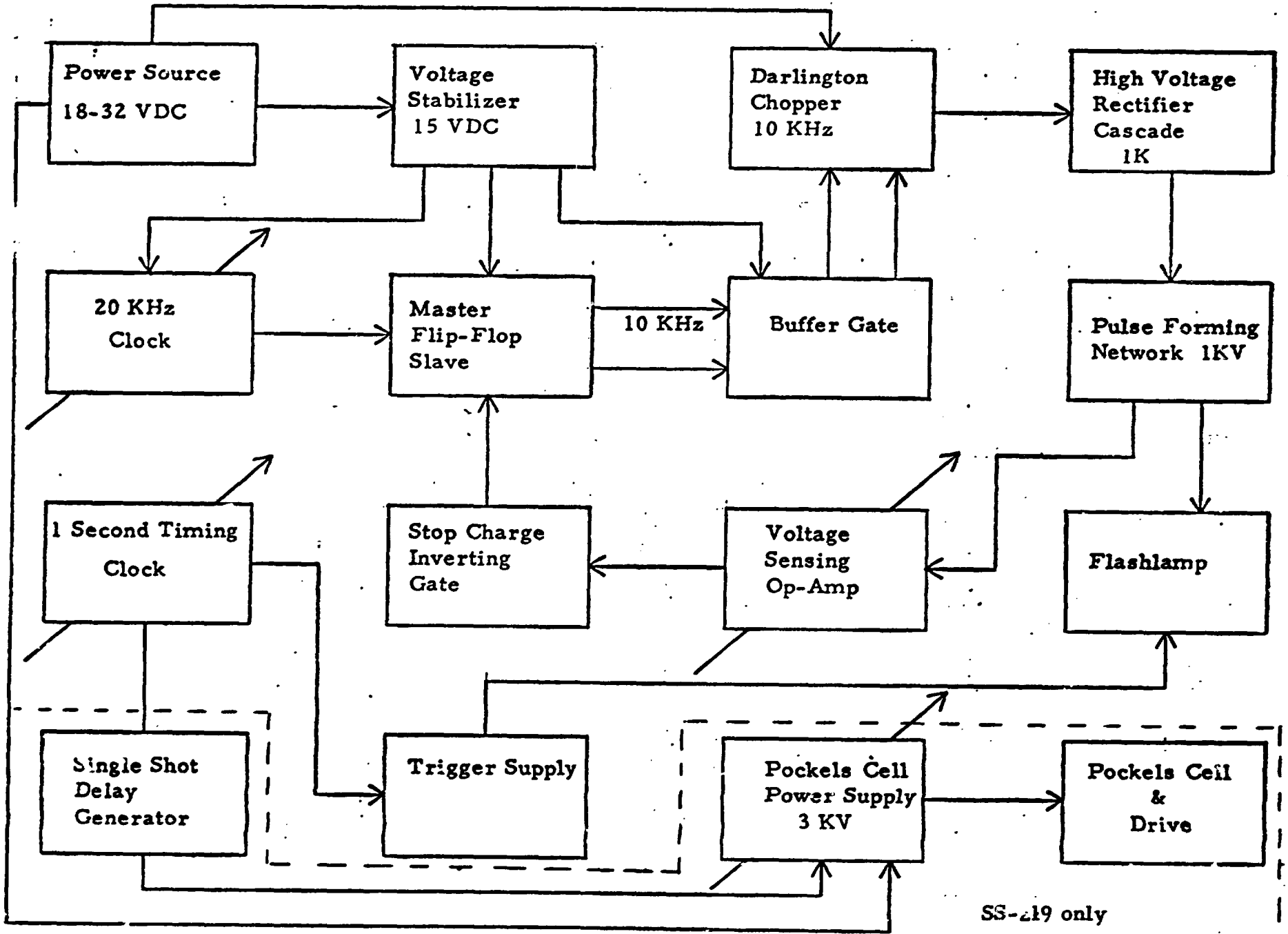

Picture #42

SS-359 and SS-219 LASER SYSTEM
LPS-100 POWER SUPPLY BLOCK DIAGRAM

REVISIONS				
ZONE	LTR	DESCRIPTION	DATE	APPROVED
1-2	B	[illegible]	[illegible]	[illegible]

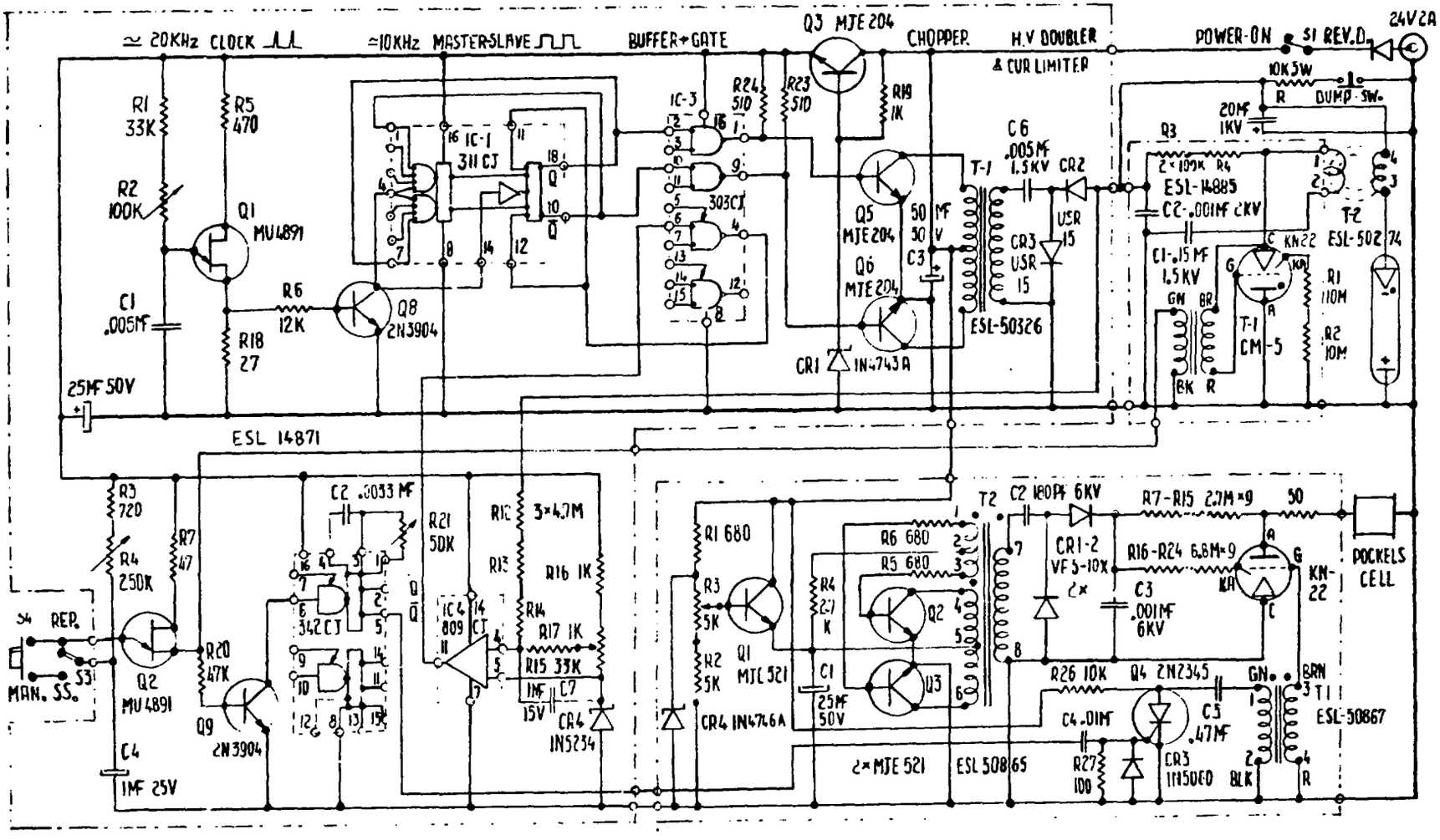

QTY REQD	CODE IDENT NO.	PART NO. OR IDENTIFICATION NO.	DRAWING OR SPECIFICATION NO.	NOMENCLATURE OR DESCRIPTION	FIND NO.

PARTS LIST

	SS 219
NEXT ASSY	USED ON
APPLICATION	

UNLESS OTHERWISE SPECIFIED DIMENSIONS ARE IN INCHES
TOLERANCES: ANGLES ±
FRACTIONS ±
3 PLACE DECIMALS ±
2 PLACE DECIMALS ±
1 PLACE DECIMALS ±
MATERIAL:

CONTR NO.
DR D. Gibson 6-14-71
CHK [illegible]
APPD
APPROVED Howard J Wargo Jr.
BY DIRECTION OF Howard J Wargo 8-29-71

RAYTHEON COMPANY
LEXINGTON, MASS. 02173

DRAWING TITLE
LPS 100AQ POWER SUPPLY
SCHEMATIC DIAGRAM

SIZE	CODE IDENT NO.	DRAWING NO.
C	49956	ESL-51268

SCALE ½ SHEET

Picture #43

The charging rate is a function of the input voltage and the value of the reactive limiting capacitor and the frequency of the clock. It is adjusted to 950 milliseconds charging time at the lowest (18V) battery voltage. With higher battery voltage, this charging time shortens to 450 milliseconds at 32V. The repetition rate of the power supply laser combination is given by the timing UJT clock. This clock is set for a 1 second rate.

When the system is switched to repetition rate mode, the clock and charging circuits start out simultaneously. At 950 milliseconds or sooner, the charging process stops and the system waits for the timer pulse. After 1 second from switch-on, the timer clock fires the trigger circuit,and through the flashlamp, the PFN capacitor voltage drops to zero. The voltage comparator starts a new cycle and the time clock fires at 1 second intervals.

In "Manual" mode, the same UJT clock starts out with the charging circuit, but it is inhibited from firing for the one second. After 1 second, depressing the manual FIRE button, the UJT fires on demand once, then it is inhibited for 1 second and the FIRE button does not operate during this inhibit interval. This feature prevents firing of the laser at lower than preset PFN levels.

4.3 Trigger Supply (See Drawing ESL-51268)

The trigger supply contains a storage capacitor .15 microfarads, a charging resistor, 200 kilo-ohm, a KN-22 Krytron, a pulse transformer, and a trigger transformer. The high voltage for the trigger capacitor is derived from the PFN capacitor and charges simultaneously with it, through the 100K ohm resistor. Upon the signal from the timing clock, the pulse transformer fires the Krytron, which in turn discharges the trigger capacitor through the primary of the trigger transformer. The secondary generates a 15 to 20 Kilovolt pulse and fires the flashlamp. This then discharges the PFN capacitor through the secondary winding of the trigger transformer.

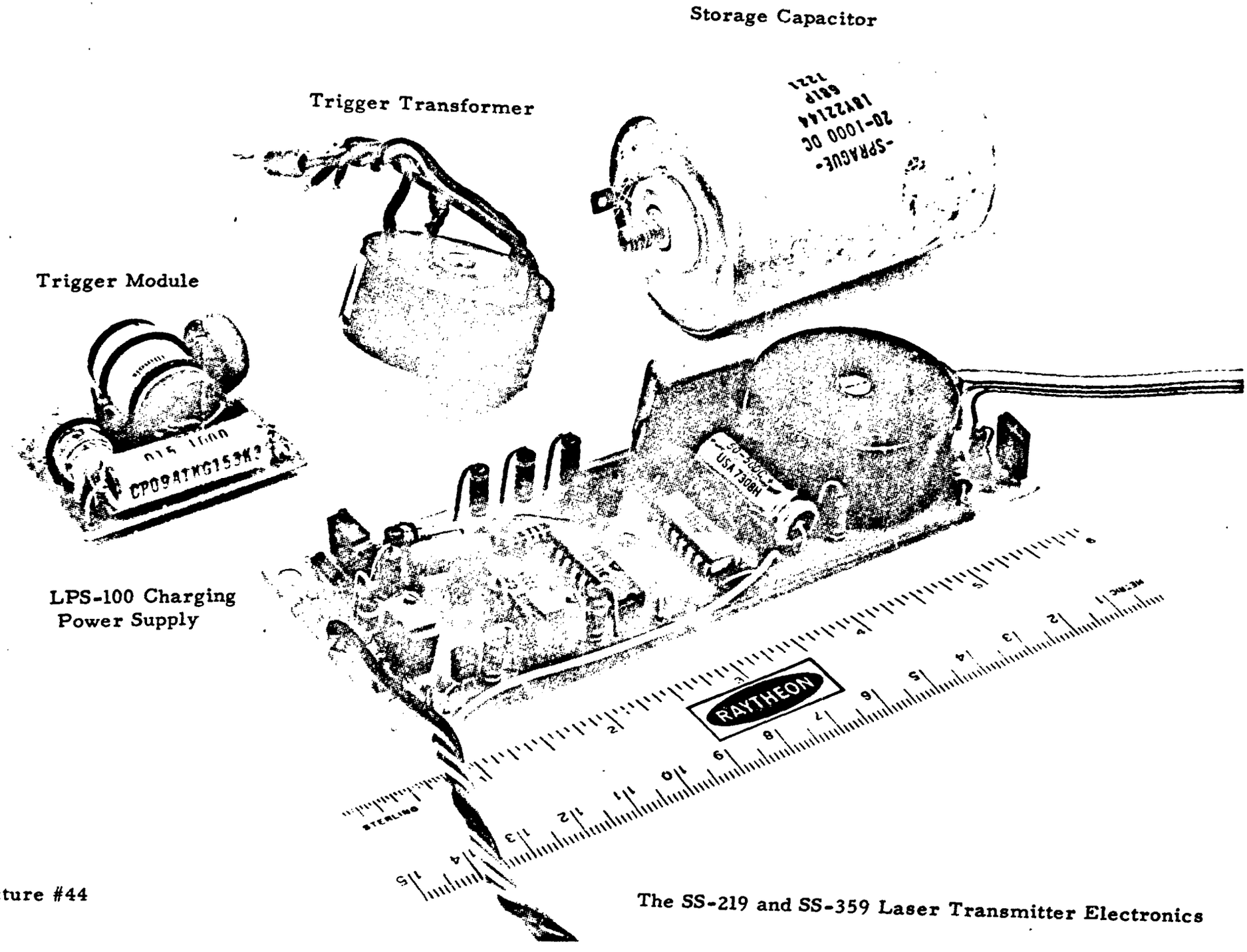

icture #44

The SS-219 and SS-359 Laser Transmitter Electronics

This trigger supply will operate satisfactorily with voltage between 700 and 2500 VDC on the PFN capacitor.

4.4 Q-Switch Supply (ESL-14872)

The Pockels Cell electronics contains a DC to DC inverter supplying 2-3 KV (adjustable), an SCR, Q-switch capacitor, pulse transformer, Krytron and the cell load resistor.

The 24 VDC id derived from the unregulated +B supply. This voltage is applied to a series regulating voltage stabilizer. The emitter-base voltage of the Q_1 series pass transistor is stabilized by the reference voltage developed across the voltage divider, R-2, and the adjustable, R-3, stabilized by CR4 reference zener diode. Adjustment or R-3 tap-off will change the level of the stabilized voltage. The stabilized voltage across capacitor C-1 supplies the self-excited chopper supply comprised of power transistors Q_2 and Q_3 and transformer T-2. The secondary of T-2 comprises a series reactance capacitor C-2, storage capacitor C-3 and two high voltage diodes CR-1 and CR-2 in voltage doubler (full wave) connection. The high voltage stored on C-3 is connected to the Pockels Cell high voltage terminal via R-7 through R-15. R16 through R-24 supplies the "keep-alive" terminal of the Krytron KN-22. The flashlamp firing pulse generated by pulse rate clock is delayed in the 342CJ delay 1C, about 120 microseconds. The delayed pulse fires SCR CR-3, which discharges capacitor C-5 through the primary of transformer T-1. The secondary of T-1 generates a pulse of about 450 VDC and applies it on the grid of the Krytron KN-22. The KN-22 is triggered into conduction, and acts as a short circuit across the Pockels Cell, removing the electrical field from the crystal. The crystal without the field applied, passes the laser radiation and permits the generation of a giant pulse.

4.5 Radiation Study of the LPS-100 AQ Power Supply

A space radiation effects analysis was conducted on the LPS-100 power supply for both permanent and transient degradation. The external free-field environmental levels were defined by

Dr. S. Mellman of NRL. The levels were based on a five-year mission life with the satellite in a synchronous orbit at approximately 600 nautical miles. The free-field environments were defined as:

Electron Fluence - 5.7×10^{10} e/cm^2 (E=1 MeV *YAG*)
Proton Fluence - 10^{13} p/cm^2 (E=1 MeV *YAG*)
Total Dose - 10^6 RADS (YAG)

The conversion factor for RADS (YAG) to RADS (Si) was defined by Dr. Mellman as 1.06. For all practical purposes, YAG may be considered to be interchangeable with Silicon with no loss to the analysis.

In translating the free-field environments down to the electronics levels, a total aluminum shielding thickness of 300 mils was used. For proton translation, it was assumed that the 10^{13} p/cm^2 free-field level had an energy spectrum based on Van Allen belt radiation. The same assumption was used for electron fluence translation.

The reason for this translation was to optimize, to the fullest extent possible, the effects of shielding of the satellite and equipment packaging for a resultant comparison to known proton fluence data in a 20 MeV monoenergetic range.

For permanent damage effects the following items were found to be deficient:

- MJE 340 Transistor
- MU4891 Unijunction Transistor
- Pockels Cell

The MJE 340 and MU4891 problems can be solved by proper preselection and adjusting circuit characteristics to accept the degradation; the Pockels Cell must be total dose tested to accurately estimate the nuclear effects.

For transient effects, it was determined that the LPS-100 can operate through the estimated transient environment.

Data/Calculations

The data and analysis presented herein are based on generalized effects and parts information within the agreed scope of work. As such, the effects data presented herein should be utilized as being only indicative of the effects on the power supply; those areas which present serious problems should be examined in greater detail and possibly be subjected to verification tests.

The Internal Radiation Environment

In order to relate the specified free-field environment to effects on components, the following steps were taken:

- The total thickness of the satellite and electronics packaging was determined (approx. 300 mils).
- The electron and proton stopping ranges (aluminum) were determined.
- The free-field fluences were then adjusted using typical Van Allen electron and proton energy spectrums (Ref. 1).

Electron Fluence

Figure A-1 shows the range curve and stopping power for electrons in aluminum. For 300 mils or 2.3 g/cm^2, it is seen that electrons with energies less than 4 MeV are stopped by this thickness of aluminum. Noting the worse case electron curve of Figure A-2, it is seen that 2-3 orders of magnitude reduction in particle fluence is obtained. This would reduce the free-field environment from 5.7×10^{10} e/cm^2 to 5.7×10^{8} e/cm^2.

Proton Fluence

Figure A-1 also presents the range curves and stopping power for protons in aluminum. For 300 mils or 2.3 g/cm^2, it is seen that protons with energies less than 70 MeV would be attenuated completely.

Referencing the proton data of Figure A-2, it is seen that a factor of 30 reduction in the free-field environment is obtained. Essentially, this reduces the internal environment to approximately 3.3×10^{11} p/cm^2. The calculation shows the typical anticipated response; specifically, proton fluence is less conducive to being attenuated than are electron fluences. In addition, the electron and proton spectrums will "harden" in content, and therefore, for the purposes of proton effects analysis, the attenuated energy spectrum will be assumed to lie above 20 MeV.

Total Dose Environment

Because the total dose environment is essentially a function of the electron/proton depositions, the external free-field total dose will be reduced by at least a factor of 10 or greater. For the purposes of analysis, the internal total dose will be assumed to be 10^5 RADS (Si).

Permanent Damage Effects

In order to assess permanent damage effects on the LPS-100, data was abstracted from References 2 and 3. In order to assess the effects of electron radiation on general power diodes, data was analogized to neutron effects on these devices. Figure A-3 presents data on the known effects of electron and proton fluences on semiconductors. Figure A-5 presents neutron effects data on capacitors; Figure A-6 presents neutron effects data on resistors. Figure A-7 and A-8 present neutron effects data on general electronic components.

Using this data, it is now possible to assess the effects of electron/proton fluences on LPS-100 components. For ease of summary, the effects analysis is presented in Table 1.

It must be stressed that the data presented in these figures is general in nature and should be used only as an indicator; failure levels defined in the data may, in particular design applications, be quite acceptable.

On the basis of the data presented in Figures A-3 through A-8, the following considerations were struck from the analysis:

- o Effects on Resistors and Capacitors
- o Effects on Tube Devices
- o Effects on General Electronic/Electrical Items (Piezoelectric crystals, meters, relays, etc.)

Transient Effects

The specified internal total dose of 10^5 RADS (Si) is produced by the energy deposited by the combined electron and proton fluences. To take the specified total dose and amortize it over a five-year operational lifetime is not acceptable.

In order to arrive at a meaningful dose rate estimate, the use of auroral and solar flare data was made. Reference 4 provides such data and this data is summarized in Table 2-2.

Table 2-2
Summary of Auroral/Solar Flare Data

Type	Fluence		Dose Rate	
	Electrons $e/cm^2/sec.$	Protons $p/cm^2/sec.$	Electrons (r/sec.)	Protons (r/sec.)
Auroral	10^{11}	10^5	2.8×10^4	1.4×10^{-1}
Solar	-	10^4	-	2.8×10^{-2}

Accordingly, the highest dose rate observed is in the order of 3×10^4 roentgens/second. It should be noted that this dose rate is a surface dose rate on the exterior of the vehicle or satellite. The proton dose rate could be lowered by an order of magnitude in passing through the satellite and electronics package skin.

In past experience on IDP's and other test programs (Ref. 5), discrete transistors and diodes showed no measurable photocurrent generation at dose rates on order of magnitude and greater above the estimated internal dose. Integrated linear/digital logic circuitry showed no false switching at dose rates an order of magnitude, and higher, in

comparison to the dose rate estimated for the ILS-100. It is therefore concluded that the ILS-100 can operate without any transient malfunction in the specified environment.

Conclusions/Recommendations

Permanent Damage Effects

In assessing permanent damage effects on the ILS-100, the following items were noted to be either failures or at least questionable:

- Transistor 2xMJE340 - Will undergo severe β decreases (60-70%). The device should have preselected β characteristics corresponding to the minimum required β for proper operation, with degradation at the specified fluence (and low temperature) taken into account.
- MU4891 - Unijunction transistor will undergo severe increases in threshold to fire voltage characteristics. Three options are available to solve this problem: a) Perform definite testing to accurately substantiate effects, or, b) Replace the device and circuit concept in entirety, or, c) Adjust circuit capability to perform with degraded threshold to fire characteristics.
- Pockels Cell - Device is questionable at the specified total dose levels. Testing must be performed to ensure operability to the same degree as the Laser YAG.

Transient Effects

The LPS-100 is sufficiently hard to withstand the estimated transient environment. Corrective action is not necessary to meet operational requirements at the estimated transient environment.
(N. B.: The radiation study of the components was conducted by Mr. Mike Gabrian of Raytheon Company, Environmental Assurance Engineering.)

Summary of Permanent Damage Effects - LPS-100 Power Supply Table 1

System/ Subsystem	Critical Items		Predominant Nuclear Effects	System Reaction
	Item	Description		
LPS-100				
Transistor Q7	2XMJE 340	NPN Silicon Med. Power Med. Freq.	Examination of available data indicates this device type/ family to be in the moderate/high power category with ft in the order of a few Megahertz.	Probable failure at specified proton fluence level. Devices will fail to provide required drive Replace MJE 340 with β preselected device
Transistor Q6	2XMJE 340	"	Analogous neutron effects data (Figure A-4) indicates device usable at specified electron fluence level.	
Transistor Q5	2XMJE 340	"	Device appears to be problematic (Figure A-3) at the specified proton fluence. Probable decrease in β of 60% - 70% anticipated; total dose effects are estimated to be negligible.	
Transistor Q4	2XMJE 340	"		
Transistor Q1	MU-4891	Silicon Unijunction	Definite failure at specified proton fluence of 5×10^9 p/cm^2. Devices will not provide sufficient drive to 2N3904, failure to fire.	Probable system failure No device substitute available. Recommend change of circuit.
Transistor Q2	MU-4891			
Transistor Q8	2N3904	NPN Silicon Low Power High Freq.	Figure A-3 indicates no significant damage at specified proton/electron fluences. β degradation is estimated at 1% - 5%; IcBO increases at 10%.	No significant damage or system reaction.
Transistor Q9	2N3904			
Zener (CR1)	-	-	Figure A-3, A-4, A-5 indicate no significant effects at specified proton/electron fluences. Shift in V_z is much less than 1%.	" " "
Zener (CR4)				
Diode (CR2)	IN 456	Silicon Low Power	Figures A-3 and A-4 indicate no significant degradation at specified proton/electron fluence levels. Increases in V_f and I_R will be in the range of 1% to 5%.	" " "
Diode (CR2)	VSR-15, 1.5KV	Silicon High Voltage Regulators	Figures A-3, A-4 and A-5 indicate no significant degradation at specified proton/electron fluence levels. Shift in regulation will be less than 1%.	" " "
Diode (CR3)	VSR-15, 1.5KV			

Picture #45

System/ Subsystem	Item	Description	Predominant Nuclear Effects	System Reaction
SCR (Q2)	Silicon Controlled Rectifier	NPNP Silicon Medium Power	Data on power diodes (Figure A-3) and analogous neutron data (Figure A-4) indicates that device is reasonably usable at specified proton/electron fluence levels. Negligible increase in I_H will occur.	No significant damage or system reaction.
IC-4	Integrated Circuit 809 CJ	Linear Op. AMP	Figure A-3 indicates linear devices are within usable proton/ electron fluence ranges.	" " "
IC-2	Integrated Circuitry	Digital Logic	Figure A-3 indicates logic elements are definitely within usable proton/electron fluence ranges.	" " "
IC-1	Integrated Circuitry	Digital Logic & Amplifier	Figure A-3 indicates digital and linear IC's are definitely within usable proton/electron fluence ranges.	" " "
IC-3	Integrated Circuitry 321CJ16	Digital Logic (HINIL)	Figure A-3 indicates digital logic to be well within usable proton/electron fluence ranges.	" " "
Transformers	T1-ESL5032c T2-ESL50274 T1-ESL14885 T1-ESL-14	Passive Electrical Elements	Cleared for use via analogous neutron data in Figure A-8. Equivalent damage levels are orders of magnitude above specified proton/electron fluence levels.	No damage or system reaction anticipated.
Tube Devices	KN22 Flash Lamp Crytron	EGG Crytron Xenon EGG	Tubes are cleared for use via analogous neutron data in Figure A-7. Threshold damage levels are an order of magnitude above specified proton/electron fluence levels.	" " "
Pockel Cell	"Q" Switch	Lithium Niobium Crystal	No specific or general nuclear data available. The device could be problematic at the specified total dose of 10^5 RADS (Si).	Questionable-device must be tested to accurately determine effects on the crystal.

* Denotes failure at the specified environment.

4.6 Space Hardened Circuit Design (see drawing ESL-51269)

Component Changes

As the result of the radiation effect study of the LPS-100 power supply, the new space hardened power supply was designed without the critical and space sensitive components.

The first basic change is in the method of the clock pulse generation for the chopper.

The LPS-100 utilizes UJT transistors for the clock pulse generation and also for the firing pulse generation. The space hardened LPS-113 power supply was designed to use positive feedback excited Schmitt trigger circuits as clocks for the choppers. A 367 CJ integrated circuit is used to produce the required clock pulses for the PFN charging supply and for the Q switch supply. The timing for the two clocks is different, since the circuits of the two choppers contain different reactances.

Circuit Changes

Another departure from the LPS-100 is the Q switch charging supply. The LPS-113 does not utilize self-excited inverters because the radiation study indicated a considerable β-change in the chopper transistors. The LPS-113 Q-switch supply utilizes the same circuit as the LPS-113 PFN charging supply. The fact is that all integrated circuits in the supply logic are equally utilized by the two charging channels. One half of each IC operates in the PFN channel and the second half of each IC operates in the Q switch supply channel.

The next departure from the LPS-100 is the duality of trigger circuits and flashlamp circuits in the LPS-113. At the very beginning of the study, we have pinpointed the flashlamps as the shortest life span components. It was evident that by utilizing a dual lamp cavity, the life of the space born laser transmitter could be doubled.

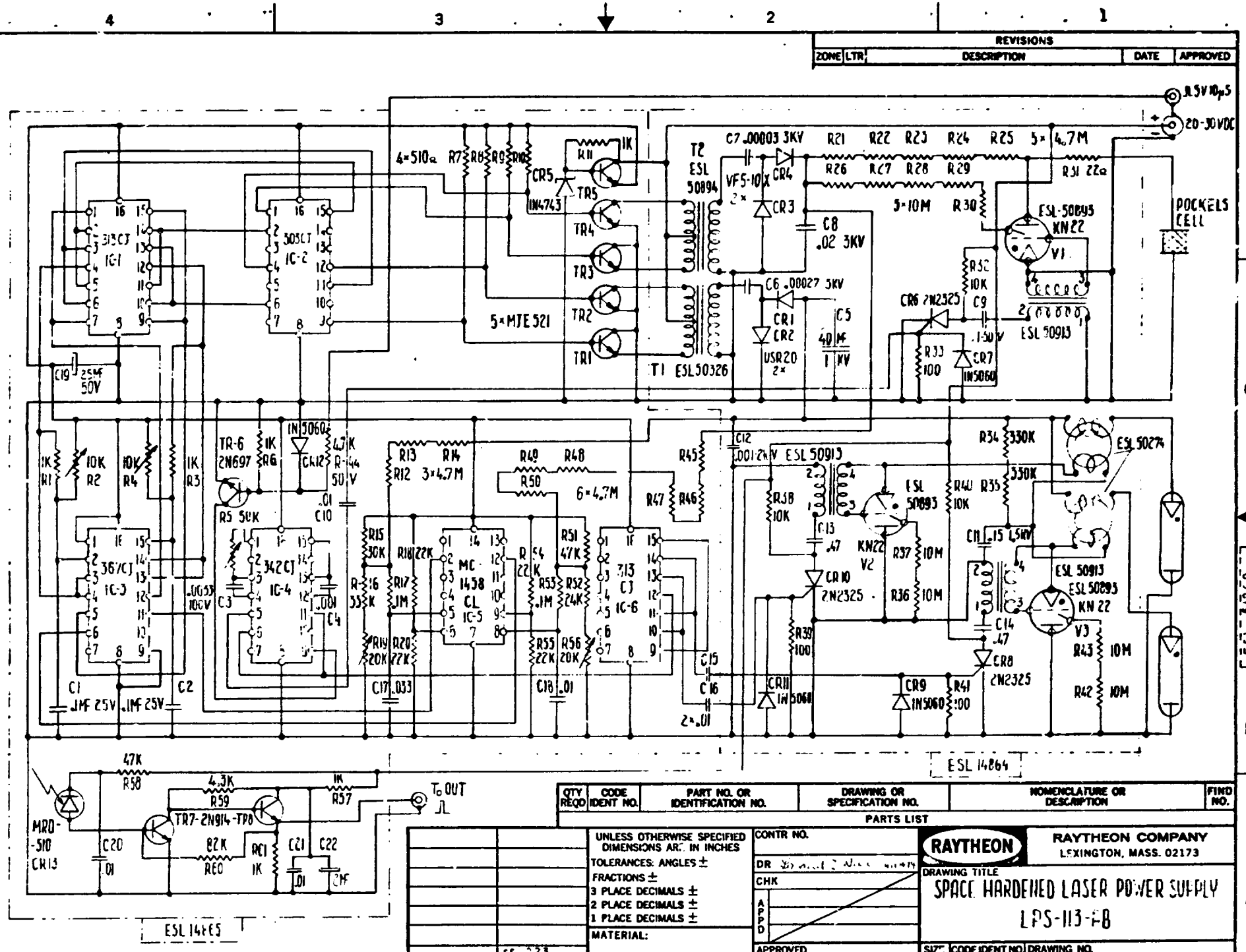
REVISIONS
ZONE LTR DESCRIPTION DATE APPROVED
11.5V 10μs
20-30 VDC
T2 ESL 50894
T1 ESL50326
VFS-10X 2×
CR3
CR4
CR1
CR2
USR20 2×
5×MTE521
4×510Ω R7 R8 R9 R10
CR5 IN4743
TR5
TR4
TR3
TR2
TR1
R11 1K
C7 .00003 3KV
C8 .02 3KV
C6 .00027 3KV
C5 40 MF 1 KV
R21 R22 R23 R24 R25 5×4.7M
R26 R27 R28 R29
5×10M R30
R31 22Ω
R32 10K
C9 .1-50V
CR6 2N2325
R33 100
CR7 IN5060
ESL-50893 KN22 V1
ESL 50913
POCKELS CELL
313CT IC-1
305CT IC-2
C19 25MF 50V
1K R1
10K R2
10K R4
1K R3
TR-6 2N697
1K R6
IN3060 CR12
4.7K R-44 50V
R5 50K
.01 C10
C3
.0063 100V
342CT IC-4
.001 C4
C1 1MF 25V
C2 1MF 25V
367CT IC-3
R13 R14 R12 3×4.7M
R49 R48 R50 6×4.7M
R45 R47 R46
C12 .001-2KV
ESL 50913
R15 30K
R16 33K
R18 22K
R17 1M
R19 20K
R20 27K
C17 .033
MC 1458 CL IC-5
R54 22K
R53 .1M
R52 24K
R51 47K
R55 22K
R56 20K
C18 .01
313 CT IC-6
C15
C16 2×.01
R38 10K
C13 .47
CR10 2N2325
R34 330K
R35 330K
R40 10K
ESL 50893 KN22 V2
R37 10M
R36 10M
C11 .15 4.5KV
ESL 50274
ESL 50913
ESL 50893 KN 22 V3
R43 10M
R42 10M
C14 .47
CR8 2N2325
R39 100
CR11 IN5060
CR9 IN5060
R41 100
ESL 14864
47K R58
4.3K R59
1K R57
TR7-2N914-TP0
MRD-510 CR13
C20 .01
82K R60
RC1 1K
C21 .01
C22 1MF
To OUT
ESL 14865
QTY REQD | CODE IDENT NO. | PART NO. OR IDENTIFICATION NO. | DRAWING OR SPECIFICATION NO. | NOMENCLATURE OR DESCRIPTION | FIND NO.
PARTS LIST
UNLESS OTHERWISE SPECIFIED DIMENSIONS ARE IN INCHES
TOLERANCES: ANGLES ±
FRACTIONS ±
3 PLACE DECIMALS ±
2 PLACE DECIMALS ±
1 PLACE DECIMALS ±
MATERIAL:
CONTR NO.
DR
CHK
APPD
APPROVED
BY DIRECTION OF
RAYTHEON
RAYTHEON COMPANY
LEXINGTON, MASS. 02173
DRAWING TITLE
SPACE HARDENED LASER POWER SUPPLY
LPS-113-FB
SIZE C
CODE IDENT NO. 49956
DRAWING NO. ESL-51269
SCALE
SHEET
55-223
NEXT ASSY
USED ON
APPLICATION
ESL-51269

Picture #47

Dual Lamp Firing

The dual lamp approach required lamp switching and a study was undertaken to find the best switching method. The involved high current (hundreds of amperes) and high trigger voltage (15-20 KV) in a small enclosure preempted the use of relays or solid state switches. The simplest approach seemed to be the use of two trigger transformers (series injection) connected to a single PFN capacitor.

Each trigger transformer, when connected to its individual flashlamp and its individual trigger supply, permits it to be fired individually. This allows alternate firing of the two flashlamps.

From the point of reliability, this circuit arrangement improves not only the life expectancy of the laser by a factor of two, but in the case of catastrophic failure of one trigger-flashlamp channel, the second half still operates at full power. The laser transmitter will continue transmitting normally, except for the slower pulse rate.

Another change in the design of the LPS-113 resulting from the radiation study was the shielded and encapsulated packaging of the radiation sensitive components, such as pulse transformers, Krytrons, detectors, etc.

Increase of the Efficiency

A special effort was spent in increasing the efficiency of the charging circuits. Certain losses are inherent in any charging circuit and almost nothing can be done about that. Such losses incorporate the forward saturation resistance of the chopper transistors, the resistance of the wire on the transformer, the losses in the magnetic core, and the reactive losses of the stray capacitances and inductances and the diode switching losses on the secondary side. All these losses amount to better than sixty percent in miniature charging systems.

Miniature charging systems must use small cores in the transformers and thin wire cross sections to meet the small volume and weight requirements; unfortunately, both contribute to considerable losses.

The forward resistance at saturation in the transistors is a function of the voltage applied and the basic nature of the junction energy gap. A typical .8 to 1.2 volts will be more significant at low voltages when the saturation voltage is a high percentage of the supply voltage than at let us say 110 V where it represents less than one percent. Also for the same amount of power transfer, the low voltage source requires high current, increasing the I^2R losses and lowering the efficiency.

Tuned Charging Circuit

The losses introduced by leakage inductance and stray capacitances were minimized by the choice of toroidal cores, fabricated from high frequency ferrite materials and the special coil winding techniques such as sectioned secondary and bifilar primary coils.

The ideal transformers would transfer only the resistive load components as reflected impedance from the secondary to the primary.

To approximate this condition, a circuit was designed where the f_o (chopper frequency) could be varied to "tune" out all the reactive components of the circuit and to draw only current through loads appearing as close as possible to pure resistances.

Tests made on several breadboard setups indicated that a sharp resonance exists in the chopper-rectifier circuit. A typical circuit drawing 5 to 6 amperes DC from the battery supply and delivering 10 Watts into a resistive load, at resonance dropped to .8 amperes, while still delivering the 10 Watts. In the final design the frequency of the toggle clock is adjustable by potentiometers (R-2 and R-4 on ESL-51269).

Supply and Load Isolation

In PFN charging power supplies, one of the prime concerns of the designer is the load line problem. At the beginning of the charging cycle the storage capacitor is a virtual short circuit load on the secondary side of the charging circuit. At the end of the charging

Conventional Voltage Doubler Circuit, No Current Limiting, No Short Circuit Protection

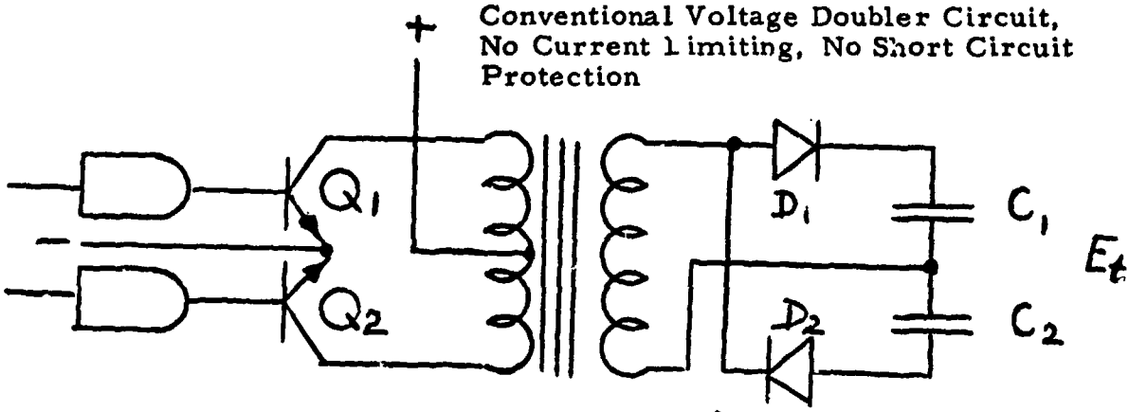

FIRST CYCLE:
C_1 is charged to E_1 through D_1, D_2 is back-biased and E_t is zero.

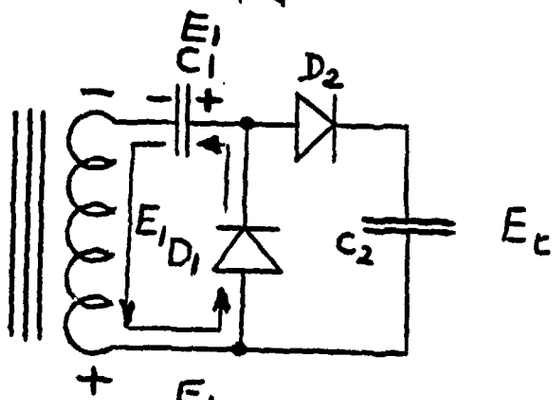

SECOND CYCLE:
Polarity on the secondary is reversed, D_1 becomes back-biased. D_2 conducts $E_1 + E_2$ in C_2 and charges to E_t

$$E_t = E_1 + E_2$$

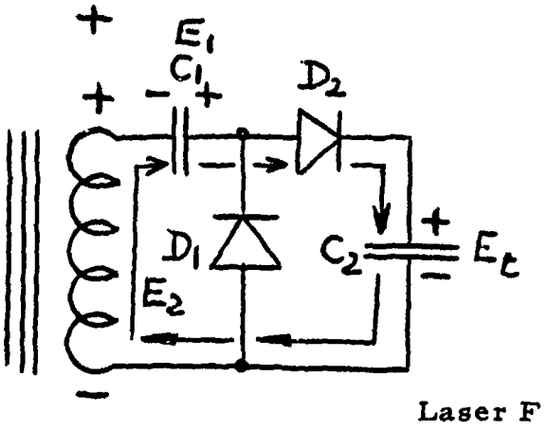

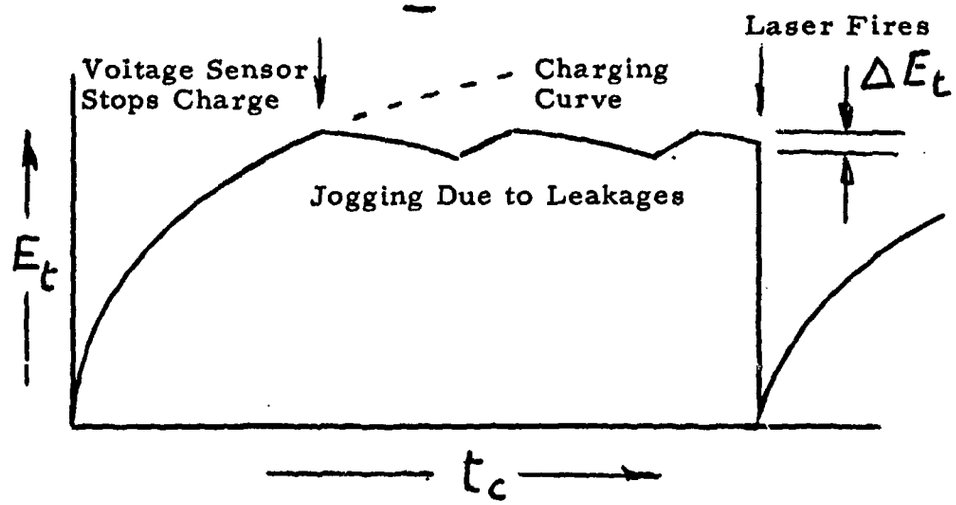

Current Limiting, Short Circuit (Load) Proof Charging Power Supply

Picture #12

cycle the load becomes an infinitely high impedance. Anywhere in between the two extremes the impedance constantly increases. The short circuit load condition will cause the chopper transistors to operate in the unsafe area and will lead to thermal puncture of the junction of the transistor. The primary current is limited in this case only by the series resistances of the components such as diodes, transformer winding resistance, etc. This indicates an equal amount of energy to be dissipated in components and stored in the capacitor.

The Constant Energy Charging

In space born power supplies, the sources of the power are invariably solar cell charged batteries. The battery life is considerably shortened, if high ratios of peak power to average power are demanded by the loads. Such loads are undesirable, because they place an unusual demand on the regulators of the supplied power.

The circuit developed for the space hardened laser power supply does have a 1.2 to 1 ratio and has a built-in short circuit protection (load). (see Picture #1)

This unique circuit utilizes the principle of full wave voltage doubler circuit, modified for reactive current limiting service and short circuit protection.

A standard voltage doubler circuit (a) charges alternately the two capacitors C_1 and C_2 and the load is connected across the two series connected capacitors.

The value of the E_{out} is $E_{in} \times K$, where K would be theoretical limit. In practice, it is less than that, depending on the losses of the circuit.

The voltage doubler circuit was chosen, because it requires only one half of the number of turns on the secondary of the high voltage transformer, and so it reduces the insulation requirements and minimizes the winding capacitance and leakage inductance and the inductive reactance of these undesired characteristics does affect the chopper circuit

performance, because they are the primary causes of "spiking", high transient switching voltages across the chopping transistors, and they generate a high amount of RF interference hash.

The modification of this circuit involves the change in the component arrangement on the secondary of the power transformer.

First, the capacitance of C_1 is reduced and the one of the C_2 is increased. The diodes D_1 and D_2 are rearranged to perform the following way (Follow picture #).

In the first half cycle of the chopper, Q is conducting. This induces a voltage into the secondary with negative polarity on the top of the secondary and positive at the bottom of the secondary. Such polarity biases D_1 into conduction and charges C_1 to approximately to $E_{primary} \times \frac{N\ secondary}{N\ primary}$. (In the actual circuit this is 700 VDC.)

The second half cycle, Q_2 conducts and this reverses the polarity across the secondary, placing positive polarity on the top of the secondary and negative on the bottom of the secondary. D_1 is back biased and will not conduct. The voltage E_2 across the secondary (700 VDC instantaneous) and the voltage stored across C_1 (700 VDC) are in series with additive polarity. Therefore, $E_1 + E_2$ forward biases D_2 and the charge is dumped into C_2. After N number of chops, the C_2 eventually charges up to E_t level, which theoretically is 2E or $E_1 + E_2$ final (1400 VDC).

The ratio of the reactances X_{C1} and X_{C2} will determine the number of cy cycles required to make $E_t \cong 2E_1$.

It is evident that not only at the beginning of the charging cycle, but well into the cycle X_{C2} is near zero. Therefore, the charging current will be determined by the terminal voltage at the transformer and the capacitance of C_1 and the chopper clock frequency. In the actual circuit, the voltage comparator circuit stops the clock when E_t reaches 1 KV. The high reactance of C_1 determines the short circuit current and also the charging current. The amount of energy stored by C_1 is constant, and therefore this charging method is constant energy type.

REVISIONS				
ZONE	LTR	DESCRIPTION	DATE	APPROVED

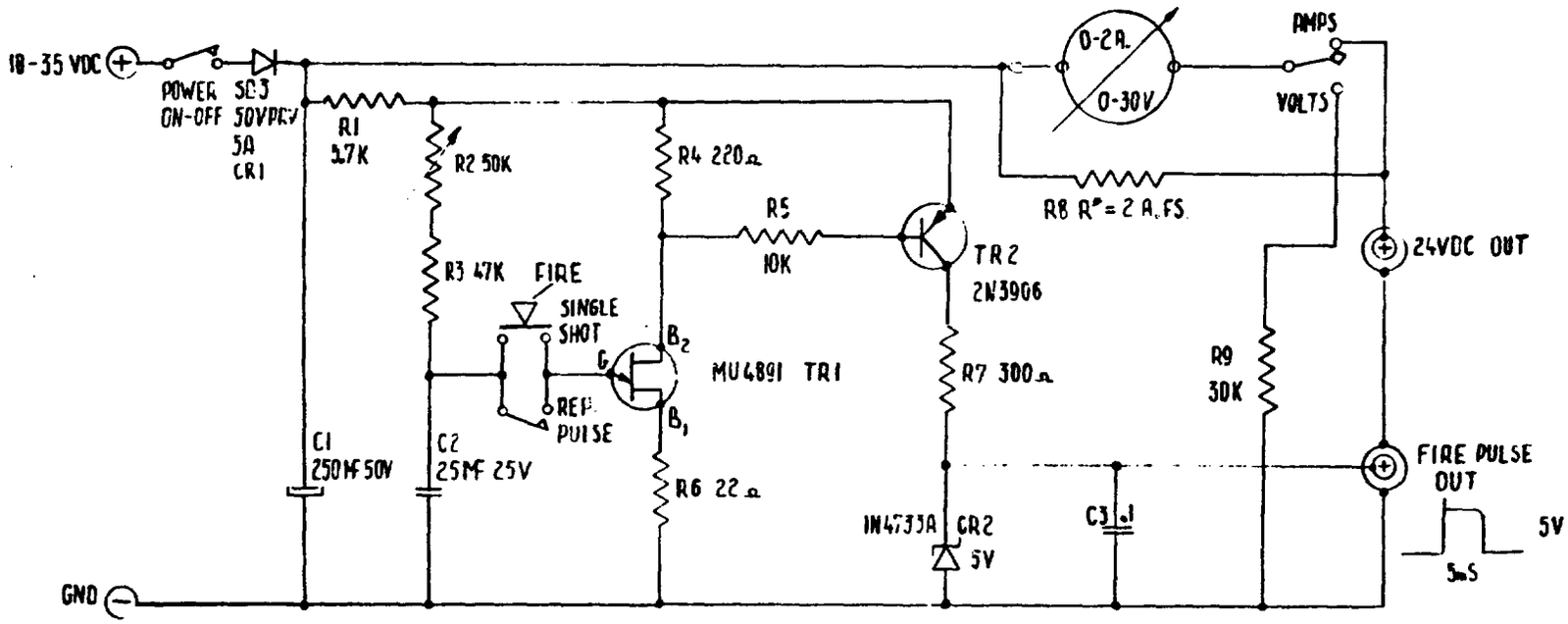

QTY REQD	CODE IDENT NO.	PART NO. OR IDENTIFICATION NO.	DRAWING OR SPECIFICATION NO.	NOMENCLATURE OR DESCRIPTION	FIND NO.
PARTS LIST					

	55-223
NEXT ASSY	USED ON
APPLICATION	

UNLESS OTHERWISE SPECIFIED DIMENSIONS ARE IN INCHES
TOLERANCES: ANGLES ±
FRACTIONS ±
3 PLACE DECIMALS ±
2 PLACE DECIMALS ±
1 PLACE DECIMALS ±
MATERIAL:

CONTR NO.
DR Leonard J Wargo 4.20.74
CHK
APPD
APPROVED Leonard J Wargo 4.20.74
BY DIRECTION OF Leonard J Wargo 4.20.74

RAYTHEON COMPANY
LEXINGTON, MASS. 02173

DRAWING TITLE
REMOTE CONTROL CIRCUIT
LPS-113-C

SIZE	CODE IDENT NO.	DRAWING NO.
C	49956	ESL-51270

SCALE | SHEET

ESL-51270

Picture #49

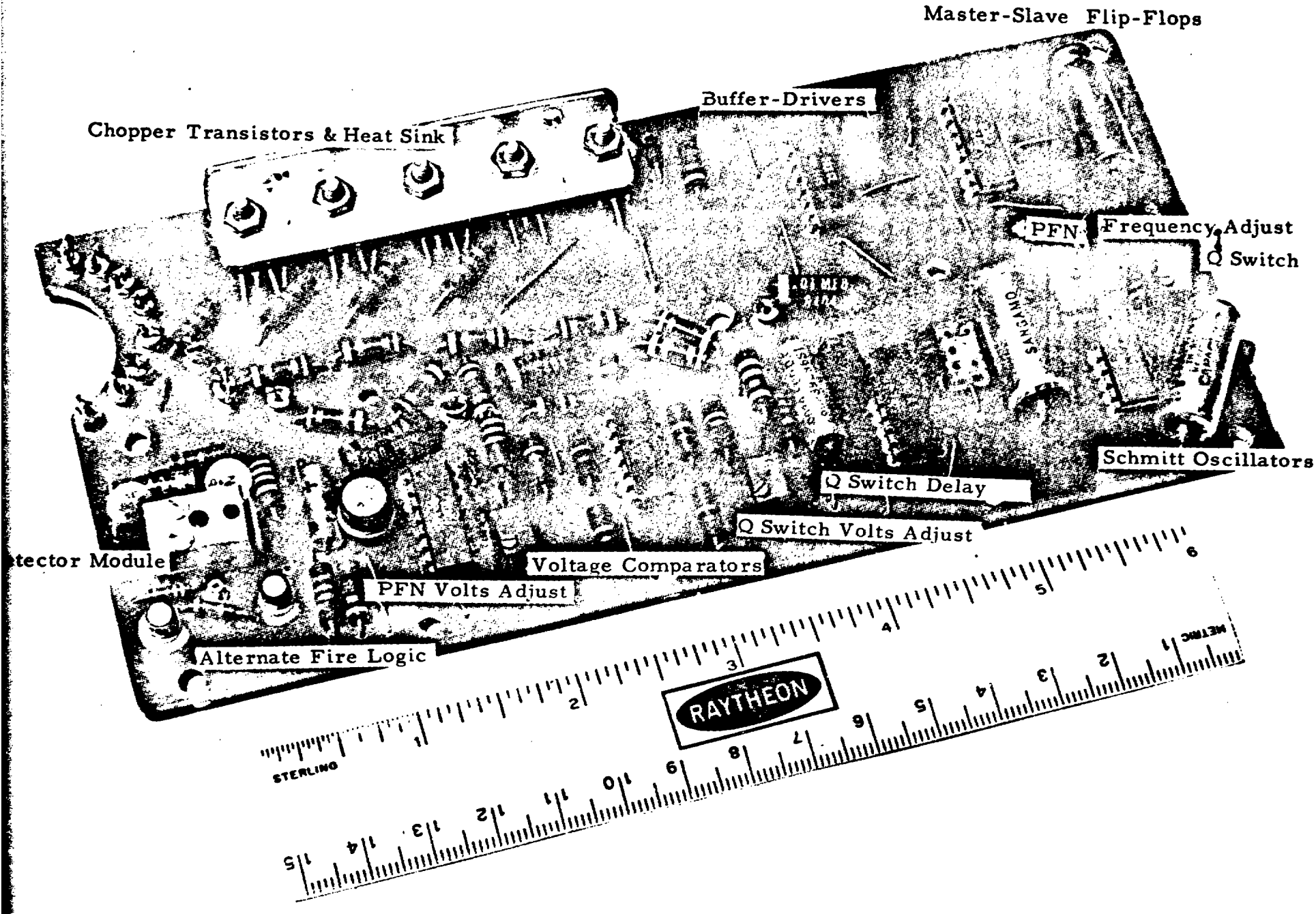

Picture #50 Top View of the Logic and Driver Board ESL-14865 of the Power Supply Model LPS-113B

4.7 Circuit Layouts

Based on the study of space environmental behavior of the LPS-100 power supply, the space hardened LPS-113 AB supply was designed and fabricated, utilizing two circuit boards with electro-magnetic shielding in between.

Since the SS-223 space hardened laser was designed for SPACE-ORBITAL SERVICE, NO PROVISIONS WERE MADE FOR SERVICE OR MAINTENANCE! The CORDWOOD type laser assembly is made layer by layer, and wire interconnections are made by solid soldering between the layers.

The lower layer, located above the Laser Transmitter and Storage Capacitor is the ESL-14864 charging supply board and the upper layer of the cordwood package is the ESL-14865 driver logic board. The two boards together are designated LPS-113A and LPS-113B. Together with the storage capacitor they constitute LPS-113AB power supply. This supply is shown on the ESL-51269 schematic diagram.

4.8 Operation of the SS-223 Laser

The SS-223 space hardened laser is designed to operate in an UNMANNED space satellite. Therefore, it does not contain any controls, indicators or meters.

For the prelaunch checkout, a remote control unit, LPS-113C is available. The diagram of the LPS-113C is shown on drawing #ESL-51270.

To operate the SS-223 laser, a DC supply of 18-32 volts, protected with a 1 ampere circuit protector should be connected to the power input coaxial connector through a shielded cable. The center conductor of the connector is POSITIVE (+); the grounded connector shell is NEGATIVE (-).

When operated from the remote control unit, a suitable cable is installed on the unit and all it needs is to be connected to the connector on the laser.

Whenever the DC power is applied to the laser, unit is ARMED AND READY TO FIRE in 10 second intervals.

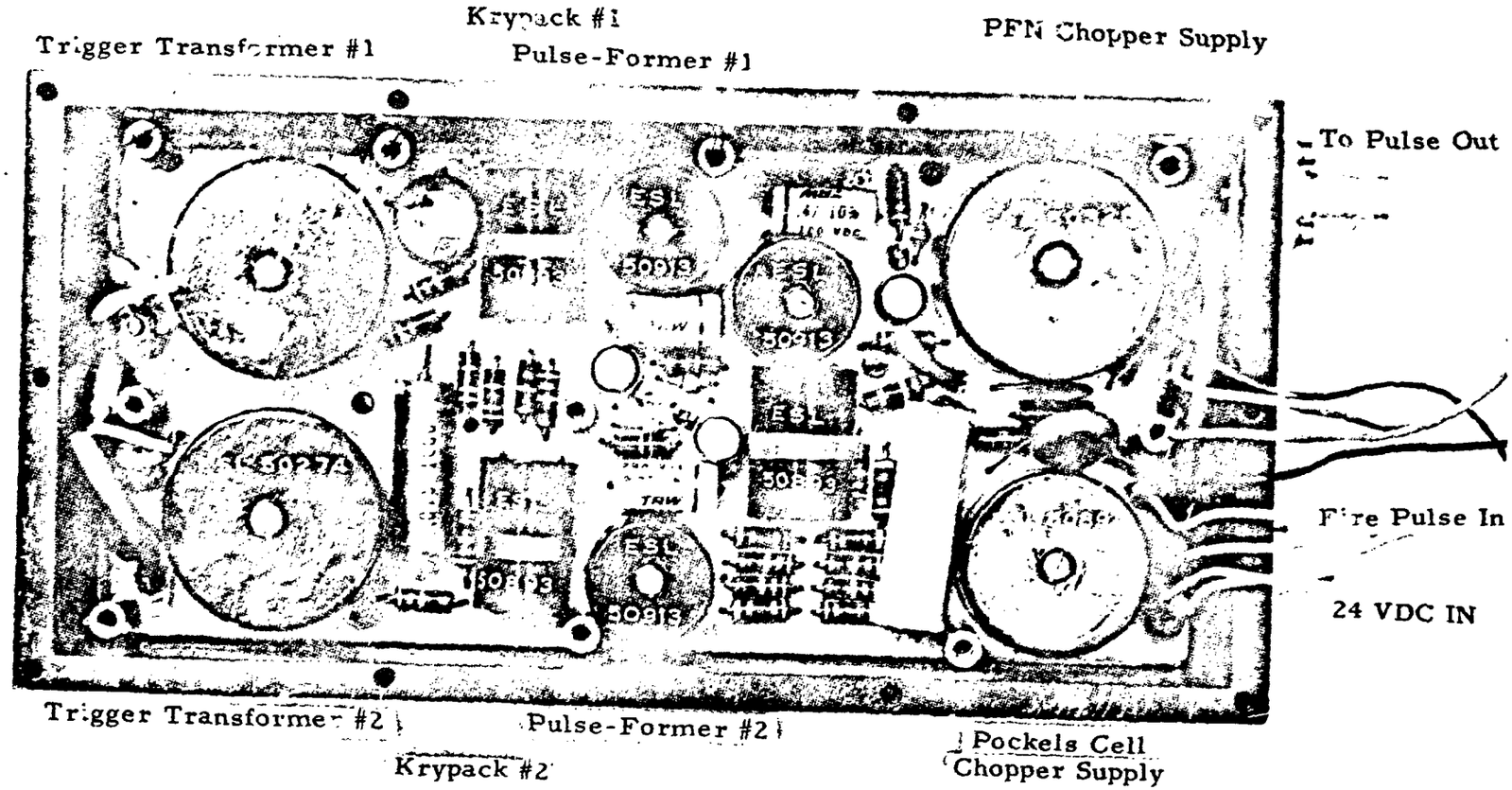

Picture #51 Top View of the Charging Supply Board ESL-14864 of the Power Supply Model LPS-113A

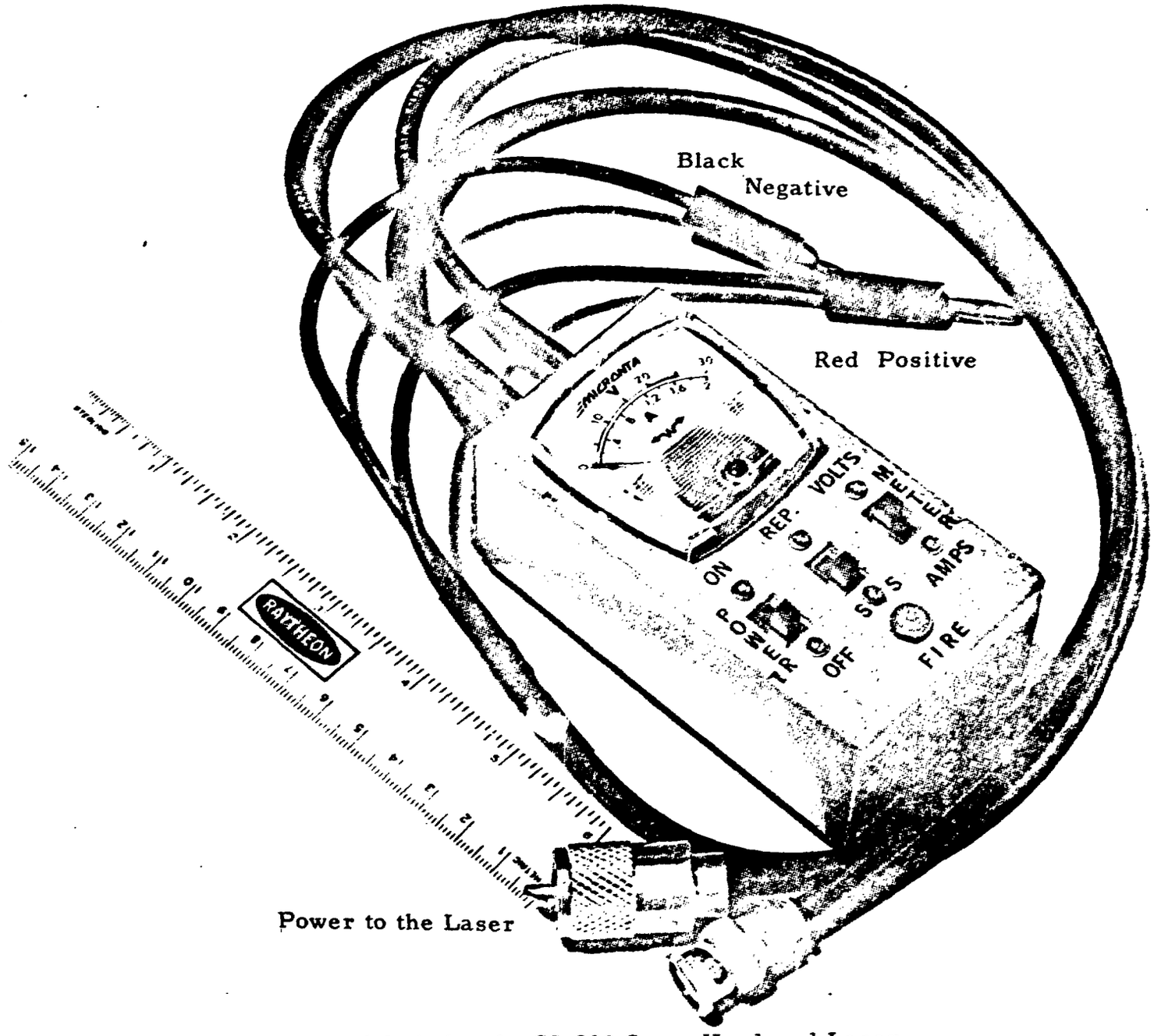

Picture #52 Terestrial Remote Control Unit for the SS-223 Space Hardened Laser

a 5 VDC, 10 microsecond or longer positive going pulse applied to the "Trigger IN" BNC connector on the laser, the laser will deliver a Q-switched pulse of 60 millijoules energy and 8 to 10 nanoseconds every 10 seconds.

The remote control box does have a 50 ohm cable with a BNC connector. This cable can be connected to the "Trigger IN" BNC on the laser for terrestrial checkout operation.

4.9 Operation from the Remote Control Box

For prelaunching checkout, connect the two cables between the remote control box and the laser transmitter as described in the previous paragraph.

Connect the input cable of the remote control box to a suitable DC power supply (24 VDC, 2 A) protected with a 1 ampere circuit protector. Connect the RED banana plug to the POSITIVE and the BLACK banana plug to the NEGATIVE terminal of the power supply.

Before turning on the power supply, make sure that all required safety measures against exposure to laser radiation are satisfied. Personnel in vicinity and exposure prone, must wear proper eye protection, and must be advised about the laser radiation. Proper provisions must be made to prevent inadvertent entry of unaided persons into the Laser Test Area! Accidental exposure probability must be zero!

The switches on the remote control unit should be in POWER OFF; SS; METER VOLTS positions. Turn on the power supply. Turn the POWER SWITCH TO ON on the remote box. The meter should read in the BLUE safety zone (20 to 25 VDC).

Switch the METER SWITCH to AMPS. The meter should read first about 600 milliamps and then drop to 290 milliamps. This indicates that the charging cycle was completed at 600 milliamps and the system is now "jogging" at 290 milliamps and is ready for firing.

If the fire button is depressed before the 10 second interpulse period, or during the charging cycle, the remot box logic will reject it and the laser will not fire. Depressing the "FIRE" button at 10 second intervals, the laser will produce a laser pulse on demand.

If automatic operation is desired, the control switch on the remote control box should be switched to REP position. To turn the system OFF, switch the "POWER" switch into OFF position.

Depending on the power supply voltage, the currents and charging and jogging times will vary. The described values apply to a 24 VDC setting on the power supply voltage dial.

New Circuit Functions

The basic functions of the circuitry of the LPS-113AB are identical with the functions of the LPS-100QA power supply. Reading the LPS-100 power supply operational description and observing the LPS-113AB schematic diagram, the operation of the Master Slave Flip-Flop, buffer gates voltage regulator, choppers, high voltage bridges, trigger supplies and Q switch supplies and voltage control circuits are identical.

The basic difference is in the dual master clock, the alternating logic, and the dual instead of a single lamp and trigger circuit arrangement.

Another difference is the absence of the timing clock and firing control in the LPS-113AB circuit, and the addition of second driver and voltage sensing circuit in the LPS-113AB (IC-5).

The locations of the major components and adjustment controls are indicated on the photographs.

Caution! If the top cover of the laser is removed, LETHAL HIGH VOLTAGES are exposed. Be sure that the power is disconnected and ALL CAPACITORS ARE DISCHARGED. Before operating the laser, READ ALL PRECAUTIONS!

4.10 FINAL AND ACCEPTANCE TESTING

The SS-223 space hardened laser parts were fabricated and final assembly was completed. The final testing of the unit was recorded in the Engineering Records Book #21554, Page 80.

The tests performed were complete functional check on all controls, pulses and circuits.

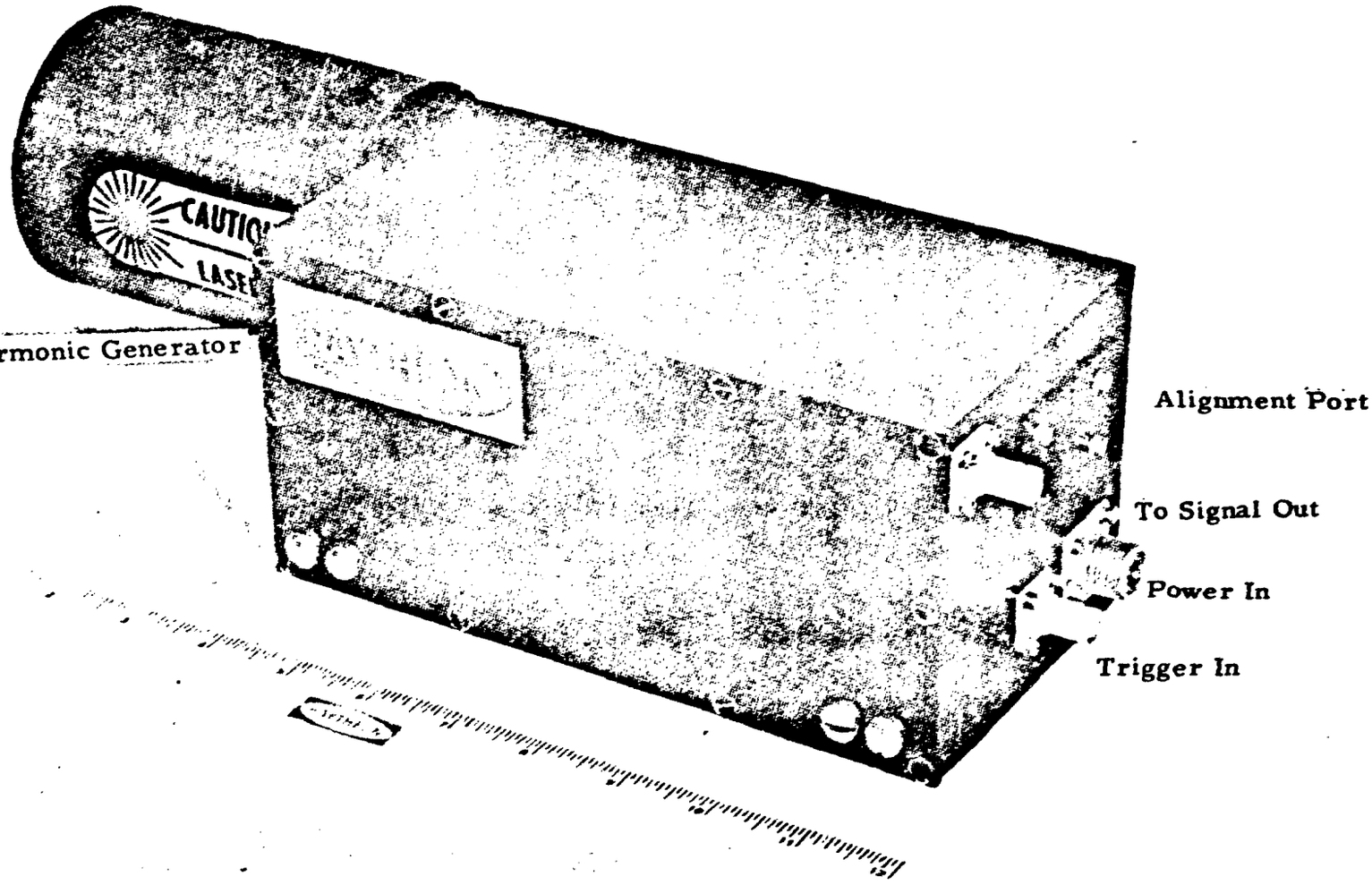

SS-223 Space Hardened Laser with the Second Harmonic Generator Attached

The final lasing test was performed with 850 VDC on the PFN capacitor of 40 microfarads. This corresponds to 14.4 joules input into one flashlamp. The Pockels Cell voltage was set at 1450 VDC and five consecutive shots were fired into a Balistic calorimeter. The Q-switched output was recorded as: 60 mJ; 63 mJ; 62mJ; 62 mJ; 61 mJ in 10 second intervals.

The output was also photographed with a TEK-519 oscilloscope and a high vacuum photodiode detector. The output pulse measured 8 nanosecond pulse width at the 1/e points.

The beam divergence was measured 2.2 milliradians at half power full angle.

The tests were concluded on April 23, 1975.

The representative of NRL, Dr. Steven Mellman, was invited to witness the consecutive tests and to effectuate the acceptance and authorize the shipment of the units.

Acceptance Testing

The acceptance testing of the SS-223 laser was registered in the Engineering Data Book #21554, Page 81, entered on June 6th, 1975 and witnessed by Lorand J. Wargo for Raytheon Company and by Dr. Steven Mellman for NRL.

The following tests were performed. The output of the laser was measured at 23 VDC input. The charging cycle was measured at 600 milliamperes, 7 seconds and then 3 seconds jogging time at 290 milliamperes. The laser fixed after 10 seconds and delivered 62 millijoules output energy in a TRG-100 Energy Meter.

Pulse width measurements were not repeated because the TEK-519 oscilloscope did not operate (no synchronization of the sweep).

A second measurement of output energy was made. The same instrument was used as at the first test. The output was 64 millijoules.

The pulse rate of the laser was measured, and confirmed to be 10 seconds.

Finally, the PFN voltage was adjusted to 900 VDC and the Q-switched output was 90 millijoules.

After this test, the SS-223 laser, the remote control box and a pair of space lamps was transferred to Dr. Mellman.

References

1) Holly, F. E., "The Geomagnetically Trapped Radiation Environment," page, 171, NASA TM-X-2440, Procedures of the National Symposium on Natural and Manmade Radiation in Space, NASA, Washington, D.C., January 1972 (U)

2) Barengoltz, J. B., "Jupiter Radiation Test Levels and Their Expected Impact on an Encounter Mission," Contract #NAS7-100, Jet Propulsion Laboratory, California Institute of Technology, NASA TM X-2440, January 1972 (U)

3) Thatcher, R. K., Hammon, D. J., Clapin, M. E., Honks, C. L., Wyler, E. N., "The Effects of Nuclear Radiation on Electronic Components, Including Semiconductors," R.E.J.C. #36, Battelle Memorial Institute, Columbus, Ohio, October 1964 (U)

4) Hansen, H. E., "Designers Guide to Space Radiation Effects," Report #347.60.00.0C-E9-09, Lockheed Missiles and Space Division, Lockheed Aircraft Corporation, Sunnyvale, California, 1961 (U)

5) Wechback, J. R., "Independent Development Program, Advanced Hardened Computer," IDP Project No. 15-02-6087-002, Volume II, Equipment Division, The Raytheon Company, Sudbury, Massachusetts, 1 March 1970 (Company Private)

APPENDIX

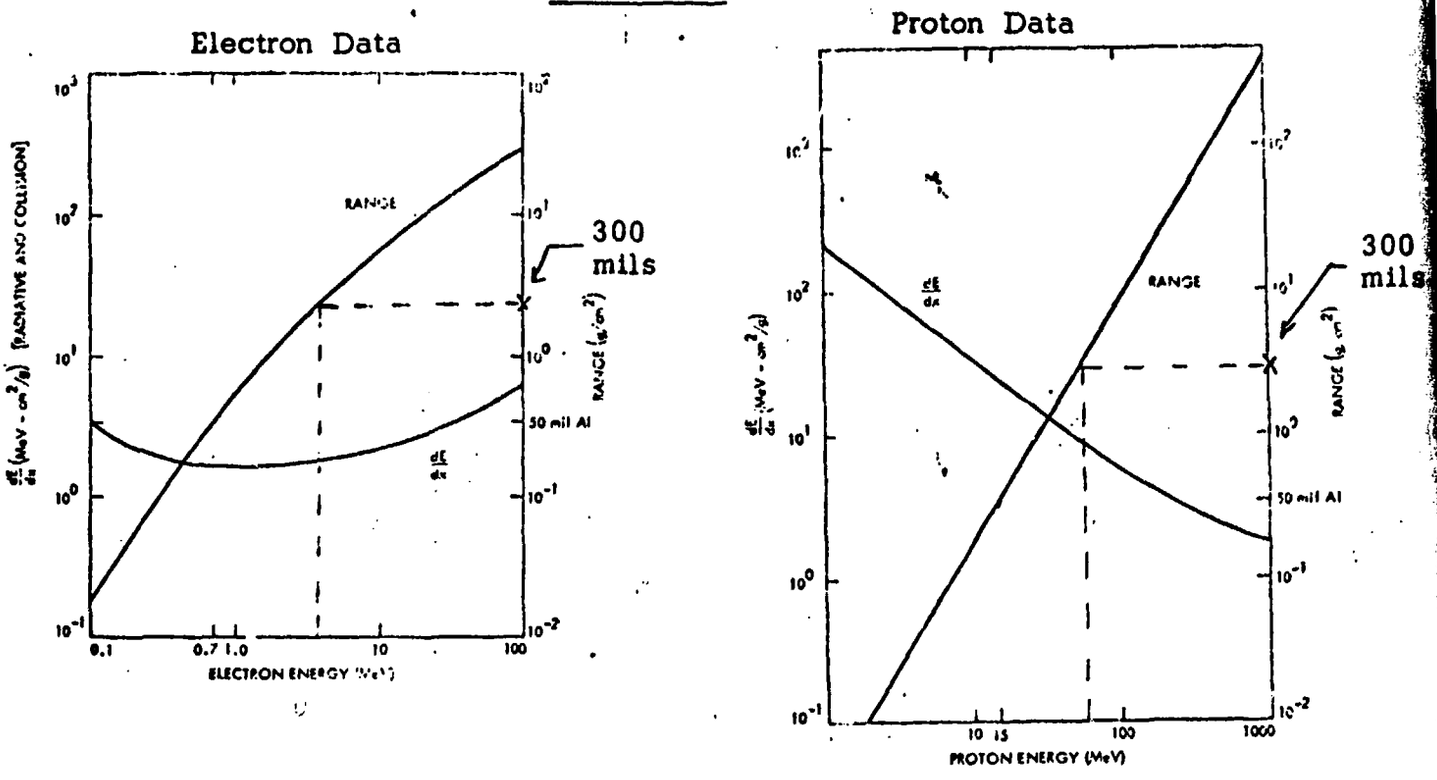

Figure A-1

Electron/Proton Range/Stopping Power Curves - Aluminum

Electron Spectrum

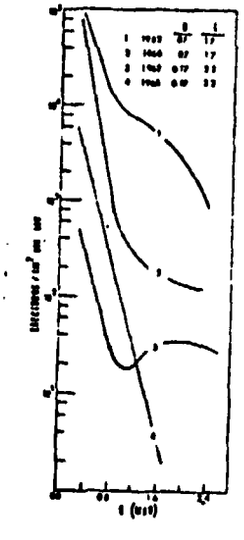

Proton Spectrum

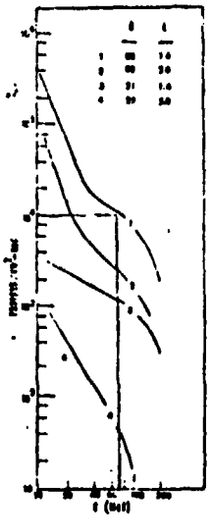

Figure A-2

Typical Electron/Proton Spectrum Data

Von Allen Belt Radiation

Electron Damage Effects Data

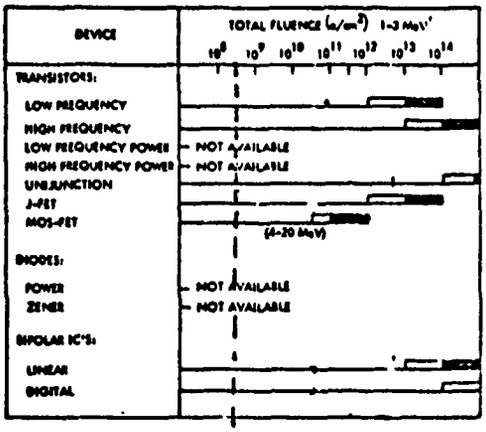

Estimated Internal Fluence Level

Proton Damage Effects Data

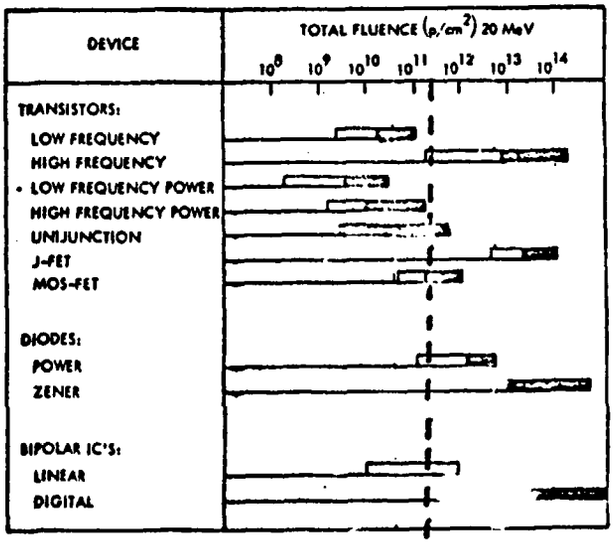

Estimated Internal Fluence Level

Figure A-3
General Damage Effects Data
for Proton/Electron Fluences

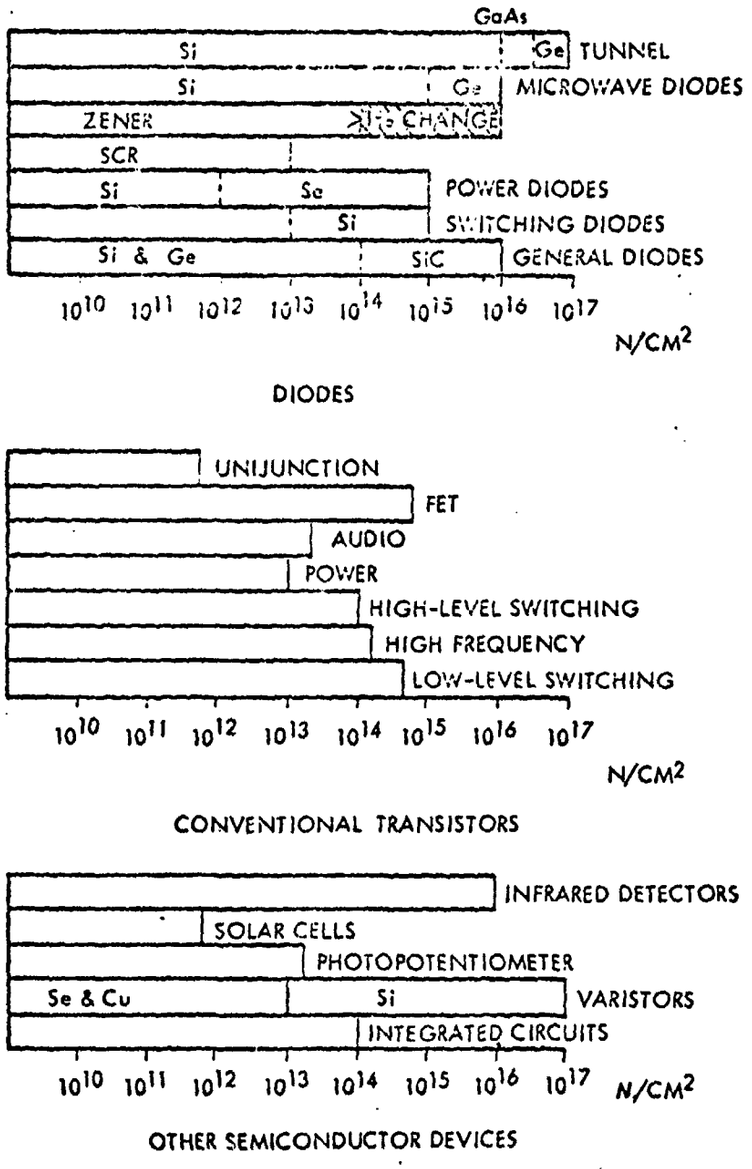

General Usage Levels for Semiconductor Devices

Figure A-4

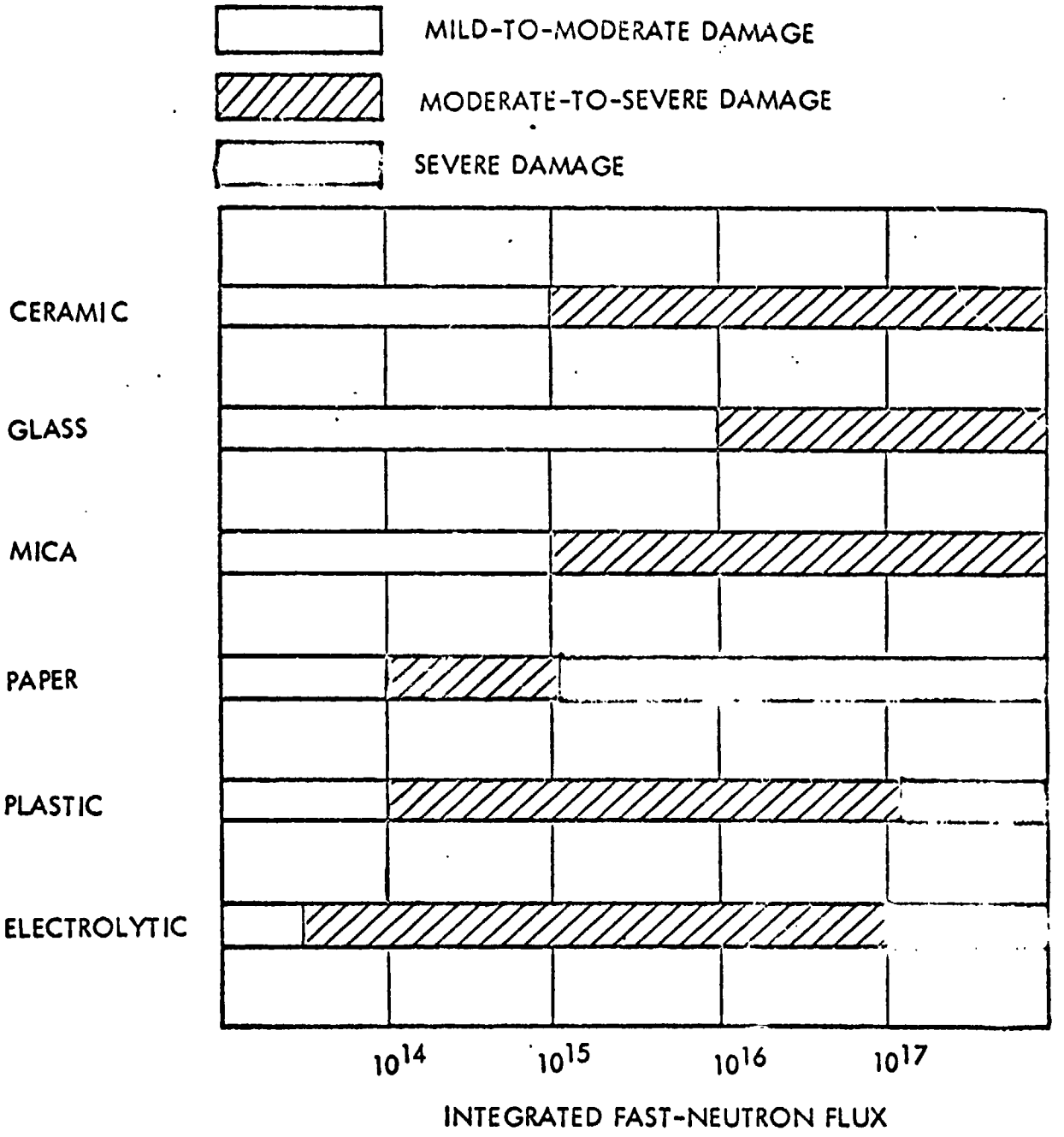

Figure A-5

Relative Radiation Sensitivity of Capacitors

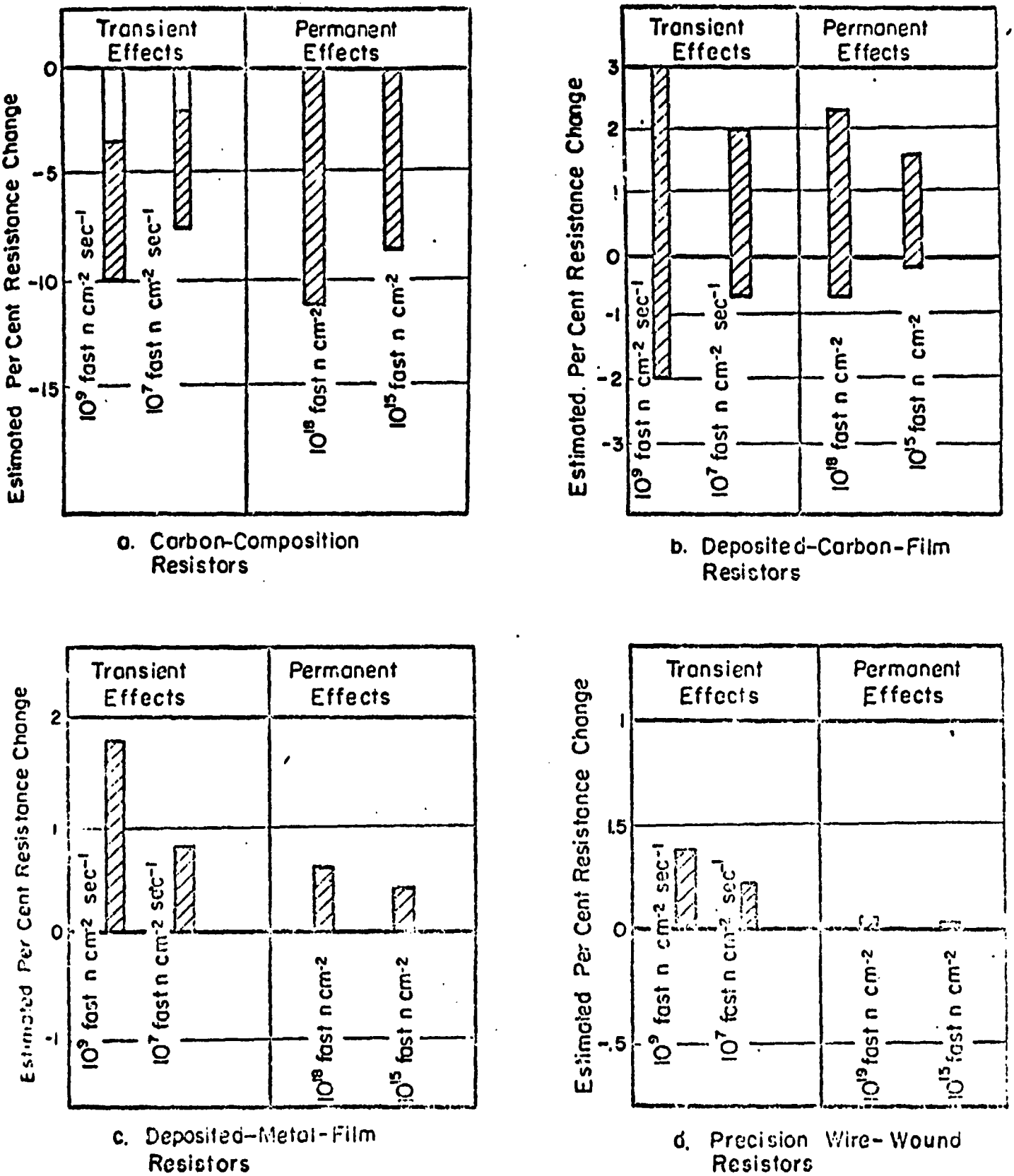

Estimated Effects of Nuclear Radiation on Carbon-Composition, Deposited-Carbon and Metal-Film, and Precision Wirewound Resistors

Figure A-6

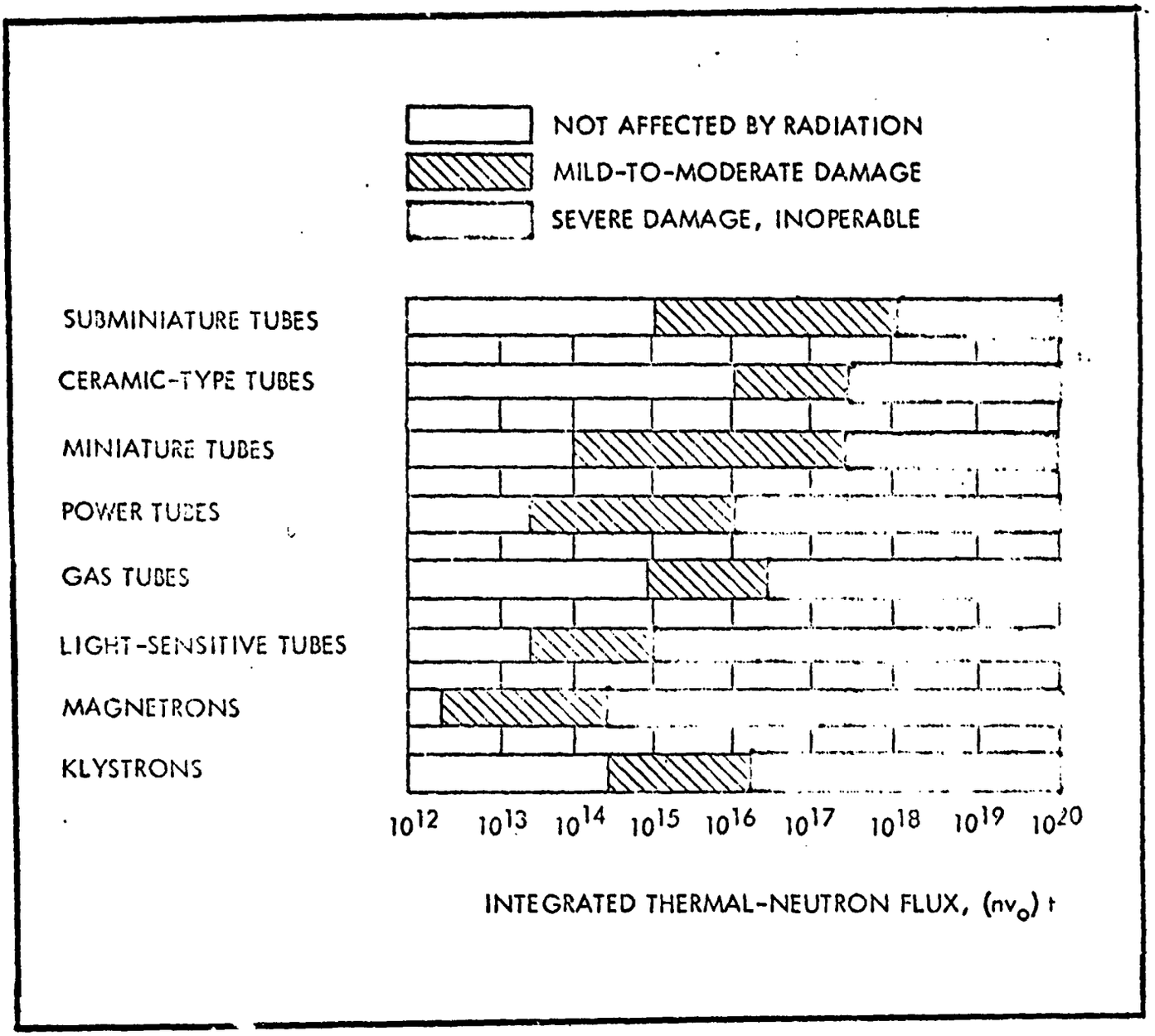

Figure A-7

Effects of Radiation on Electron Tubes as a Function of Integrated Thermal-Neutron Flux $(nv_o)t$

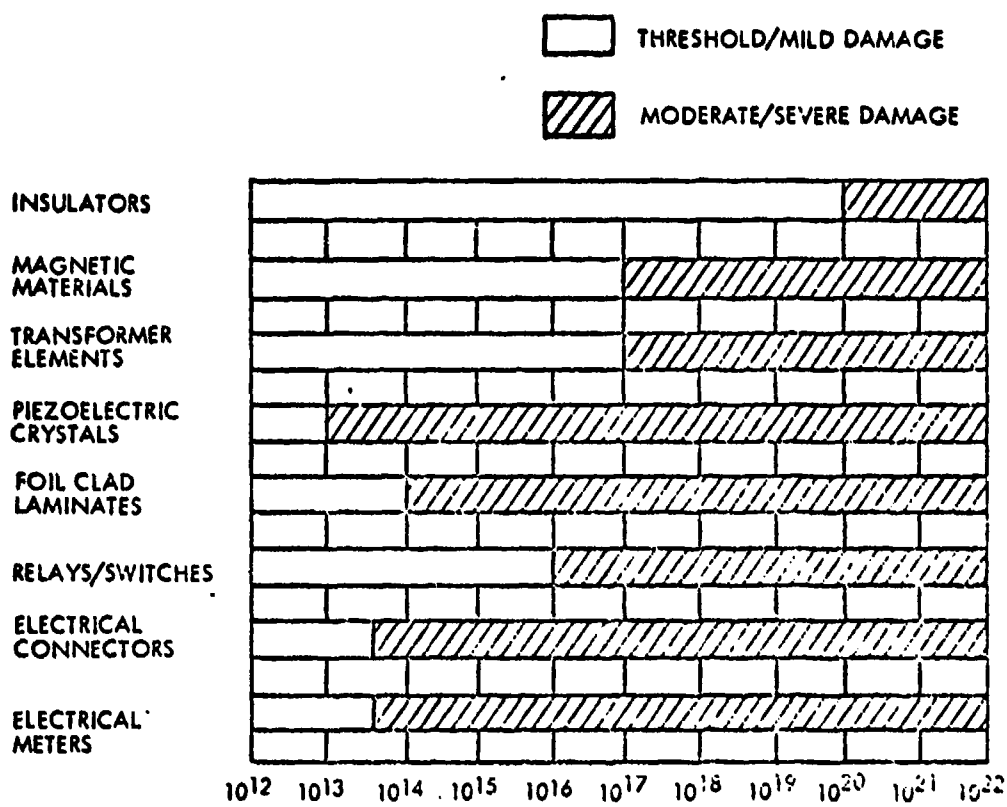

Abstracted Neutron Degradation Levels
for General Electronic Components

Figure A-8